1-1-2013

Modifications on A-F Hardening Rule to Assess Ratcheting Response of Materials and Its Interaction with Fatigue Damage under Uniaxial Stress Cycles

Gholamreza Ahmadzadehrishehri
Ryerson University

MODIFICATIONS ON A-F HARDENING RULE TO ASSESS RATCHETING RESPONSE OF MATERIALS AND ITS INTERACTION WITH FATIGUE DAMAGE UNDER UNIAXIAL STRESS CYCLES

By

Gholamreza Ahmadzadehrishehri
B.Sc. in Mechanical Engineering, Shiraz University, July 1999
M.Sc. in Mechanical Engineering, Guilan University, July 2002

A dissertation
presented to the Ryerson University
in partial fulfillment of the
requirement for the degree of

Doctor of Philosophy

in the Program of
Mechanical Engineering

Toronto, Ontario, Canada, 2013

AUTHOR'S DECLARATION FOR ELECTRONIC SUBMISSION OF A DISSERTATION

I hereby declare that I am the sole author of this dissertation. This is a true copy of the dissertation, including any required final revisions, as accepted by my examiners.

I authorize Ryerson University to lend this dissertation to other institutions or individuals for the purpose of scholarly research.

I further authorize Ryerson University to reproduce this dissertation by photocopying or by other means, in total or in part, at the request of other institutions or individuals for the purpose of scholarly research.

I understand that my dissertation may be made electronically available to the public.

ABSTRACT

Modifications on A-F Hardening Rule to Assess Ratcheting Response of Materials and Its Interaction with Fatigue Damage under Uniaxial Stress Cycles

Gholamreza Ahmadzadehrishehri, Doctor of Philosophy in Mechanical Engineering, Ryerson University, Toronto, Canada, 2013

Ratcheting deformation is accumulated progressively over three distinct stages in materials undergoing asymmetrical cyclic stresses. The present thesis evaluates the triphasic ratcheting response of materials from two stand points:

(i) Mechanistic approach at which stages of ratcheting progress over stress cycles was related to mechanistic parameters such as stress level, lifespan, mechanical properties and the softening/hardening response of materials. Mechanistic approach formulated in this thesis was employed to assess ratcheting strain over triphasic stages in various steel and copper alloys under uniaxial stress cycles. Good agreements were achieved between the predicted ratcheting strain values based on the proposed formulation and those of experimentally reported.

(ii) Kinematic hardening rule approach at which the hardening rule was characterized by the yield surface translation mechanism and the corresponding plastic modulus calculated based on the consistency condition.

Various cyclic plasticity models were employed to assess ratcheting response of materials under different loading conditions. The Armstrong-Frederick (A-F) hardening rule was taken as the backbone of ratcheting analysis developed in this thesis mainly due to less complexity and number of coefficients in the hardening rule as compared with other earlier developed hardening rules in the literature.

To predict triphasic ratcheting strain over stress cycles, the A-F hardening rule has been further developed by means of new strain rate coefficients γ_2 and δ. These coefficients

improved the hardening rule capability to calibrate and control the rate of ratcheting over its progressive stages. The modified hardening formulation holds the coefficients of the hardening rule to control stress-strain hysteresis loops generated over stress cycles during ratcheting process plus the ratcheting rates over stages I, II, and III. These coefficients were calibrated and defined based on the applied stress levels. The constructed calibration curves were employed to determine strain rate coefficients required to assess ratcheting response of materials under uniaxial loading conditions at various cyclic stress levels. The predicted ratcheting strain values based on the modified hardening rule were found in good agreements with the experimentally obtained ratcheting data over stages I and II under uniaxial loading conditions.

The capability of the modified hardening rule to assess ratcheting deformation of materials under multi-step uniaxial loading spectra was also assessed. Subsequent load steps were considerably affected by previous load steps in multi-step loading conditions. Ratcheting strains for low-high stress steps were successfully predicted by the modified hardening rule. High-low loading sequences however resulted in an overestimated reversed ratcheting strain in the later load steps.

The modified hardening rule proposed in this thesis was then employed to predict the ratcheting strain and its concurrent interaction with fatigue damage over stress cycles in steel alloys. The interaction of ratcheting and fatigue damage was defined based on mechanistic parameters involving the effects of mean stress, stress amplitude, and cyclic softening/hardening response of materials. The extent of ratcheting effect on the overall damage of steel samples was defined by means of the product of the average ratcheting strain rate over the stress cycles and the applied maximum cyclic stress, while fatigue damage was analysed based on earlier developed energy-based models of Xia-Ellyin and Smith-Watson-Topper. Overall damage induced by both ratcheting and fatigue was calibrated through a weighting factor at various ratios of mean stress/cyclic amplitude stress (σ_m/σ_a). The estimated lives based on the proposed algorithm at different mean stresses and stress amplitudes showed good agreements as compared with experiments.

ACKNOWLEDGEMENTS

I would like to express my sincere gratitude to my supervisor Professor A. Varvani-Farahani for his encouragement, advice, and support. He has provided me with guidance, inspiration and motivation, helping me greatly throughout my work on this thesis. He has definitely contributed to the success of this work very much.

Sincere thanks are extended to Dr. H. Haftchenary who morally supported me over the period of this study. I would like to thank Mostafavi's and Bahrani's families for their countless assistance. Thanks also go to Matin Sarchami for helping in banking the ratcheting data.

The Financial supports through Ontario Graduate Scholarship Program (OGS) and Natural Sciences and Engineering Research Council (NSERC) of Canada are greatly appreciated.

I would like to express my deepest indebtedness and thanks to my parents, brother and sisters for their love, and support during the course of my study.

I would like to express my sincerest appreciation for my lovely wife for her patience, inspiration, unconditional support, and love. I undoubtedly owe her greatly for being able to complete my studies and perform this work.

And, thanks to Mighty God for all the blessings he has given me.

تقدیم به مادرم، آن نادرهٔ وجود

و پدرم که، هستیم از اوست

To my beloved mother and father

درخت تو گر بار دانش بگیرد به زیر آوری چرخ نیلوفری را

"ناصر خسرو"

Your fruitful tree of knowledge enables you to dominate the whole universe.

"Nasir Khusraw"

TABLE OF CONTENTS

LIST OF TABLES

LIST OF FIGURES

NOMENCLATURE

f	Yield surface function and mean stress function
$\bar{s}$	Deviatoric stress tensor
$\bar{a}$	Total backstress tensor
σ_y	Yield stress
$d\bar{\varepsilon}$	Total strain increment
$d\bar{\varepsilon}_p$	Plastic strain increment
$d\bar{\varepsilon}_e$	Elastic strain increment
$d\bar{\sigma}$	Stress increment
G	Shear modulus
υ	Poisson's ratio
E	Elastic modulus
$\bar{I}$	Unit tensor
$\bar{\sigma}$	Stress tensor
H_p	Plastic modulus function
$d\bar{s}$	Deviatoric stress increment
$\bar{n}$	Unit exterior normal to the present yield surface at the stress state
C	Material constant in Prager, A-F, Bower and modified hardening rules
$\bar{v}$	Mroz translation vector
$R_{(i+1)}$	Radius of the (i+1) th surface in the Mroz multi-surface type hardening rule
$R_{(i)}$	Radius of the ith surface in the Mroz multi-surface type hardening rule
$\bar{a}_{(i+1)}$	Center of the (i+1) th surface in the Mroz multi-surface type hardening rule
$\bar{a}_{(i)}$	Center of the ith surface in the Mroz multi-surface type hardening rule
$d\bar{a}_{(i)}$	Increment of center of the ith surface in the Mroz multi-surface hardening rule
$\bar{v}'$	Garud translation tensor

$\bar{n}'$	Unit exterior normal to the next yield surface at the stress state
γ	Material constant in the A-F hardening rule
dp	Increment of equivalent plastic strain
$d\bar{a}^{(i)}$	Increment of ith backstress tensor
$C^{(i)}$, $\gamma^{(i)}$	Material constant in Chaboche hardening rule
$\bar{a}^{(i)}$	ith backstress tensor
γ_1	The first feedback rate of the Bower and modified hardening rules
γ_2, δ	Stress level dependent coefficients in the modified hardening rule
$\bar{b}$	Second kinematic variable in the Bower hardening rule
ε_r	Ratcheting strain
N	Number of stress cycles
N_f	Life cycles
$\Delta\sigma$	Stress range
σ_a	Stress amplitude
σ_m	Mean stress
σ_{ult}	Ultimate tensile strength
n	Cyclic strain hardening exponent
K	Cyclic strength coefficient
P, Q, ρ and β	SWT equation constants
b and c	Coffin-Manson equation exponents
ε'_f	Fatigue ductility coefficient
σ'_f	Fatigue strength coefficient
C_m, λ and k_m	Xia-Ellyin equation constants
C_r, χ and k_r	Ratcheting damage equation constants
D	Overall damage
D_r	Ratcheting damage
D_m	Fatigue damage

$D_{\exp}$	Experimentally obtained damage
N_f	Number of cycles to failure
ΔW_p	Plastic energy per cycle
ΔW_e	Elastic energy per cycle
ε_a	Strain amplitude
$\sigma_{\max}$	Maximum tensile stress value during a cycle
$\dot{\varepsilon}^r_{avg}$	Average ratcheting strain rate
ξ	Weighting factor
$\overline{\rho}$	Multiaxial constrain factor

Preface

The following provides a brief description of materials covered in the chapters that follow.

Chapter 1 presents an overview and background for ratcheting assessment and its interaction with fatigue damage of materials. This chapter highlights the objectives and scope of the research work.

Chapter 2 discusses ratcheting deformation mechanism and classifies various ratcheting types. This chapter also examines the capability of linear, multi-surface and non-linear hardening rules to address the stress-strain response of materials undergoing uniaxial and multiaxial strain- and stress-controlled loading conditions. Cyclic plasticity models of Prager, Garud, A-F, Chaboche and Bower were reviewed in detail.

Chapter 3 develops the mechanistic formulation to assess triphasic ratcheting response of materials over stress cycles. The ratcheting formulation was defined based on mechanistic parameters involving stress level and material properties. Effects of mean stress, stress amplitude and cyclic softening/hardening response of materials were included to define and calibrate the mechanistic equation. This chapter further modifies the A-F kinematic hardening rule to assess the ratcheting response of materials. The modified hardening rule including stress level and material dependent coefficients is introduced to address ratcheting strain over larger domain of stress cycles. This chapter also presents the formulations to interact material damages induced due to concurrent ratcheting and fatigue phenomena. The algorithm for component life prediction has been detailed in this chapter.

Chapter 4 verifies (i) the mechanistic equation developed to assess triphasic ratcheting response, (ii) the modified hardening rule and (iii) concurrent ratcheting-fatigue damage assessment introduced in the previous chapter. Ratcheting data extracted from the literature for

steel and copper samples tested under uniaxial stress cycles were employed to assess both mechanistic ratcheting equation and the modified hardening rule developed in chapter 3. Newly developed ratcheting strain rate coefficients were calibrated based on variations of mean stress and stress amplitude in this chapter. Constructed family curves enabled an easy estimation of these coefficients at any given stress levels through interpolation. The modified hardening rule to assess ratcheting response of four steel alloys under various multi-step loading histories with different loading sequences was further evaluated. In this chapter, concurrent interaction of ratcheting and fatigue damage for two steel alloys of 42CrMo and 1020 experiencing uniaxial stress cycles was investigated.

Chapter 5 discusses the outcomes of ratcheting analysis based on the mechanistic and the hardening rule approaches developed in this thesis. The modified hardening rule and its capability to assess ratcheting response of materials for single- and multi-step loading sequences were discussed. This chapter also confers the effect of concurrent interaction of ratcheting-fatigue damage in the life of components.

Chapter 6 summarizes the conclusions obtained from this study and presents future recommendations.

Appendix A tabulates experimental data employed in chapter 2 to evaluate stress-strain as well as ratcheting responses of steel alloys under various loading conditions. This appendix also lists material properties and constants for plasticity models required to predict stress-strain response of materials. Hysteresis loops obtained based on different hardening rules is also presented in this appendix.

Appendix B consists of tables of ratcheting experimental strain values employed in chapter 4.

Appendix C presents MATLAB program listings to assess ratcheting response based on the mechanistic approach and the modified hardening rule with related subroutines.

CHAPTER ONE

INTRODUCTION

1.1. Overview and background

Prevention of fatigue failure is an essential aspect of design for many engineering components and structures in service which are subjected to repeated loading. Fatigue damage occurs on the microscopic scale and progressive localized deformation takes place under cyclic loading conditions. Many machines, vehicles and structural components experience cyclic loads with mean stress in both low-cycle fatigue (LCF) and high-cycle fatigue (HCF) regimes. Material response in HCF regime is mainly elastic and tensile mean stress causes an increase in crack opening and accelerates fatigue damage accumulation. However, in the LCF regime, the elastic-plastic response of materials results in fatigue damage progress associated with irreversible plastic deformation. Ratcheting phenomenon occurs in materials subjected to cyclic stress-controlled loading conditions with mean stress when the applied cyclic stress stays larger than the yield strength of the material resulting in progressive plastic deformation. Ratcheting deformation induced due to the asymmetric stress cycles can integrate with fatigue damage leading to the catastrophic failure of components.

Unlike existing hardening rules that have tried to characterize ratcheting behaviour over a relatively small number of cycles, the present research aims to further modify A-F kinematic hardening rule enabling ratcheting assessment of materials for longer number of stress cycles whereas the framework of the modified hardening rule involves less complication and a limited number of coefficients.

A ratcheting-fatigue damage assessment algorithm was developed to interact the involvement of both ratcheting deformation and fatigue damage concurrently experienced by

materials over stress cycles. The present thesis developed a model for material ratcheting response over stress cycles enabling engineers to design reliable load-bearing as well as safe and risk-free manufactured components. To realistically predict life of cyclically loaded material, the interaction of ratcheting deformation and fatigue damage stays as one of main outcomes of this research.

1.2. Objective and scope

This research aims to investigate on the ratcheting behaviour and fatigue failure and their interaction for different materials under asymmetrical cyclic stressing and to develop a unique yet simple method for the evaluation of ratcheting strain and life prediction of materials under uniaxial stress-controlled loading conditions. The first objective of this work is to evaluate cyclic stress-strain hysteresis loops of materials under strain-controlled condition based on linear, multi-surface and non-linear hardening rules under various uniaxial loading conditions. These plasticity models are within the framework of unchanged yield surface shape and yield surface translation and are limited to room temperature testing condition.

This research is to further assess ratcheting deformation over triphasic stages of lifespan by means of mechanistic parameters. Linear and nonlinear functions as a combined formulation include terms of amplitude stress, mean stress, mechanical properties, lifespan and stress cycle. In addition to these terms, the effect of softening/hardening response of material was taken into account to characterize triphasic ratcheting deformation in various materials over life cycles.

The A-F hardening rule is chosen as the backbone formulation to modify the kinematic hardening rule capable of analysing triphasic ratcheting response of materials. The modified hardening rule encountered the influence of stress levels over stages by means of γ_2 and δ coefficients. The modified hardening rule was evaluated to assess ratcheting response of materials under various single- and multi-step loading spectra. Modifications on the hardening rule by direct means of such calibrating coefficients are relatively novel in open literature for classical hardening rules.

The ultimate objective of this research work is to investigate the interaction of damages induced by both ratcheting and fatigue phenomena over stress cycles and quantitatively evaluate

the extent of ratcheting and fatigue damage contributions in the life of components. Fatigue damage values are calculated based on Smith-Watson-Topper (SWT) and Xia-Kujawski-Ellyin energy-based models and the corresponding predicted ratcheting values are respectively defined as upper and lower curves. The upper curve presents the pure fatigue damage and the lower curve represents ratcheting damage. The components experiencing asymmetric loading conditions fall between these boundaries. The predicted overall damage values are compared with the experimentally values obtained under uniaxial loading conditions.

CHAPTER TWO

LITERATURE SURVEY: CYCLIC PLASTICITY AND HARDENING RULES

2.1. Introduction

Many engineering components and structures in service are continuously subjected to multiaxial stress cycles at which the plastic deformation results in a severe damage of components/structures and catastrophic failures. Such examples include airplane landing gears, structures operating in offshore and earthquake zones, pressure vessels, and nuclear reactors. The elastic-plastic deformation and cyclic response of these structures become of a prime step for a reliable design of heavily loaded components and structures when the cyclic stress level exceeds the yield limit.

Over stress cycles, metallic materials may harden or soften in the first 100-200 cycles until a stabilized hysteresis loop is achieved. Prager linear kinematic hardening model [1] was first developed to translate yield surface in the stress space over loading and unloading exceeding the elastic limit while shape and size of surface stayed unchanged. To analyse the behaviour of materials subjected to complex cyclic strain-controlled loading histories, Mróz [2] proposed multi-surface hardening rule based on the concept of field of work-hardening moduli. The multi-surface model was employed by several researchers to characterize materials plasticity under various loading conditions. To simplify Mróz multi-surface hardening rule and to address consistency condition some researchers introduced two- and three-surface models [3-7]. Modifications on the multi-surface hardening rule proposed by Garud [8-9] resolved inconsistency problem and surfaces intersection involved in Mróz model. In spite of close agreement results with experimental data provided by Mróz and Garud multi-surface models in strain-controlled loading conditions, this class of hardening rule is yet to describe ratcheting

strain behaviour of materials under uniaxial and proportional stress-controlled loading conditions [10-12].

2.2. A-F type hardening models and ratcheting assessment

Armstrong-Frederick [13] further developed Prager's hardening rule by introducing a nonlinear term (referred as recall term). Under uniaxial loading conditions and at the presence of mean stress, this nonlinear term resulted in open hysteresis loops and accumulated plastic strains in direction of the applied load. Analytical solution of A-F hardening rule simplified identification of the model and nonlinear relationship between evolution of backstress and plastic strain increments. A-F model also addressed Bauschinger's effect however it overestimated ratcheting strain over stress cycles [14]. To overcome this shortcoming, A-F nonlinear hardening rule has been modified, generalized and widely used in many constitutive models to characterize ratcheting behaviour of the materials subjected to various loading conditions. A constitutive model has been introduced by Chaboche [15] in the form of superposition of the series of decomposed A-F nonlinear hardening rules. In this model the variables acted independently to improve description of ratcheting strain. Chaboche [16] further improved the capability of A-F rule in predicting ratcheting strain by introducing a dynamic recovery term in the form of a power function and a threshold. Ohno and Wang [17-18] proposed the model with critical state of dynamic recovery containing a power law nonlinearity in the second term of the hardening rule to increase the effect of dynamic recovery. In uniaxial loading cases, ratcheting prediction by Ohno-Wang model showed close agreement with the experimental results [11, 19]. Jiang-Sehitoglu [20, 21] and McDowell [22] modified exponents of Ohno-Wang model to improve the ability of simulation of multiaxial ratcheting strain. To achieve better correlation between the predicted ratcheting strain values and the experimental results in various cyclic loading conditions over an extended domain of stress cycles, further improvement of Chaboche model to simulate ratcheting strain was presented by Bari and Hassan [23] using the ideas of Delobelle et al. [24] and Burlet and Cailletaud [25]. Modifications on A-F hardening rule through these models [11, 15, 17-21] resulted in better predictions. They were however limited due to their complexity in ratcheting analysis, several number of constants and the limited coverage of stress cycles undergoing ratcheting phenomenon.

Bower [26, 27] modified A-F rule by introducing the second kinematic variable to decrease the A-F constant ratcheting strain rate as the number of stress cycles advanced. Bower's model addressed ratcheting assessment of materials with a relatively higher number of stress cycles before ratcheting arrest as compared with other earlier modified A-F rules. This model due to its less number of coefficients and a uniform knee transition beyond the initial stage of ratcheting is considered as a potential model for further development.

2.2.1. Mechanism of Ratcheting Deformation

To realistically address the ratcheting response of materials, the ratcheting deformation mechanism was distinctly defined over stages of lifespan. In a material undergoing asymmetrical cyclic stresses, ratcheting strain is accumulated progressively in three stages. Triphasic trend of cyclic plastic strain accumulation in materials has been earlier reported [28-38]. This deformation mechanism is associated with plastic slip, dislocation movement and cell formations [28, 36, 38,39]. Ratcheting strain accumulation begins quickly in stage I and as the number of cycles advances the rate of ratcheting decreases gradually due to reduction of the number of active dislocations. The ratcheting rate reduction continues till rate of accumulation of strain becomes stabilized. Secondary region commences with steady-state ratcheting rate. In this stage gradual stabilization of dislocations takes place as cycling continues and 80%-90% of materials life cycles are spent in this stage [38, 40]. The later stage of ratcheting process is typified as ratcheting strain rate increases. Deformation at this stage is related to the formation of dislocation cells as the number of cycles increases. The ratcheting accelerates uncontrollably in successive cycles during stage III resulting in the cross sectional area reduction. This increases maximum true stress, leading to necking and ductile fracture in materials [28, 36, 38, 39].

2.2.2. Ratcheting Deformation and Types

Based on experimental observations, uniaxial ratcheting strain process can be divided into three types I, II and III as depicted in figure 2.1. For type I of ratcheting , at the beginning of cyclic stressing, ratcheting strain evolves with higher rate and then decreases gradually till ratcheting is arrested and shakedown takes place. In some cases, shakedown in ratcheting deformation occurs while the influence of the low cycle fatigue under cyclic stressing is significant. Therefore, fatigue damage in material under stress cycling accelerates and results in

failure in subsequent cyclic stage. Ratcheting is defined as type II when the ratcheting strain rate begins quickly in stage I and as the number of cycles advances in stage II, strain deformation accumulates in a constant rate. Ratcheting strain increases gradually till specimen failed in subsequent cyclic period. Type III of ratcheting is defined for those cases which ratcheting strain rate declines quickly to a certain value and then goes up rapidly leading specimen to failure. The present research will mainly focus on type I ratcheting where shakedown and fatigue are interacted [41].

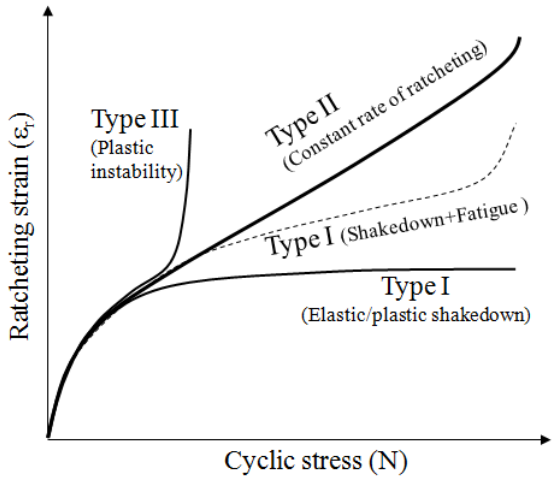

Figure 2.1 Various types of ratcheting of metallic materials [41]

In this chapter, linear, non-linear and multi-surface hardening rules to assess cyclic plasticity and ratcheting response of steel alloys over stress cycles were examined. Hardening rules were first employed to quantitatively evaluate the stabilized stress-strain hysteresis of 1045 steel alloy experiencing 90° out-of-phase straining condition. Prager, Garud, A-F and Bower model were employed to assess ratcheting responses of various steel alloys of 42CrMo, SS304, SS316L and rail steel under uniaxial loading condition. The same hardening rules were then employed to evaluate ratcheting response of 1070 steel alloy over stress cycles. Experimentally obtained values of ratcheting strain over stages I/II stress cycles were found in good agreements with those predicted based on Bower model.

2.3. Constitutive models and formulations

Of several developed cyclic plasticity models, this chapter mainly addresses five classic approaches of linear hardening (Prager [1]), nonlinear kinematic (A-F [13]), multi-surface (Garud [8]), decomposed nonlinear kinematic (Chaboche [15]) and nonlinear kinematic with second kinematic variable (Bower [26]). These hardening rules are classified into three categories of linear, multi-surface and non-linear kinematic hardening rules.

2.3.1. Linear hardening rule

Unlike the isotropic hardening, the kinematic hardening rule describes stress-strain response of materials under cyclic loading realistically and it takes into account of Bauschinger's effect and material memory due to plastic deformation. The first kinematic hardening rule has been introduced by Prager [1] in which the yield surface is linearly translated in the stress space without changes in size and shape of yield surfaces during plastic deformation:

$$d\bar{a} = Cd\bar{\varepsilon}_p \tag{2.1}$$

where C is a material constant which is found from the slope of the uniaxial stress-strain curve [11, 19]. Based on the linear hardening rule, if the shape of yield surface stays unchanged the value of plastic modulus will be identical with the value of constant C.

2.3.2. Multi-surface hardening rule

Mróz introduced concept of the field of work-hardening moduli to improve linear kinematic hardening rule and predict the responses of stress for multiaxial strain-controlled loading. This concept is a generalization of the uniaxial stress-strain curve and instead of using one point as a border of elastic and plastic region, cyclic uniaxial stress-strain curve is divided into a number of segments each having constant plastic modulus. Von Mises yield criterion is used to describe plastic surfaces as field of plastic moduli. The first surface is the yield surface and the other surfaces represent plastic modulus functions. Mróz proposed that translation direction of a yield surface is dependent on the vector joining the current state of stress P on the

i^{th} surface with the state of stress P' on the $(i+1)^{th}$ surface at which two surfaces have a common exterior normal $\bar{n}$ as shown in figure 2.2 [11, 42, 43].

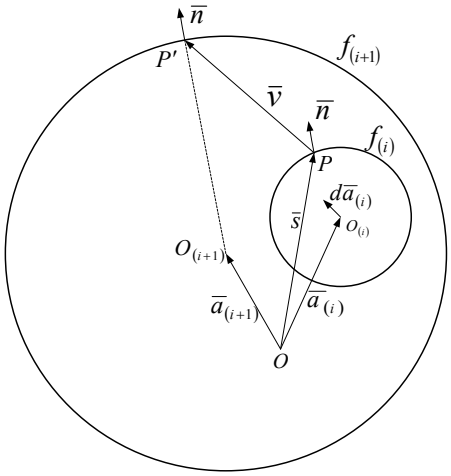

Figure 2.2 Mróz hardening rule and surface translation illustration

Vector $\bar{v}$ is expressed as:

$$\bar{v} = (R_{(i+1)} - R_{(i)})\bar{n} + \bar{a}_{(i+1)} - \bar{a}_{(i)} \tag{2.2}$$

where $\bar{a}_{(i+1)}$ and $\bar{a}_{(i)}$ are the translation vectors for the center points and $R_{(i+1)}$ and $R_{(i)}$ represent radii of $(i+1)^{th}$ and $(i)^{th}$ surfaces, respectively. Translation of i^{th} center of surface based on Mróz model is determined by:

$$d\bar{a}_{(i)} = \frac{d\bar{s} \cdot \bar{n}}{\bar{v} \cdot \bar{n}} \bar{v} \tag{2.3}$$

Garud [8, 9, 11] found that yield surface translation in Mróz hardening rule is not dependent on the stress increment and it causes inconsistency in the finite stress increment calculation. To solve consistency problem, Garud proposed a modified hardening rule that surface translation direction is related to stress increment vector. As figure 2.3 illustrates, due to stress increment if point P on the i^{th} yield surface translates to the point P' on the $(i+1)^{th}$ surface, then two surfaces are tangential. Translation direction of i^{th} surface is presented by vector joining O_i to O'_i and the magnitude of translation is determined by consistency condition.

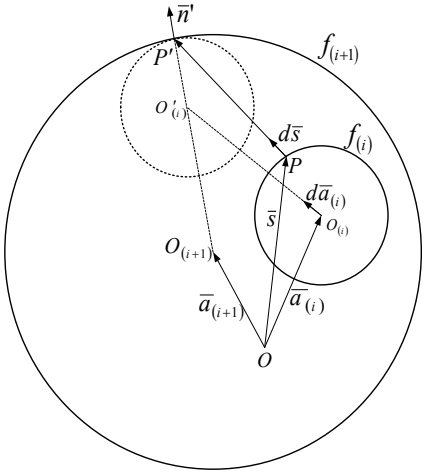

Figure 2.3 Garud hardening rule and surface translation illustration

Unit normal $\bar{n}'$ at point P' is evaluated by determining of point P' on the $(i+1)^{\text{th}}$ surface. Vector joining point P to P' is expressed as:

$$\bar{v}' = (R_{(i+1)} - R_{(i)})\bar{n}' + \bar{a}_{(i+1)} - \bar{a}_{(i)} \tag{2.4}$$

The Garud hardening rule incorporating the new tensor is defined as:

$$d\bar{a}_{(i)} = \frac{d\bar{s} \cdot \bar{n}'}{\bar{v}' \cdot \bar{n}'} \bar{v}' \tag{2.5}$$

The only difference between the Garud and the Mróz models is that the translation direction in Mróz hardening rule is calculated by normal vector of current state of stress while in the modified rule of Garud, the translation direction is determined by the normal vector of stress increment [11, 42, 43].

2.3.3. Nonlinear kinematic hardening rule

Armstrong-Frederick modified Prager linear hardening model by adding a non-linear term as:

$$d\bar{a} = Cd\bar{\varepsilon}_p - \gamma \bar{a} dp \tag{2.6}$$

The first term of Equation (2.6) includes the plastic strain rate (tensor) and the second term accounts for the plastic strain rate modulus (scalar). Terms C and γ are material constants and are

determined from the uniaxial stress-strain hysteresis loop under strain-controlled condition. The second term in Equation (2.6) is called recall or dynamic recovery term and dp is defined as the equivalent plastic strain increment. Under uniaxial loading conditions with non-zero mean stress, this nonlinear term resulted in open hysteresis loops and accumulated plastic strains in direction of the applied load. Constants C and γ are employed to determine plastic modulus in forward and reversed loading. In uniaxial loading condition, plastic modulus is defined based on $H_p = C \pm \gamma\bar{a}$ at which (-) sign corresponds to the forward loading and (+) sign corresponds to reversed loading. Figure 2.4 presents the schematic progress of open stress-strain hysteresis loops for forward and reversed loading [11, 14, 19].

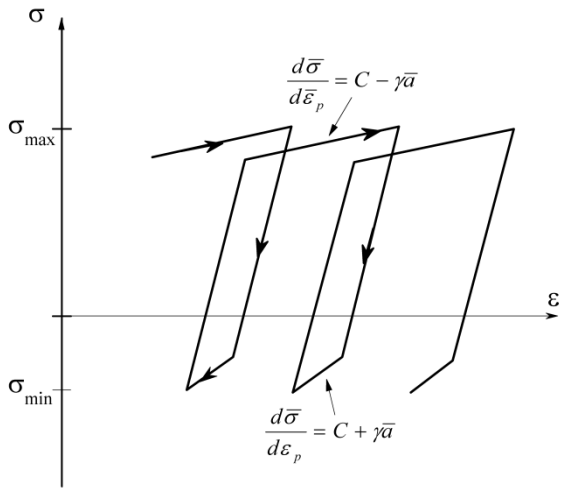

Figure 2.4 Schematic hysteresis loops with different slopes in forward and reversed loading based on A-F hardening rule.

A-F model also addresses Bauschinger's effect however it overestimates ratcheting strain over stress cycles [14]. To overcome this shortcoming, Chaboche et al. [15] extended A-F hardening rule by decomposing hardening rule $d\bar{a}$ to several parts M in the form of:

$$d\bar{a} = \sum_{i=1}^{M} d\bar{a}^{(i)} \tag{2.7}$$

Each of the backstress parts of $d\bar{a}^{(i)}$ works independently and is defined as:

$$d\bar{a}^{(i)} = C^{(i)} d\bar{\varepsilon}_p - \gamma^{(i)}\bar{a}^{(i)} dp \qquad (i = 1,2,...,M) \tag{2.8}$$

A-F hardening rule was further modified by Bower [26] as he introduced a second kinematic variable and the evolution of backstress was defined based on plastic strains as:

$$d\bar{a} = Cd\bar{\varepsilon}_p - \gamma_1(\bar{a} - \bar{b})dp \tag{2.9}$$

and

$$d\bar{b} = \gamma_2(\bar{a} - \bar{b})dp \tag{2.10}$$

where C, γ_1 and γ_2 are material constants. Equations (2.9) and (2.10) hold 3 independent material constants as well as the initial material yield stress. The size of the stress-strain hysteresis loop is controlled by material constants *C* and the first feedback rate γ_1. Magnitude of the second feedback rate, γ_2, determines the ratcheting rate. The tensor $\bar{b}$ has been introduced as an additional kinematic variable with the initial value of zero. Equation (2.10) controls the movement of $\bar{b}$ that follows $\bar{a}$ with 'exponential lag' during cyclic loading. Gradual decreasing in the rate of mean value of $(\bar{a} - \bar{b})$ is defined by second feedback rate of γ_2 over stress cycles [11, 26]. When γ_2=0, the model predicts constant ratcheting rate and reduces to A-F nonlinear kinematic hardening rule and by setting γ_2=γ_1=0 the hardening rule converts to the simple linear kinematic hardening.

The hardening rules have been categorized by their yield surface translation mechanism and their corresponding plastic modulus. Prager and A-F models are referred as coupled models as these models define the magnitude and direction of yield surface translation and then plastic modulus H_p is calculated using the consistency condition while Mróz and Garud models initially determine the plastic modulus and the yield surface translation direction and then consistency condition is enforced to obtain the magnitude of the surface translation. In this class, plastic modulus calculation is not coupled with its kinematic hardening rule through the yield surface consistency condition.

2.4. Comparison of the hardening rules

To evaluate cyclic stress-strain and ratcheting response of materials based on various kinematic hardening models under strain- and stress-controlled conditions, experimental data of steel alloys were extracted from literature [11, 26, 29-30, 34-35, 44-45].

2.4.1. Non-proportional strain-controlled condition

1045 steel samples were tested under strain-controlled 90° out-of-phase condition at frequency range of 0.1 to 3 Hz. The tests were conducted at the different axial and torsional strain levels. These tests were carried out with a sinusoidal waveform at room temperature [46]. Cyclic stress-strain response of 1045 steel subjected to 90° out-of-phase strain-controlled axial-torsion loading condition were examined and compared with experimental results. These tests were conducted with a sinusoidal waveform with an axial strain amplitude 0.192% and shear strain amplitude 0.187%. [11].

Figure 2.5 presents experimental data of axial stress versus shear stress for a 1045 steel sample tested under 90° out-of-phase cyclic straining condition. This figure also shows how closely the experimental data agree with the predicted curves based on different kinematic hardening rules. The hardening rules constants required to predict curves in figure 2.5 are listed in Table A.2.

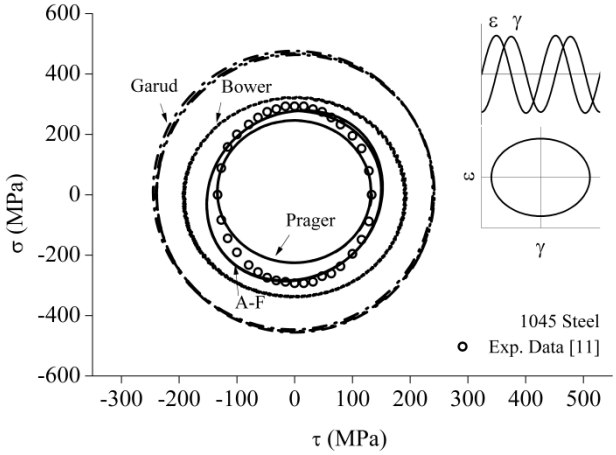

Figure 2.5 Predicted axial and shear stress values based on various hardening rules compared with experimental data [11]

A-F nonlinear kinematic hardening was found to closely agree with the experimental results in this figure. Figure 2.6 presents the stabilized axial and the shear stress-strain hysteresis loops based on the Prager, Garud, A-F and Bower hardening rules under a 90° out-of-phase cyclic strain-controlled condition.

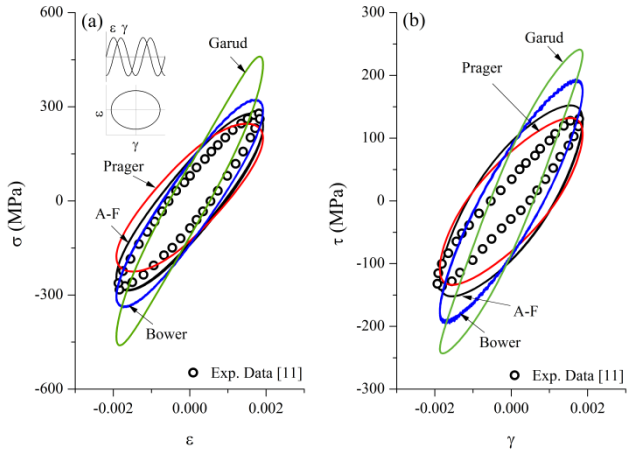

Figure 2.6 Stabilized stress-strain hysteresis loops: a) axial and b) shear hysteresis loops of A-F, Prager, Bower and Garud models under a 90° out-of-phase cyclic strain-controlled for 1045 steel

Figure 2.6 shows that at the constant range of straining, the axial stress range is twice the shear stress range. The linear hardening rule of Prager underestimated the magnitudes of both axial and shear stresses. The predicted hysteresis loop based on A-F model closely agreed with the experimentally obtained stress-strain data for 1045 steel under a 90° out-of-phase strain-controlled condition as compared with other hardening rules. Prager hardening rule underestimated both the axial and shear hysteresis loops. Axial and shear hysteresis loops generated based on Garud model resulted in an extra hardening and largely overestimated the experimental data as compared with other rules. Bower model predicted the axial stress-strain loop more closely than the shear stress-strain loop of figure 2.6b.

2.4.2. Uniaxial stress-controlled condition

Experimental ratcheting strain values of 42CrMo, SS304, SS316L and rail steel alloys over uniaxial stress cycles were evaluated based on Prager, Garud, A-F and Bower hardening rules. 42CrMo, SS304, and SS316L steel specimens were tested under uniaxial cyclic stressing rate of 500, 400, and 250 MPa/s respectively [29-30, 45] and rail steel specimen was tested under uniaxial load-controlled condition with axial load rate of 3.33 KN/s [26].

Prager, A-F and Bower material constants required to assess ratcheting strain over stages I/II stress cycles for four different steel alloys were presented in Table A.5 in appendix A. Predicted ratcheting strain curves based on Prager, Garud, A-F and Bower models for 42CrMo, SS304, SS316L and rail steel alloys at different stress levels are presented in figure 2.7.

The relationship between ratcheting strain and number of stress cycles would be a practical index to evaluate the ability of hardening rules in predicting the ratcheting strain. The ratcheting strain is obtained by taking the average of maximum and minimum values of strain in a hysteresis loop. Figure 2.7 presents ratcheting response of 42CrMo, SS304, SS316L and rail steels evaluated based on Prager, Garud, A-F and Bower models. A-F highly overestimated ratcheting data and both Garud and Prager underestimated the experimental ratcheting strain values under uniaxial stress cycles. Over first few cycles Bower predicted a constant ratcheting rate, as the number of cycles advanced its ratcheting rate decreased and eventually arrested. Employing second kinematic variable, $\overline{b}$, and feedback rate γ_2 in Equation (2.9) and (2.10) enabled Bower's model to control the ratcheting rate decay over stress cycles however after a number of cycles the predicted ratcheting was arrested. Ratcheting strains of 42CrMo, SS304, SS316L and rail steel alloys under uniaxial stress cycles were found in good agreements with those predicted based on Bower over stages I/II of ratcheting curve. Figures 2.7a-2.7b and 2.7c-2.7d respectively show ratcheting strain of 42CrMo and SS304 steels in two different stress amplitudes while the mean stress was kept constant. Better correlation is observed by Bower's model in smaller cyclic stress amplitudes. In 42CrMo steel, predicted ratcheting strain in early stage of cyclic stressing was found in good agreement with the experimental data. For SS304 and SS316L (figures 2.7c-2.7d and 2.7e-2.7f), Bower model initially well predicted ratcheting strain rate at the stage I, then ratcheting strain was overestimated when stress cycles exceeded this stage. Over larger number of stress cycles (stage II) where ratcheting strain builds up with a constant rate, Bower's model simulated ratcheting response in good agreement with the experimental data. Based on hardening rule of Bower, the motion of hysteresis loops over stress cycles resulted in the change of ratcheting strain rate while ratcheting strain over stress cycles accumulated with a constant rate when assessed by A-F hardening rule. Both Prager and Garud models however generated closed hysteresis loops and lacked to address ratcheting response of materials. Bower's hardening rule successfully predicted ratcheting strain of steel alloys over

uniaxial stress cycles within stages I/II. Beyond these stages, hardening rule of Bower tends to arrest the ratcheting and shakedown occurs.

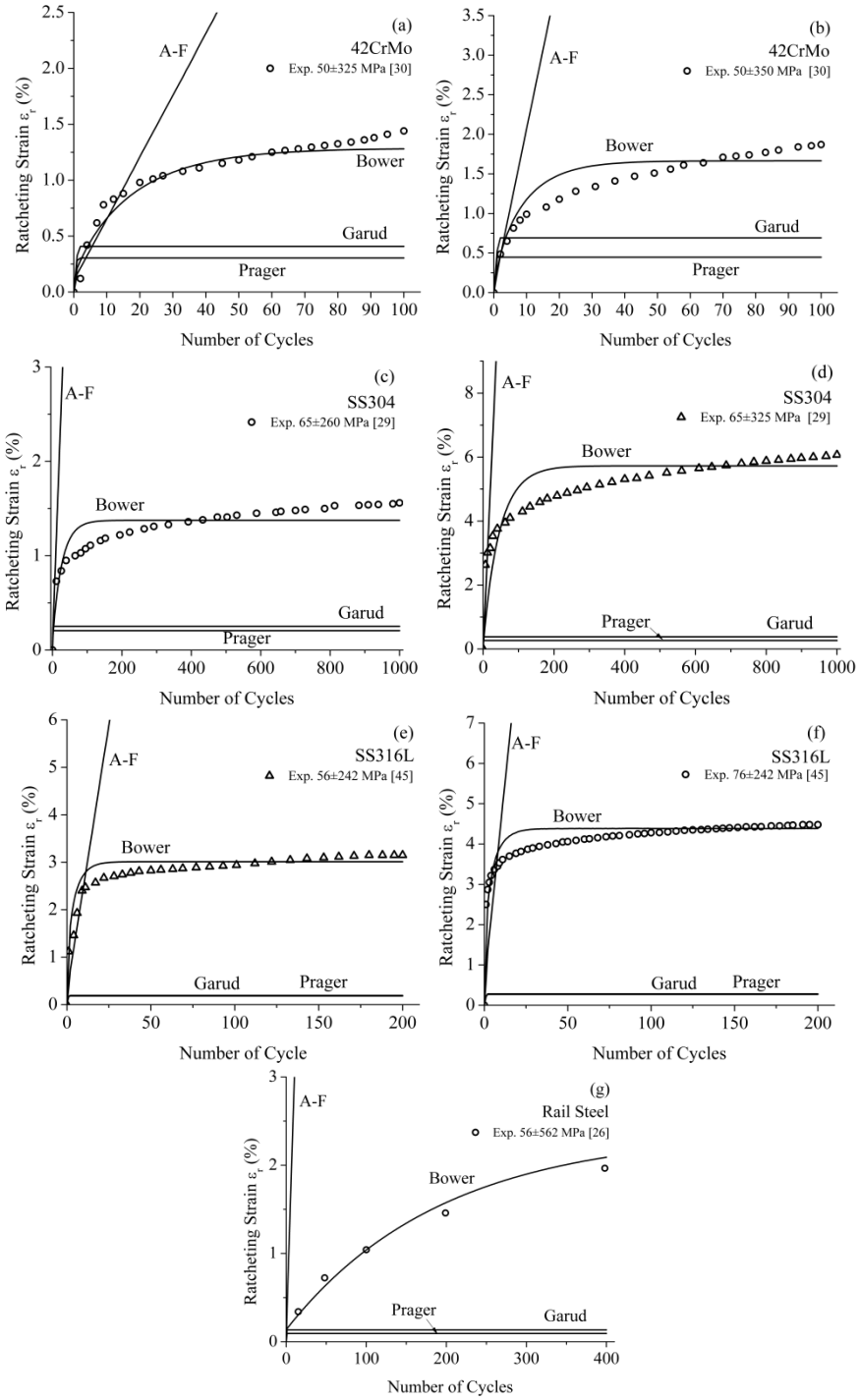

Figure 2.7 Experimental and predicted ratcheting strain values over stress cycles within stages I/II based on Prager, Garud, A-F and Bower hardening rules for different steels: (a and b) 42CrMo, (c and d) SS304, (e and f) SS316L, and (g) Rail steel

2.4.3. Non-proportional stress-controlled condition

Ratcheting response of 1070 Steel alloy tested under a 90° out-of-phase stress cycles were evaluated based on various hardening rules. The ratcheting strain values were reported extensively in reference [11]. Non-proportional cyclic stressing test with 90° phase difference was carried out. This test was performed at a frequency of 0.5 Hz. The Test was conducted under axial stress amplitude of 222 MPa with a mean stress value of 222 MPa in the presence of the shear stress amplitude of 224 MPa. Hardening rules constants required to assess ratcheting of 1070 steel are listed in Table A.7 reported in appendix A.

The predicted ratcheting strain values based on hardening rules over the first 16 cycles are presented in figure 2.8. Figure 2.8f also presents experimental ratcheting data for 1070 steel. Figures 2.8e and 2.8f show a close agreement of Bower ratcheting strain prediction with those of obtained experimentally.

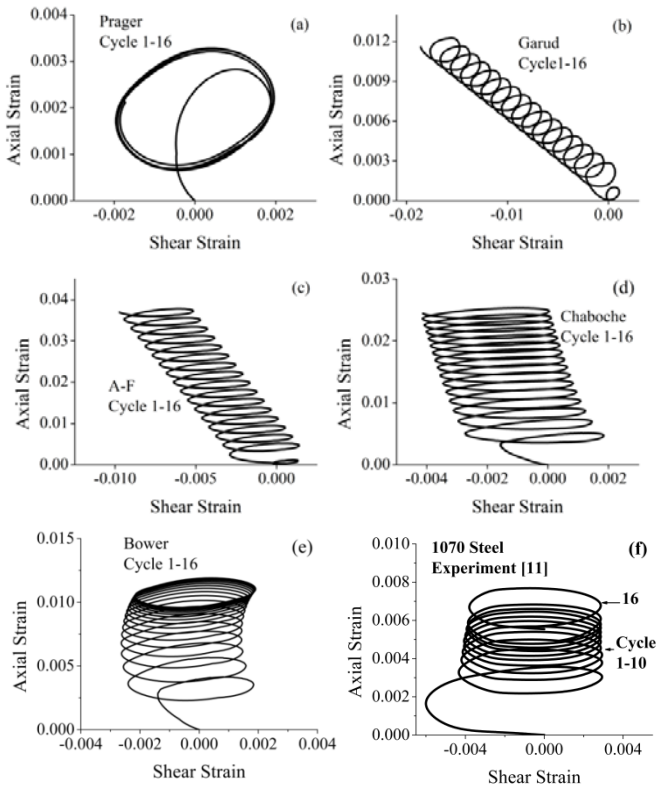

Figure 2.8 Ratcheting strain over first 16 stress cycles: a) Prager, b) Garud, c) A-F, d) Chaboche, e) Bower models as compare with f) experimental data over elliptical loading path

Figure 2.9 presents the predicted axial ratcheting strains for the first 100 cycles based on various hardening models. The predicted ratcheting strain curve based on Bower's model shows a relatively better agreement with the experimental data as compared with other hardening rules in this figure.

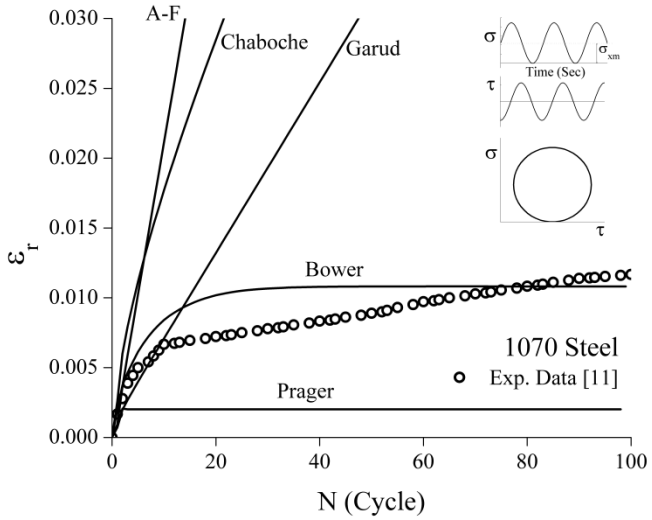

Figure 2.9 Ratcheting strain vs. stress cycles in 1070 steel: predicted based on various hardening rules

In Prager linear hardening rule, translation of yield surface is proportional to plastic strain increments through material constant C which corresponds to the slope of uniaxial stress-plastic strain curve. Material constants C and γ in A-F nonlinear hardening rule were determined using uniaxial stress-plastic strain curve under strain-controlled condition. The material constants C and γ_1 in Bower hardening rule were obtained from the unsymmetrical uniaxial stress-strain hysteresis loops. The hardening coefficient C was selected to coincide with the size of measured stress-strain loops and two feedback rates γ_1 and γ_2 were found trough iteration to achieve correct values of accumulated strain in two arbitrary cycles. The second feedback rate γ_2 was found dependent on material properties, mean stress and stress amplitude. The rate of ratcheting, motion of hysteresis loops over stress cycles, the shape and size of loops and their consistency are crucial variables to control constants C, γ_1 and γ_2. Constant values in this hardening rule were defined to retain the consistency condition.

Ratcheting response of 1070 Steel alloy tested under a 90° out-of-phase stress cycles were evaluated based on various hardening rules. The results showed that the Prager linear hardening rule was unable to model ratcheting strain and this model produced a closed hysteresis loop

within asymmetric cyclic stress loading. Prager linear kinematic hardening model predicted ratcheting at the beginning of cyclic loading and shortly after the ratcheting was stabilized (shakedown occurred). Garud hardening rule predicted a closed loop under proportional loading while under non-proportional loading, Garud overestimated the strain ratcheting. Garud and A-F hardening rules demonstrated constant ratcheting rate under 90° out-of-phase condition while the experimental data showed that ratcheting rate decreases continuously as stress cycles advanced. Unlike these two models, Chaboche hardening rule showed a slight decrease in ratcheting rate over stress cycles. Despite implementing the nonlinear terms (recall term), A-F model overestimated the ratcheting rate. The predicted ratcheting rates based on Garud and A-F models were found larger than those experimentally reported. Under non-proportional loading, Garud predicted ratcheting strains within first few cycles and then overestimated largely ratcheting data while predicted ratcheting curve based on Prager fell below ratcheting data. Hardening rule of Bower predicted ratcheting strains well agreed with the experimental data.

2.5. Summary

Several kinematic hardening rules under strain- and stress-controlled conditions were studied. The Prager linear hardening rule underestimated both stress-strain hysteresis loops and ratcheting strain respectively under the strain- and stress-controlled conditions. Garud multi-surface model estimated the ratcheting strain under non-proportional stress-controlled conditions during very early stage of stress cycles. Under the strain-controlled condition however Garud model resulted in a higher non-proportionality effect than the other models. Under stress-controlled condition, ratcheting response was predicted by A-F hardening rule while the constant ratcheting strain rate caused large deviation from the experimental results. Chaboche model predicted ratcheting strain with slight decay at the first few stress cycles. Bower's model extended A-F hardening rule to describe plastic strain through an internal state variable and the model was found to well predict ratcheting strain of materials. Implementing second kinematic variable in Bower's hardening rule resulted in ratcheting rate decay. Bower's model was found capable of predicting ratcheting strain for larger number of stress cycles within stages I/II as compared with Prager, Garud and A-F models. Hardening rule of Bower offered a simple hardening rule to assess ratcheting response of materials resulting in an arrest in ratcheting beyond stages I/II stress cycles.

CHAPTER THREE

RATCHETING-FATIGUE MODELING

3.1. Introduction

Many engineering components and structures in service experience progressive accumulation of deformation known as ratcheting when they are subjected to cyclic loading, which can result in failure. In this case ratcheting strain evolves over stress cycles experiencing plastic deformation [47]. Cyclic plasticity deals with ratcheting phenomenon and many researchers have experimentally and theoretically studied the elastic-plastic response of various materials undergoing different cyclic loading spectra [40, 48-50]. Uniaxial and multiaxial ratcheting has been investigated in the last three decades leading to develop many constitutive models to characterize ratcheting responses. Some renowned works include of Bower [26] Chaboche [7,16], Guionnet [51] Hassan et al. [47, 52-53] Bari and Hassan [19, 23, 54] Jiang and Sehiyoglu [20-21] Ohno and Wang [17-18] and Chen et al. [55-56]. These researchers however concentrated mainly on the ratcheting behaviour and its constitutive models where the number of applied cycles was relatively small and the ratcheting-fatigue damage interaction was not concurrently evaluated. Several researchers [29, 57-59] have reported that ratcheting strain produced in the asymmetrically cyclic stressing resulted in extra fatigue damage and shortened fatigue life. The effect of mean stress with/without ratcheting strain on fatigue life on ASTM A-516 Gr. 70 was investigated by Xia et al. [57] and verified that the ratcheting strain contributes to the acceleration of the fatigue damage process. It is well-documented that the ratcheting phenomenon depends on several factors including mean stress, stress amplitude, loading history, loading frequency, microstructural characteristics, and cyclic hardening/softening of the materials [15, 30-31, 47, 57]. The effects of mean stress, stress amplitude and stress ratio on the ratcheting-fatigue interaction of SS304, 42CrMo and Al-6061-T6 alloys were investigated at

various loading conditions [29-30, 60]. Kwofi and Chandler [61] and Liu et al. [59] have developed stress-based fatigue failure models while the effect of mean stress was taken into account. Kwofi-Chandler's approach however is limited in application due to its numerous empirical constants. A fatigue-ratcheting damage model was developed by Jiang and Sehitoglu [62] for the prediction of the rolling contact failures by means of their proposed ratcheting model [20-21]. Gao and Chen [63] modified Coffin-Manson equation to take the effect of ratcheting into account on torsional fatigue life of the lead-free solder joints.

It is well-documented that cyclic hardening causes to decelerate the rate of ratcheting. In contrary, increase in the rate of ratcheting is expected in a material with a cyclic softening response [47]. Based on experimental results in [47], in materials with softening characteristics, higher mean stress and higher stress amplitude result in an increase in rate of ratcheting. The higher mean stress values also cause expansion of the hysteresis loop area over stress cycles. In the hardening case, the rate of ratcheting was reported to be less dependent of the applied stress amplitude and mean stress [47, 53]. The area and the width of hysteresis loops decreased both with an increase in the mean stress value.

3.2. Phenomenological ratcheting response

Ratcheting deformation of materials over stress cycles was formulated based on the progressive strain accumulation over three distinct stages of lifespan. Triphasic stages of ratcheting deformation were related to stress cycles, lifespan, mechanical properties and amplitude and mean stress components by means of linear and logarithmic functions. Mathematical description for such triphasic response has been developed based on earlier research works [64-65]. Equation (3.1) integrated stages of ratcheting deformation over stress cycles N and calibrated the ratcheting response over life cycles N_f to quantitatively evaluate ratcheting strain of materials as:

$$\varepsilon_r = \alpha \left(A\left(\frac{\ln N}{\ln N_f} + C\left(\frac{N}{N_f} - \frac{\ln N}{\ln N_f} \right) \right) + B^2 \frac{\ln\left(1 - \frac{N}{N_f}\right)}{\ln \frac{1}{N_f}} \right) \quad (3.1)$$

In equation (3.1) coefficients *A*, *B*, and *C* are defined as:

$$A = -2\ln\left(\frac{\sigma_y}{E}\right) \tag{3.2a}$$

$$B = \ln\left(\frac{\Delta\sigma}{E}\right) \tag{3.2b}$$

$$C = \frac{1}{2}\left(1 - \frac{\sigma_m}{\Delta\sigma}\right)^{1/2n} \tag{3.2c}$$

where $\Delta\sigma = 2\sigma_a$ is the stress range , σ_m is the mean stress, σ_y and σ_{ult} denote respectively the yield stress and the ultimate tensile strength of materials and *E* is the modulus of elasticity. Term *n* corresponds to cyclic strain hardening exponent.

The coefficient α in equation (3.1) was introduced to include the effect of softening/hardening response of materials on the ratcheting deformation. This coefficient was defined as the ratio of ultimate tensile strength to the yield stress of materials powered with exponent *n* as $\left(\alpha = (\sigma_{ult}/\sigma_y)^n\right)$. For materials with softening response as the cyclic load is applied, a rearrangement of dislocations takes place and the material deforms with less resistance and this ratio corresponds to a smaller magnitude as compared with materials with hardening response. For cyclically hardened materials, on the other hand the dislocation density is initially low. As a cyclic load is applied, the dislocation pile-up increases and material shows a greater strength. Coefficient α is always more than unity.

Equation (3.1) mathematically integrated triphasic stages of progressive ratcheting strain over life cycles. This equation was normalized by N_f to distinctly define the ratcheting strain over three stages of lifespan. Figure 3.1 schematically demonstrates stages I, II and III of ratcheting strain over fatigue cycles. Ratcheting strain was accumulated from the very first stress cycles to the cycle at which failure took place. Stage I consisted of a rapid accumulation of the ratcheting strain and a drop in the ratcheting strain rate. A steady-state ratcheting strain rate occurred over stage II and the third stage suddenly raised the ratcheting strain rate to failure stage.

Coefficients A and C calibrate the primary and secondary stages of ratcheting strain curve over stress cycles. The effect of amplitude stress is more pronounced in variation of coefficient C than the mean stress magnitude. Coefficient C is less than unity and stress amplitude is introduced as a denominator in equation (3.2c) to amplify the sensitivity of coefficient C with stress level changes over stages I and II. Coefficient B calibrates stage III of the ratcheting strain curve over last few cycles of lifespan and is influenced by stress amplitude. Coefficients A and B are defined by logarithmic functions and influence respectively stage I and III of ratcheting strain curve over stress cycles. Coefficients A and B shift up and control respectively the outward and inward trends of stages I and III of the ratcheting curve as the magnitude of E increases.

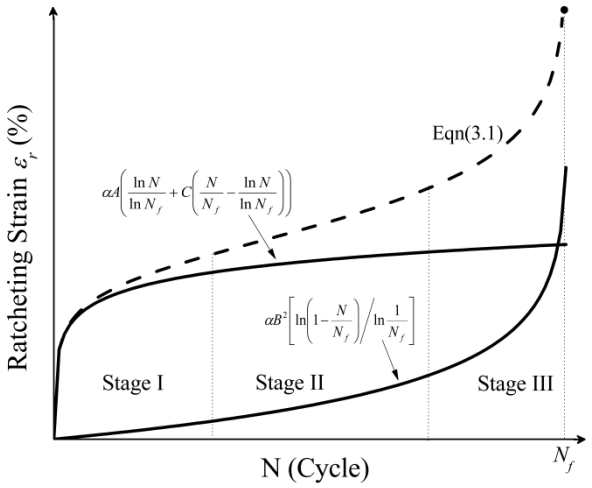

Figure 3.1 Partitions of equation (3.1) to construct the triphasic stages of ratcheting strain over fatigue cycles.

3.3. The modified hardening rule and ratcheting assessment

3.3.1. Elements of cyclic plasticity and hardening rule

Framework of cyclic plasticity theory is established based on the small deformation and total strain increment consists of elastic and plastic strain components:

$$d\bar{\varepsilon} = d\bar{\varepsilon}_e + d\bar{\varepsilon}_p \tag{3.3}$$

and the elastic part is represented by Hooke's law as:

$$\bar{\varepsilon}_e = \frac{\bar{\sigma}}{2G} - \frac{\upsilon}{E}(\bar{\sigma}.\bar{I})\bar{I} \tag{3.4}$$

where terms $\bar{I}$ and $\bar{\sigma}$ correspond respectively to unit and stress tensors while plastic part is defined on the basis of the associated flow rule as:

$$d\bar{\varepsilon}_p = \frac{1}{H_p}(d\bar{s}.\bar{n})\bar{n} \tag{3.5}$$

Where H_p and $d\bar{s}$ are the plastic modulus and the increment of deviatoric stress tensor respectively and vector $\bar{n}$ is the normal vector to the yield surface. $\bar{s}$ is the deviatoric stress and expressed as:

$$\bar{s} = \bar{\sigma} - \frac{1}{3}(\bar{\sigma} \cdot \bar{I})\bar{I} \tag{3.6}$$

It is assumed that yield surface can translate but cannot rotate and during loading and unloading the shape of the yield surface stays unchanged and during plastic loading, yield surfaces must follow the stress points in the stress space through satisfying consistency condition. The von-Mises yield criterion is used in this study as:

$$f(\bar{s},\bar{a},\sigma_y) = \frac{3}{2}(\bar{s}-\bar{a})\cdot(\bar{s}-\bar{a}) - {\sigma_y}^2 = 0 \tag{3.7}$$

The most important constituent in cyclic plasticity constitutive models is the hardening rule that distinguishes one plasticity model from another. A hardening rule dictates the movement direction of yield surface in the stress space during plastic deformation.

Armstrong-Frederick (A-F) [13] developed the non-linear hardening model as:

$$d\bar{a} = Cd\bar{\varepsilon}_p - \gamma\bar{a}dp \tag{3.8}$$

where

$$dp = \sqrt{d\bar{\varepsilon}_p \cdot d\bar{\varepsilon}_p} \tag{3.9}$$

Coefficients C and γ are material constants and the first term of equation (3.8) includes strain hardening and the second term is referred as recall or dynamic recovery term causing nonlinear trend in the hardening rule and accounts for the accumulated plastic strain increment which is defined by equation (3.9) [11, 14, 19, 66]. Constants C and γ are determined from the uniaxial stress-strain hysteresis loop under strain-controlled condition [13].The plastic modulus is defined by implementing consistency condition as:

$$H_p = C - \gamma(\bar{a} \cdot \bar{n}) \tag{3.10}$$

A-F model overestimates ratcheting response over stress cycles [19]. To predict ratcheting strain rate decay, Bower [26] modified A-F hardening rule by introducing a second kinematic variable. The increment of backstress was defined based on Bower's hardening rule [26-27] as:

$$d\bar{a} = Cd\,\bar{\varepsilon}_p - \gamma_1(\bar{a} - \bar{b})dp \tag{3.11}$$

where

$$d\bar{b} = \gamma_2(\bar{a} - \bar{b})dp \tag{3.12}$$

This hardening rule consisted of 3 independent material constants C, γ_1 and γ_2. Material constant C and the first feedback rate γ_1 controlled the size of the stress-strain hysteresis loop. The ratcheting rate was determined by the second feedback rate, γ_2. The tensor $\bar{b}$ has been introduced as an additional kinematic variable with the initial value of zero. Under cyclic loading conditions, predicted values of ratcheting strain based on Bower's model resulted in better agreements with the experimental data as compared with those of predicted based on A-F, Chaboche, Garud, and Mróz models. Bower's predictions showed ratcheting strain rate decay over stress cycles while other hardening rules kept the ratcheting rate constant. Hardening rule of Bower addressed the ratcheting strain rate decay over limited number of cycles and beyond stage I Bower's model experienced a premature plastic shakedown and ratcheting arrested.

To further extend the capability of this A-F based hardening rule and to address ratcheting response of various materials over wider range of stress cycles, coefficients γ_2 and δ were introduced into the hardening rule:

$$d\bar{a} = Cd\,\bar{\varepsilon}_p - \gamma_1(\bar{a} - \delta\bar{b})dp \tag{3.13a}$$

where

$$d\bar{b} = \gamma_2(\bar{a} - \bar{b})dp \tag{3.13b}$$

Coefficients C and γ_1 in the modified hardening rule (Equation (3.13)) are responsible to control the width of stress-strain hysteresis loops over ratcheting progress. Coefficient δ avoided ratcheting arrest after certain number of cycles and resulted in a constant rate followed by ratcheting strain rate decay over stage I. Coefficient γ_2 along with term δ intends to control ratcheting rate and calibrate the ratcheting response for various materials and stress levels. New adapted coefficients γ_2 and δ compromise over-prediction of ratcheting of A-F over stage I and the premature plastic shakedown beyond stage I resulted by Bower's model. Involvement of these coefficients improved the hardening rule capability to extend ratcheting of materials over stress cycles beyond stage I. These coefficients controlled rate of ratcheting in stages I and II and calibrated the modified hardening rule to predict ratcheting strain over prolonged stress cycles. Figure 3.2 present a typical ratcheting response in 42CrMo steel tested under uniaxial stress cycles (σ_a=350MPa, σ_m=50MPa) and the dependency of the modified hardening rule on coefficients γ_2 and δ.

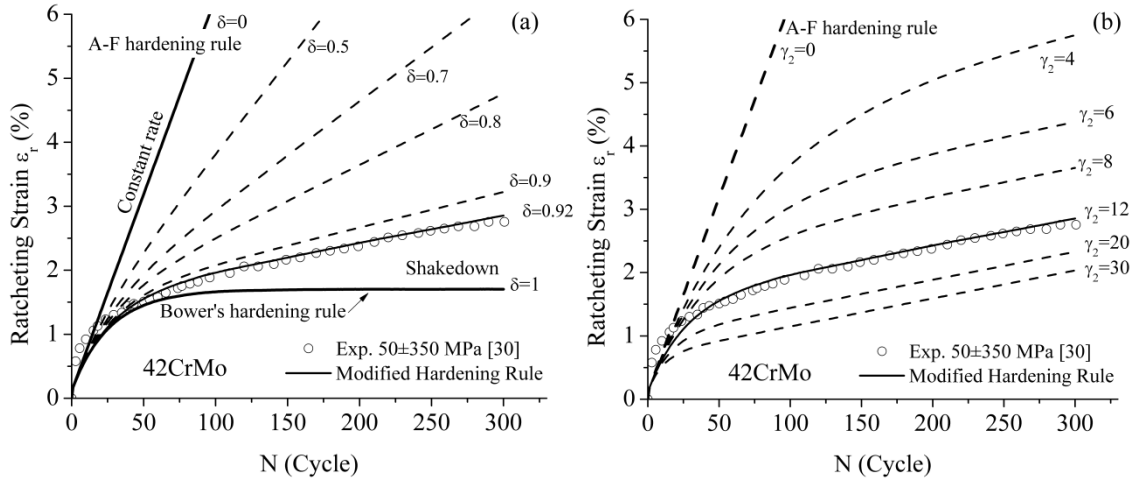

Figure 3.2 Variations of (a) $0 < \delta < 1$ and (b) $0 < \gamma_2$ coefficients and their effects on the ratcheting strain over stress cycles

As shown in figure 3.2 for $\delta=0$, the modified hardening rule reduced to the A-F hardening rule resulting in a constant ratcheting rate. For values of δ greater than zero, ratcheting progress decreased in rate and continued over limited domain of stress cycles in stage I. Beyond this stage, ratcheting strain rate remained unchanged. As constant δ increased in magnitude, the pace of ratcheting strain accumulation decreased. At $\delta=1$, the modified hardening rule reduced to Bower's model resulting in shakedown followed by a decay in the ratcheting strain rate. Similarly at $\gamma_2=0$, the modified hardening rule (equation (3.13)) reduced to A-F hardening rule leading to a constant ratcheting rate. At $\gamma_1=\gamma_2=0$ the modified hardening rule was further converted to the simple linear hardening of Prager. Figure 3.2 also highlights that as the magnitude of coefficient δ drops from unity to zero, both ratcheting magnitude and rate over stages I and II increase noticeably. A decrease in the constant γ_2 in this figure corresponds to an increase in the magnitude of ratcheting strains and rates over stages I and II.

The modified hardening rule (equation (3.13)) calibrated ratcheting by means of coefficients γ_2 and δ estimated from ratcheting data over stages I and II. These coefficients were found to be dependent on the applied stress level for materials examined in this study. This enables the modified hardening rule to predict ratcheting response of materials for prolonged stress cycles by estimating coefficients γ_2 and δ based on applied uniaxial stress levels.

The MATLAB programing was developed to assess ratcheting response of materials based on the modified kinematic hardening rule in the framework of cyclic plasticity theory. Figure 3.3 presents the algorithm of the MATLAB programing including main ingredients of cyclic plasticity theory and procedure to analyse ratcheting response of materials over stress cycles based on the modified hardening rule.

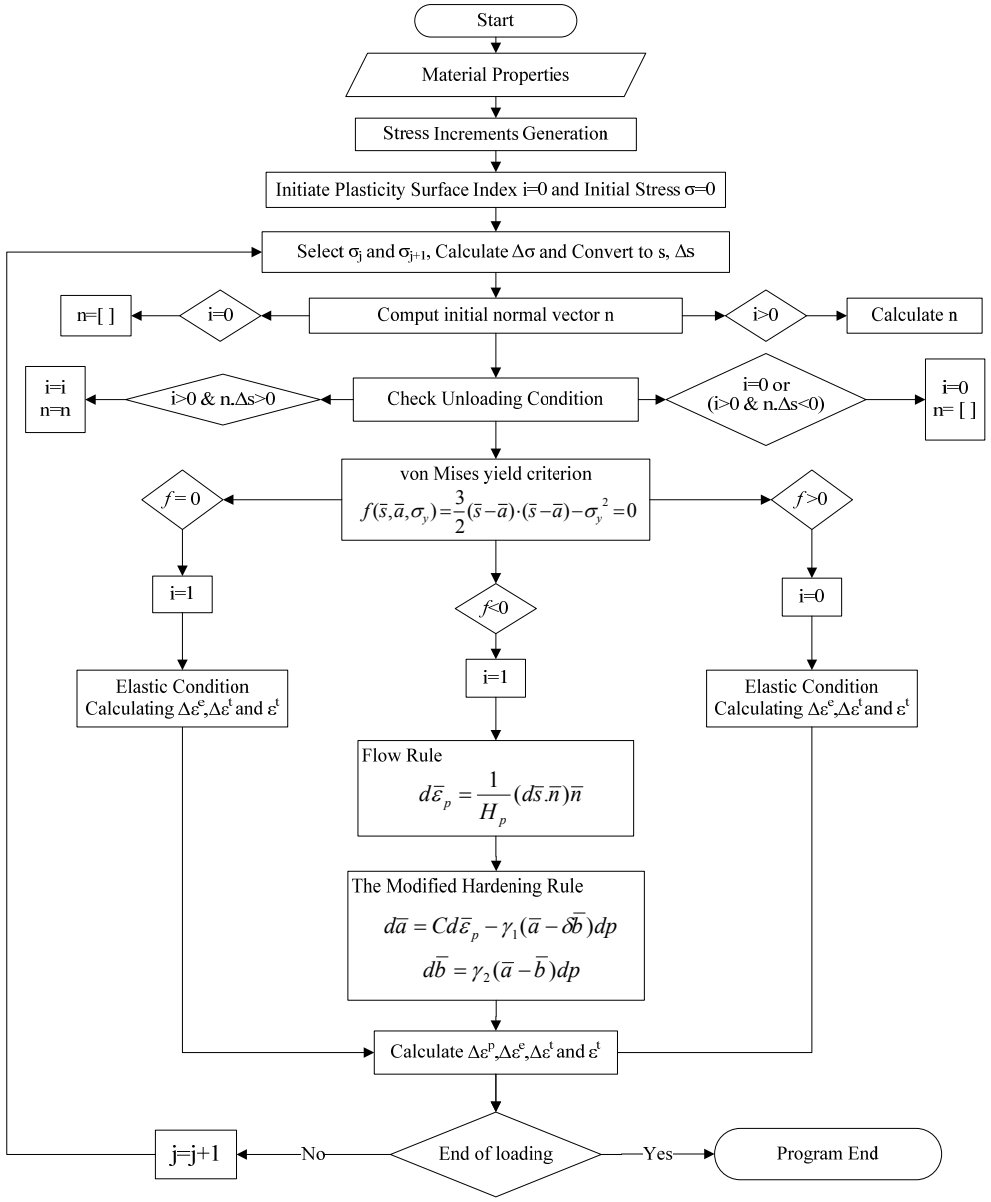

Figure 3.3 Algorithm for prediction of ratcheting strain of materials based on the modified hardening rule under stress-controlled condition.

3.4. Ratcheting-fatigue damage formulations

The interaction of ratcheting and fatigue damage over stress cycles was investigated and the extend of ratcheting and fatigue damage contributions in the overall damage was quantitatively evaluated. Fatigue damage values were calculated based on Xia et al. , and SWT energy-based models and the ratcheting effect was included by means of the average of

normalized ratcheting strain rate and the maximum stress of applied cycles. Overall Damage values were calibrated by means of a weighting factor at various mean stress and cyclic stress amplitudes. The damage values predicted by the proposed model were compared with the experimentally obtained damage values for 42CrMo and 1020 steel alloys tested under uniaxial fatigue loading conditions.

3.4.1. Overall damage assessment

The overall damage of material is composed of the cyclic fatigue damage component D_m and the ratcheting damage component, D_r. The extent of ratcheting effect is defined by product of the normalized average ratcheting strain rate, $\dot{\varepsilon}^{r}_{avg} \Big/ \varepsilon^{r}_{(0-N_f)}$ and the maximum applied stress, σ_{max} and is expressed as:

$$D_r = \sigma_{\max} \frac{\dot{\varepsilon}^{r}_{avg}}{\varepsilon^{r}_{(0-N_f)}} = k_r N_f^{\chi} + C_r \tag{3.14}$$

where $\varepsilon^{r}_{(0-N_f)}$ is defined as $\frac{1}{2}\varepsilon^{r}_{N_f}$. The right hand side of equation (3.14) relates the ratcheting damage to life N_f in the form a power law equation as well as materials constants k_r, χ and C_r which are determined empirically [57].

To include the effect of ratcheting on the overall damage of components under stress cycles, concurrent damage values of ratcheting and fatigue stress cycles were realistically integrated through a factor ξ as an index factor representing unequal damage contributions due to both phenomena. This factor calibrates contribution of ratcheting and fatigue damage in the overall damage of components under cyclic stresses. The overall damage D is composed of ratcheting and fatigue damage values and is expressed as:

$$D = \xi D_m + (1 - \xi) D_r \tag{3.15}$$

The factor ξ has been introduced to partition the efficiency of mean stress and accumulated ratcheting to calculate overall damage exerted on materials. This factor is estimated from the D_r-N_f curve, the D_m-N_f curve and corresponding damage data of sample obtained experimentally. Factor ξ is defined as:

$$\xi = \frac{D_{\exp} - D_r}{D_m - D_r} \tag{3.16}$$

The weighting factor ξ is related to the applied mean stress and ratcheting behaviour of materials. Since changes in mean and amplitude stress values significantly influence the ratcheting strain and corresponding damage values, the overall damage was defined to be dependent of the ratio of mean stress and amplitude stress. Equation (3.15) is applicable for a series of cyclic tests under different stress amplitudes and mean stresses. A family of damage curves possesses different weighting factors ξ and are non-linearly related to the σ_m/σ_a ratio.

3.4.2. Fatigue damage assessment

To assess fatigue damage of materials over stress cycles, two well-known energy-based damage models of Xia et al. [57] and SWT [68] were employed. Energy-based damage models were chosen as the stress and strain components in these models address both low-cycle and high-cycle fatigue regimes. Energy-based damage models were used to calculate damage values D_m as a main component of equation (3.15). Damage models were then compared for their capability in assessing fatigue damage of materials discussed in this study.

3.4.2.1. Xia et al. energy-based damage model

Based on the strain-energy density, Xia and coworkers [69] have proposed fatigue failure criterion for fully reversed cyclic loading as follows:

$$\frac{\Delta W^p}{\overline{\rho}} + \Delta W^e = k_m N_f^{\lambda} + C_m \tag{3.17}$$

where ΔW^p is the irreversible plastic energy over a stress cycle, $\overline{\rho}$ is a multiaxial constrain factor, and ΔW^e is a properly defined elastic energy. In the uniaxial cyclic loading it is assumed that ΔW^p is the area of the stress-strain hysteresis loop, $\overline{\rho} = 1$ and $\Delta W^e = \sigma_a^2 / 2E$ where E is the modulus of elasticity. N_f denotes the number of cycles to failure and the material constants k_m, λ and C_m are determined based on fully-reversed uniaxial fatigue test data [57].The non-damaging energy value C_m corresponds to the materials fatigue limit. It has been shown that predicted results for fully reversed cyclic loading are in good agreement with equation (3.17). Xia et al.

[57] further modified equation (3.17) to account for the effect of mean stress through the function *f*. Equation (3.18) shows how this function influences the fatigue damage D_m through its elastic energy range term ΔW^e as:

$$D_m = \Delta W^p + f\Delta W^e = k_m N_f^{\lambda} + C_m \tag{3.18}$$

Xia et al. [57] defined function $f(\sigma_m/\sigma_a)$ by a quadratic equation (3.19):

$$f^2 - \frac{\sigma_m}{\sigma_a} f - 1 = 0 \tag{3.19}$$

For the fully reversed loading condition (σ_m =0), equation (3.19) reduces to f=1. For non-zero mean stress cases, the positive root of this equation is representative of fatigue damage progress in materials [70].

3.4.2.2. SWT model

Smith, Watson and Topper (SWT) proposed a stress-strain function [68] to include the effect of mean stress to predict fatigue behaviour in metals. The function has been defined by $\sigma_{max}\varepsilon_a$ where σ_{max} is the maximum tensile stress and ε_a is the strain amplitude. SWT can be obtained at given fatigue life for fully reversed by manipulating the Coffin-Manson equation in the form of:

$$\sigma_{\max}\varepsilon_a = \sigma'_f N_f^b \left(\frac{\sigma'_f}{E} N_f^b + \varepsilon'_f N_f^c \right) \tag{3.20}$$

where E is elastic modulus, b and c are material constants and σ'_f and ε'_f are fatigue strength coefficient and fatigue ductility coefficient, respectively. The general form of SWT equation is given as:

$$D_m = \sigma_{\max}\varepsilon_a = PN_f^{\rho} + QN_f^{\beta} \tag{3.21}$$

The procedure of overall damage assessment is developed in an algorithm presented in figure 3.4:

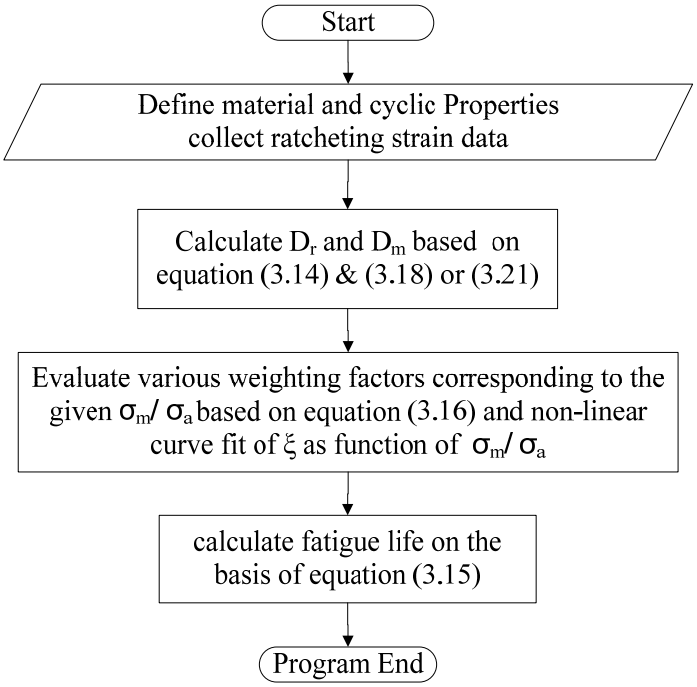

Figure 3.4 Algorithm flow chart for life prediction

3.5. Summary

Ratcheting formulations were developed based on (i) mechanistic approach and (ii) kinematic hardening rule approach. Based on the mechanistic approach, ratcheting formulation was defined based on parameters involving the effects of stress level and material properties. Effects of mean stress, stress amplitude and cyclic softening/hardening response of materials were included to define and calibrate the mechanistic equation. The triphasic ratcheting strain equation was developed based on mechanism of ratcheting deformation over stress cycles. The next employed approach to assess ratcheting response of materials was modified based on A-F kinematic hardening rule. The modified hardening rule was developed based on the framework of A-F nonlinear hardening rule consisted of materials coefficients C and γ_1 and ratcheting rate coefficients γ_2 and δ. Modifications on the hardening rule by direct means of such calibrating coefficients are relatively novel for classical hardening rules. The modified hardening rule successfully addressed stages I and II of ratcheting process at which ratcheting strain rate decay was followed by constant ratcheting strain rate. Coefficients γ_2 and δ enabled the hardening rule

to successfully predict ratcheting strain values between plastic shakedown of Bower's model and overestimation of ratcheting strain response of materials in A-F model.

Ratcheting-fatigue interaction formulation was developed to address the effect of both coupled ratcheting and fatigue phenomenon concurrently. The interaction of ratcheting and fatigue phenomena was defined based on mechanistic parameters involving the effects of mean stress, stress amplitude, and cyclic softening/hardening response of materials. The magnitude of ratcheting damage was calculated by the product of ratcheting strain rate and the maximum applied cyclic stress values over stress cycles, whereas fatigue damage was analysed based on energy-based models of Xia-Kujawski-Ellyin and Smith-Watson-Topper.

CHAPTER FOUR

RESULTS OF RATCHETING-FATIGUE ASSESSMENT

4.1. Triphasic ratcheting strain prediction of materials over stress cycles

To formulate ratcheting strain evolution, a parametric equation was proposed in previous chapter (section 3.1). The formulation includes mechanistic parameters of stress amplitude and mean stress over triphasic stages of ratcheting lifespan. Stages of ratcheting deformation were related to stress cycles, lifespan, mechanical properties and amplitude and mean stress components by means of linear and non-linear functions. Terms of mechanical properties in the ratcheting formulation enabled to characterize ratcheting response of various materials over life cycles. These terms were further employed to interpret the influence of softening/hardening response of materials on ratcheting deformation. Ratcheting data for 42CrMo, 20CS, SA333 steels and OFHC copper reported in the literature are employed to evaluate the proposed ratcheting formulation.

4.1.1. Materials and experimentation

In order to evaluate the ratcheting strain response of materials under stress cycles, four different materials of 42CrMo, 20CS, SA333 steels and OFHC copper were cyclically loaded under stress-controlled at various mean and amplitude stresses [28, 33, 37-38, 71-72]. Table 4.1 presents properties of these materials. Figure 4.1 presents monotonic and cyclic stress-strain responses of the materials used in this investigation.

Table 4.1 Material and cyclic properties

Material	E (GPa)	σ_y (MPa)	σ_{ult} (MPa)	n	K (MPa)
42CrMo [71]	190.5	310	670	0.10	637
20CS [33, 72]	203	350	441	0.24	1221
SA333 Gr. 6 C-Mn [37-38]	203	304	494	0.142	830
OFHC copper [28]	70.8	52	234	0.443	545

The cyclic stress-strain curves for 20CS, SA333 steels and OFHC copper show hardening responses of these materials. The monotonic stress-strain curves of annealed 42CrMo and 20CS steels present a yielding plateau. Cyclic stress-strain diagram of annealed 42CrMo shows a softening response for strain values exceeding 2%. Geometry and dimensions of tested samples have been reported in references [28, 33, 37-38, 71-72].

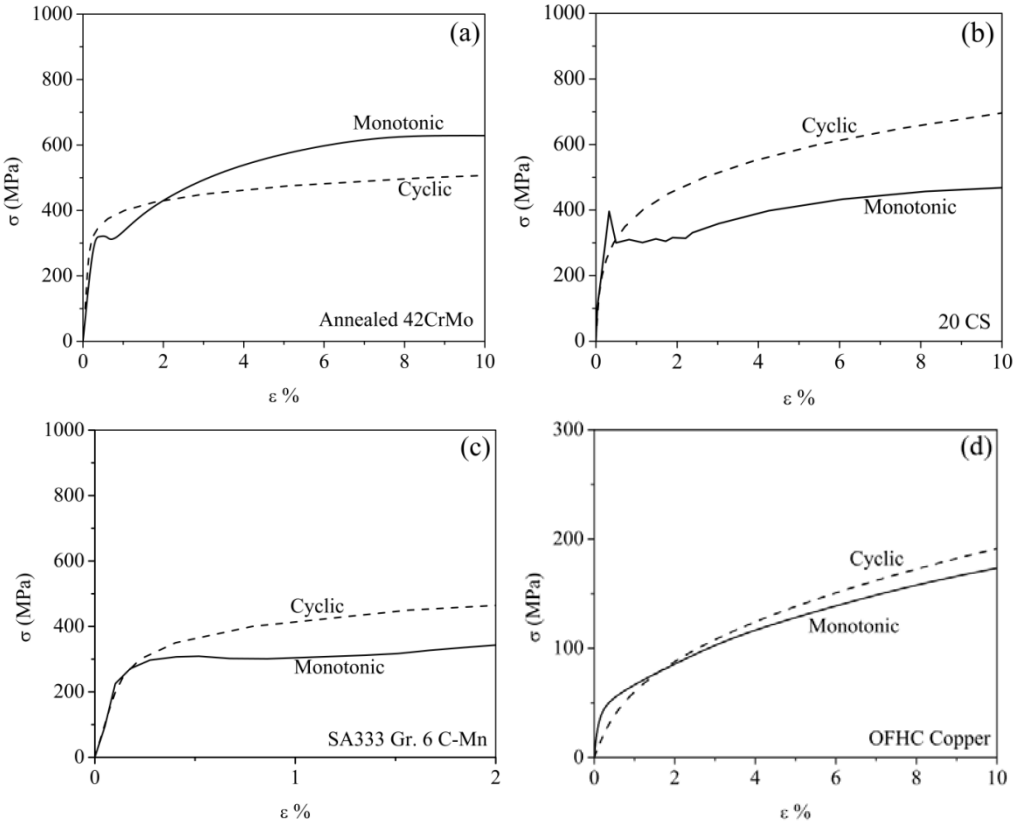

Figure 4.1 Monotonic and cyclic stress-strain curves of a) annealed 42CrMo steel [71], b) 20CS [33] and c) SA333 steel [38] and d) OFHC copper [28]

All cyclic tests were performed under the stress-controlled condition and at room temperature. Uniaxial ratcheting tests were conducted under different combinations of mean and

amplitude stresses at various stress rates. Table 4.2 lists the testing conditions at which various materials were cycled.

Table 4.2 Uniaxial testing conditions for 42CrMo, 20CS, SA333 steel and OFHC copper samples.

Materials	σ_m (MPa)	σ_a (MPa)	Stress ratio, R	Stress Rate (MPa/s)	Life (Cycle)
42CrMo [71]	100	350	-0.555	500	4918
	150	350	-0.40	500	2789
	50	400	-0.777	500	1793
20CS [33, 72]	50	275	-0.692	400	9334
	50	300	-0.714	400	2000
	50	320	-0.730	400	552
SA333 [37-38]	40	310	-0.77	50	3300
	80	310	-0.590	50	1184
	120	310	-0.442	50	570
OFHC copper [28]	50	120	-0.412	500	10187
	50	140	-0.474	500	1015
	50	160	-0.524	500	186
	30	140	-0.647	500	2060

The ratcheting strain values correspond to $\varepsilon_r = 1/2\left(\varepsilon_{\max} + \varepsilon_{\min}\right)$ where ε_{max} and ε_{min} are the experimentally obtained maximum and minimum true strain values from stress-strain hysteresis loops over uniaxial life cycles.

4.1.2. Verification of the proposed formulation and results

To evaluate the capability of ratcheting strain equation presented in previous chapter, four different alloys of 42CrMo, 20CS, SA333 steels and OFHC copper were examined. Ratcheting plastic strain of alloys undergoing stress-controlled cyclic tests were used to evaluate ratcheting deformations of alloys quantitatively. Ratcheting strain was calculated over stress cycles through the proposed ratcheting strain equation (3.1). The coefficients B and C are dependent on the amplitude and the mean stress magnitudes (listed in Table 4.2) and calibrated equation (3.1) by means of material properties (listed in Table 4.1) over ratcheting stages.

Coefficients *A* and *C* calibrate the stages I and II of ratcheting strain curve over stress cycles. Coefficient *C* is more affected by the amplitude stress magnitude as compared with the mean stress level. Coefficient *B* calibrates final stage of the ratcheting strain curve and is influenced by stress amplitude level. Coefficients *A* and *B* are defined by logarithmic functions and influence respectively stage I and III of ratcheting strain curve over stress cycles. The

ratcheting curve over stages I and III are being affected as the magnitude of E increases. This may be associated to the cyclic softening response of harder materials upon cyclic loading conditions. Stress-strain hysteresis loops of these materials widen over stress cycles resulting in higher ratcheting strain values. This verifies how an increase in *E*-dependent coefficients *A* and *B* shifts up the ratcheting strain curves over stress cycles.

Figures 4.2a, b, c and d compare experimental data of ratcheting strain of four different materials tested under uniaxial stress cycles with the calculated ratcheting strain curves over the materials life cycles based on equation (3.1). These figures verify how closely the calculated ratcheting strain values agree with the experimentally obtained data tested at given materials and loading conditions.

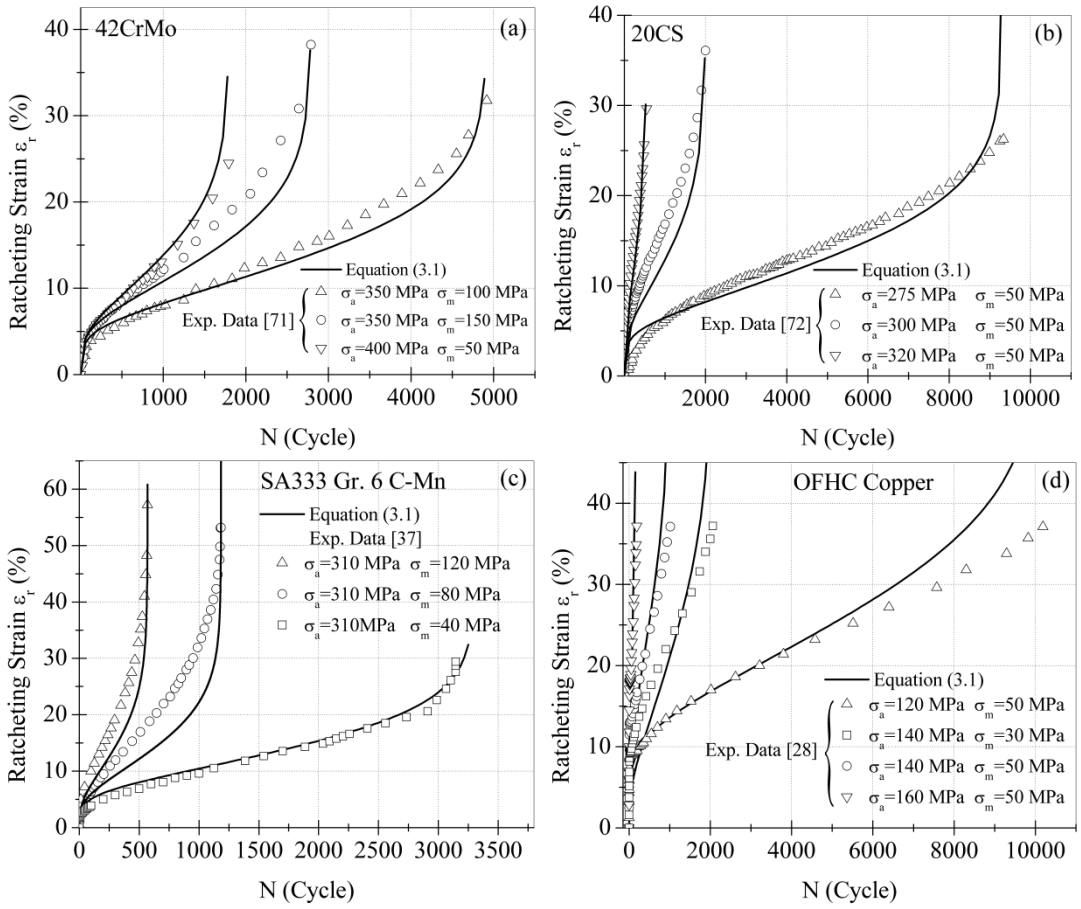

Figure 4.2 The calculated and the experimental ratcheting strain values over stress cycles for (a) 42CrMo steel, (b) 20 carbon steel, (c) SA333 steel and (d) OFHC copper under various mean and amplitude stresses

The calculated triphasic response of ratcheting strain for all materials were found in good agreements with the ratcheting experimental data tested in steel and copper alloys (see figure 4.2). In equation (3.1) as the stress level (mean stress and stress amplitude) increases both ratcheting rate and ratcheting strain magnitudes increase accordingly. Ratcheting strain and its rate however increase till certain stress ratio and then drops. The progressive ratcheting strain over triphasic lifespan in equation (3.1) is further calibrated by coefficient α to address the cyclic hardening/softening response of materials. This equation successfully evaluated ratcheting strain of various materials of 42CrMo, 20CS, SA333 steels and OFHC copper involving stress components and materials properties as main contributing elements of ratcheting phenomenon.

4.2. Ratcheting assessment based on the modified hardening rule

Ratcheting response of materials by means of modified hardening rule based on new introduced coefficients is evaluated. The implemented modifications on the A-F based hardening rule aims to address stages of ratcheting over stress cycles. The modified hardening rule predicts the ratcheting strain rate decay over stage I and the constant rate of strain accumulation during stage II. The modified hardening rule consisted of the coefficients of the hardening rule controlling stress-strain hysteresis loops generated over stress cycles during ratcheting process (Bower's modification on A-F rule) plus the coefficients controlling rates over stages of materials ratcheting deformation. Ratcheting strain rate coefficients improve the hardening rule capability to calibrate and control the rate of ratcheting in stages I and II and enable the modified hardening rule to predict ratcheting strain over a prolonged domain of stress cycles.

4.2.1. Materials, experimentation and testing conditions

To evaluate the capability of the modified hardening rule in predicting the ratcheting response of materials over stress cycles, four different materials of 304, 42CrMo, 316L steel alloys and copper were extracted from works of Kang and his coworkers [29-30, 45]. These materials were cyclically loaded under stress-controlled and room temperature conditions. Table 4.3 presents materials examined in this study and the ratcheting coefficients C and γ_1.

The cylindrical test sample bars of 304, 42CrMo, 316L steel alloys and copper consisted of gauge length of 30 mm and diameter of 10 mm were tested using a MTS809-250KN test

machine. Samples of 304, 42CrMo, 316L steel alloys and copper were tested under uniaxial cyclic stress rates of 250, 500, 100 and 100 MPa/s, respectively [29-30, 45]. Uniaxial ratcheting tests were performed under different mean and alternating stresses at various stress rates. Table 4.4 lists the ratcheting tests performed for various materials examined in this research.

Table 4.3 Properties of materials examined in this study and their ratcheting coefficients

Material	E (GPa)	σ_y (MPa)	C (Gpa)	γ_1
304 steel [29]	190	209	27	180
42CrMo steel [30]	190.5	310	35	200
316L steel [45]	190	285	20	150
Copper [45]	129	60	9	100

Table 4.4 Ratcheting tests for 304, 42CrMo, 316L steel and copper samples performed under uniaxial loading conditions [29-30, 45]

Materials	σ_m (MPa)	σ_a (MPa)	Stress ratio, R	Life cycles (Tested)
304 [29]	10	260	-0.93	5775
	10	280	-0.93	2930
	10	300	-0.94	1620
	10	350	-0.94	690
	5	300	-0.97	1810
	20	300	-0.88	2495
	30	300	-0.82	3435
	40	300	-0.77	3870
	95	281	-0.50[a]	21200
	60	313	-0.67[a]	5570
	40	337	-0.80[a]	1600
	20	356	-0.90[a]	955
42CrMo [30]	50	350	-0.75	6315
	50	400	-0.78	2000
	100	350	-0.56	5080
	150	350	-0.40	2735
	106	319	-0.50[b]	10100
	50	370	-0.75[b]	3830
	20	400	-0.90[b]	2315
316L [45] [e]	69	300	-0.62	---
	69	327	-0.65[c]	---
	69	346	-0.67	---
	10	346	-0.94	---
	30	346	-0.84	---
	99	297	-0.50[c]	---
Copper [45] [e]	18	73	-0.6	---
	18	91	-0.67	---
	18	109	-0.71	---
	36	73	-0.33	---
	55	73	-0.14	---
	55	90	-0.25[d]	---
	45	100	-0.38[d]	---

[(a)] σ_{max}=375MPa, [(b)] σ_{max}=425MPa, [(c)] σ_{max}=396MPa, [(d)] σ_{max}=145MPa
[(e)] Data reported up to 1000 cycles

4.2.2. Estimation of the coefficients of the modified hardening rule

4.2.2.1. Estimation of C and γ_1 coefficients

Coefficients C and γ_1 are material dependent and these coefficients govern the shape and size of hysteresis loops. Under uniaxial cyclic stressing with non-zero mean stress, proper selection of C and γ_1 results in constructing continuous stress-strain hysteresis loop and satisfying consistency condition during forward and reversed loading conditions. Figure 4.3b presents how different values of coefficients C and γ_1 affect shape and size of hysteresis loops in SS304 subjected to stress level 20±300MPa. Different values of C and γ_1 are examined through a closed form solution of the modified hardening rule in each iteration to achieve consistent hysteresis loops in shape and size. Figures 4.3c, 4.3d, 4.3e show the results of three typical iterations with pairs of (C=10GPa, γ_1=150), (C=40GPa, γ_1=450) and (C=27GPa, γ_1=180) and their corresponding predicted hysteresis loops over cyclic stress level 20±300MPa. Figures 4.3c and 4.3d present violation of consistency condition during plastic loading resulting in large strain jumps and distortions in hysteresis loops while in figure 4.3e with C=27GPa and γ_1=180 consistency condition is satisfied and hysteresis loops progress over cycles.

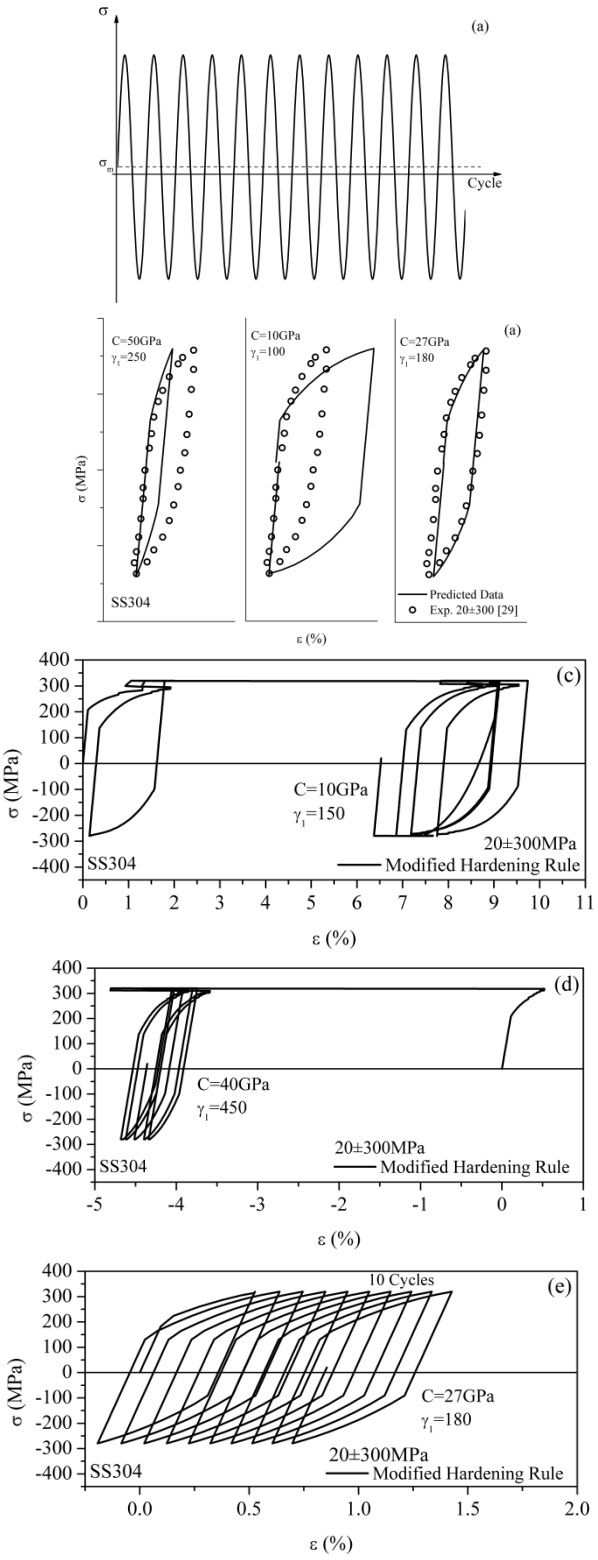

Figure 4.3 The effect of coefficients C and γ_1 on the hysteresis loops and consistency condition.

4.2.2.2. Estimation of γ_2 and δ coefficients

Coefficients γ_2 and δ controlled the ratcheting strain rate over stages and were found to be material and stress level dependent as presented in figures 4.4-4.7. These figures show the trend of dependency of coefficients γ_2 and δ with material types and stress levels. Such trend agreed with an earlier study by Jiang and Zhang [73]. They found that the ratcheting strain rate is sensitive to the magnitude of applied stresses.

To estimate Coefficients γ_2 and δ, a family of curves was constructed to present variations of these coefficients with magnitudes of stress amplitude and mean stress. Curves converged and met each other at materials yield stress σ_y level. The sharp decreasing trend of coefficient γ_2 over stress amplitude gained a steady response at amplitude stress levels beyond $1.3\sigma_y$. To estimate coefficient δ, a family of curves was defined to present the decreasing trend of this coefficient as stress amplitude increased. This trend showed a higher rate at stress magnitudes beyond yield stress. For both coefficients γ_2 and δ as mean stress values increased the family curves were shifted up. To construct the family dashed-curves presented in figures 4.4-4.7, continuous master curves were first constructed to correlate coefficients γ_2 and δ with stress amplitude at constant mean stresses (see parts a and b in figures 4.4-4.7). The constructed curves for various stress levels were then employed to predict coefficients γ_2 and δ at any given amplitude and means stress levels. Open symbol data in figures 4.4-4.7 represent values of coefficients γ_2 and δ at different stress levels to closely coincide the predicted and experimental ratcheting data over stress cycles. These curves readily enable estimating both γ_2 and δ values for any given stress levels on the curves or by means of interpolation if the curve for the desired stress level is not given in figures 4.4-4.7.

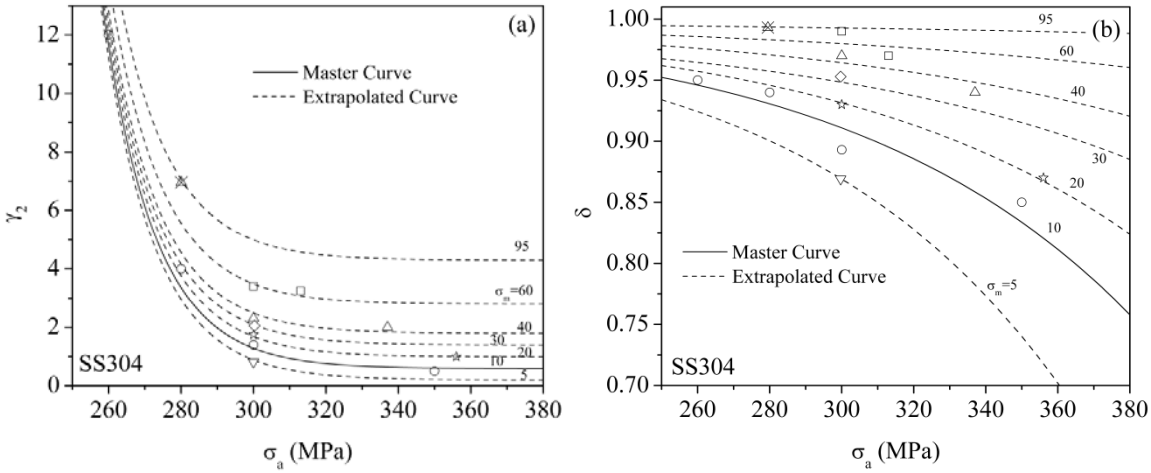

Figure 4.4 (a) and (b) Family curves representing the variations of coefficients γ_2 and δ as function of mean and amplitude stress values for 304 steel samples.

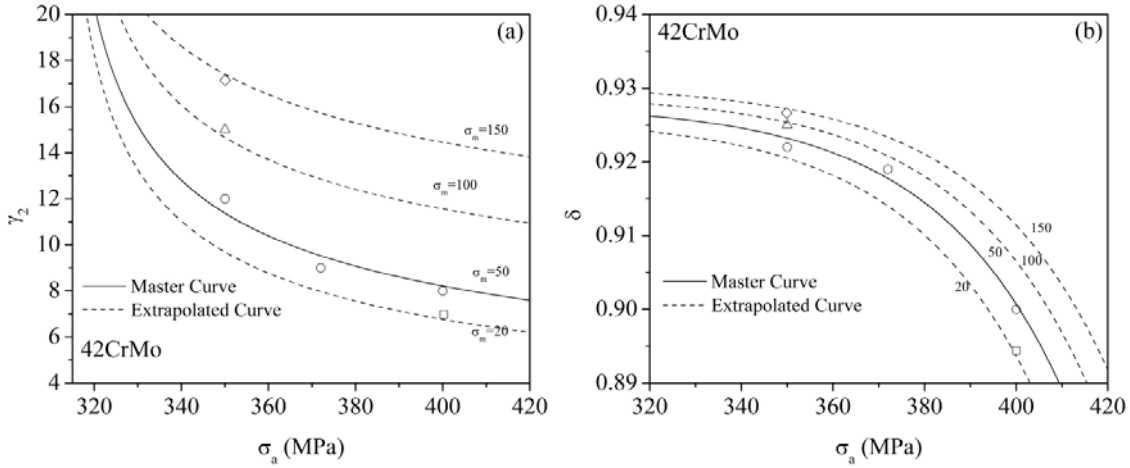

Figure 4.5 (a) and (b) Family curves representing the variations of coefficients γ_2 and δ as function of mean and amplitude stress values for 42CrMo steel.

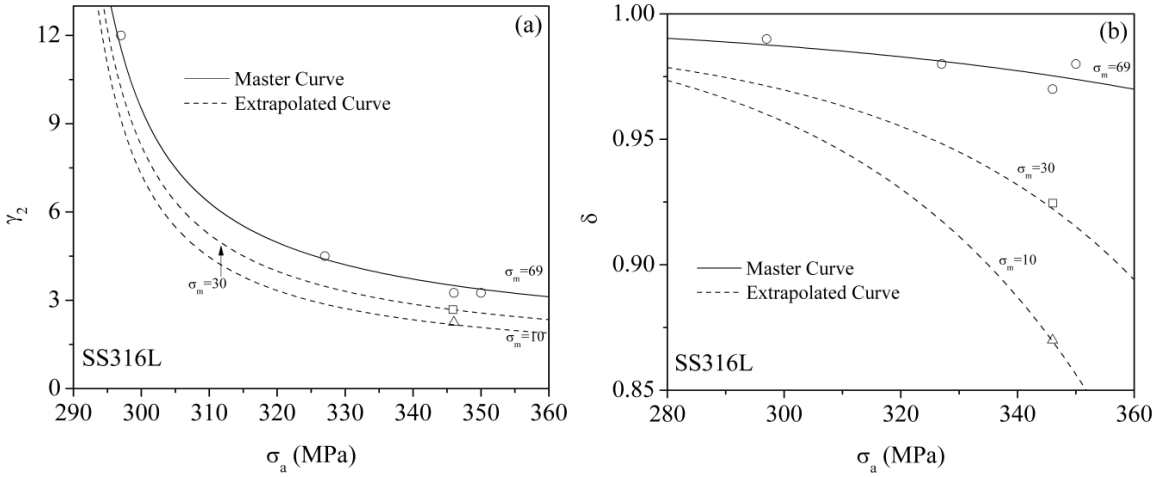

Figure 4.6 (a) and (b) Family curves representing the variation of coefficients γ_2 and δ as function of mean and amplitude stress values for SS316L steel samples.

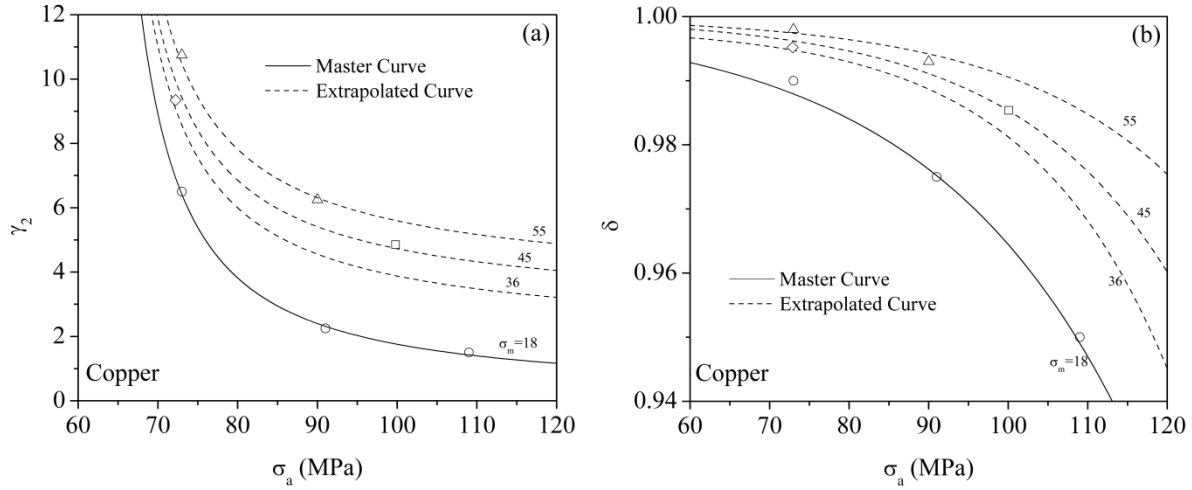

Figure 4.7 (a) and (b) Family curves representing the variations of coefficients γ_2 and δ as function of mean and amplitude stress values for copper samples.

4.2.3. Predicted ratcheting results

The modified hardening rule was employed to assess ratcheting strain values of 304, 42CrMo, 316L steel and copper alloys over uniaxial stress cycles. Predicted ratcheting strains for steel samples using equation (3.13) were plotted in figures 4.8-4.10 versus those of experimentally obtained values. These figures verify that the predicted ratcheting values over stress cycles based on the modified hardening rule are in good agreements with experimentally obtained ratcheting strain values over stages I and II at various stress levels. The capability of the modified hardening rule due to inclusion of constants γ_2 and δ is quite evident when compared with Bower's model (see figure 3.2). Ratcheting strains predicted by Bower's model were limited within the stage I and beyond this stage Bower's model showed an arrest of ratcheting where shakedown took place.

Figure 4.8 shows that as the magnitude of stress amplitude increases, the ratcheting strain values over stages I and II increase. At a constant mean stress, as the magnitude of stress amplitude increased, the ratcheting strain rate over stages I and II increased.

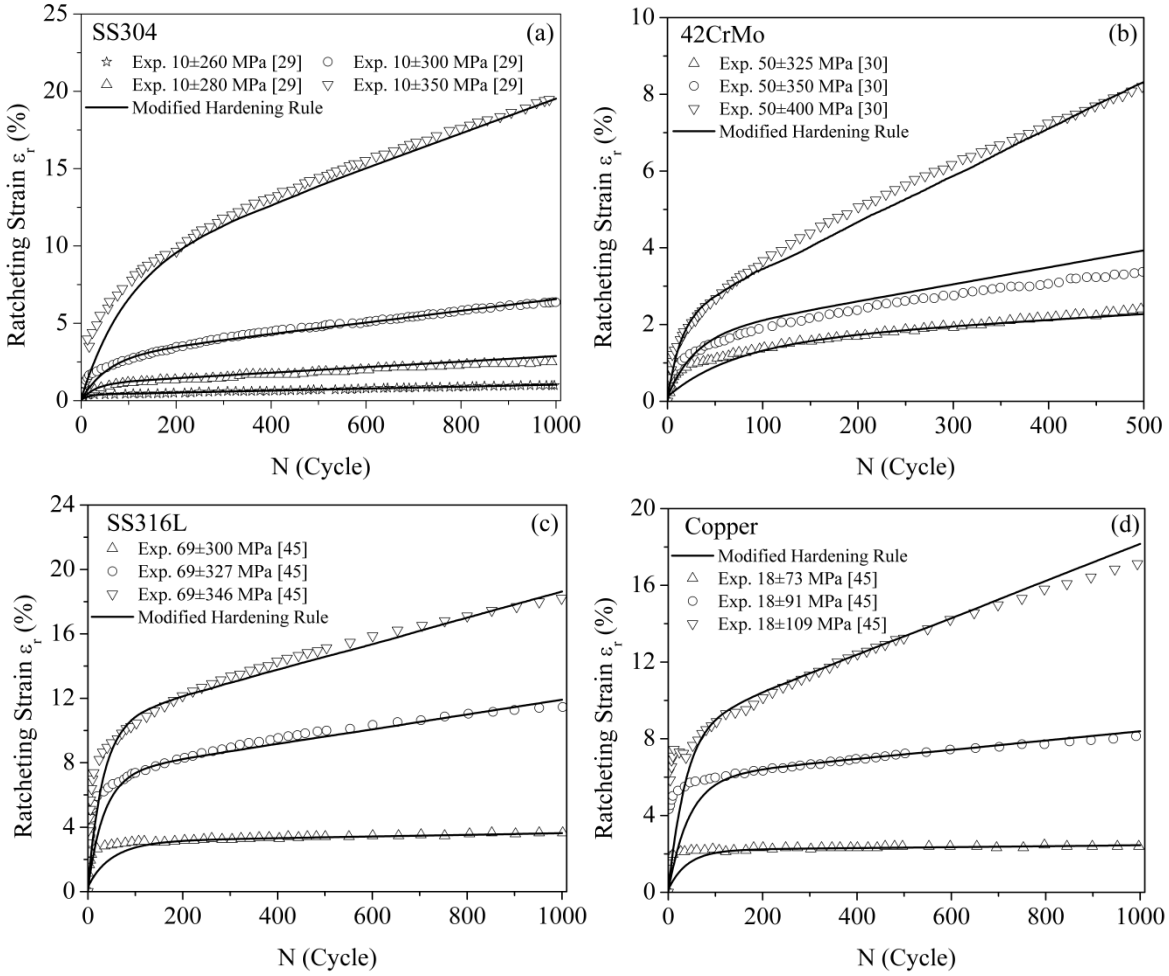

Figure 4.8 The predicted ratcheting strain based on the modified hardening rules versus the experimental ratcheting values over stress cycles at a constant mean stress and various stress amplitudes for (a) 304 steel, (b) 42CrMo, (c) 316L, and (d) copper.

In figure 4.9 as the magnitude of mean stress increases, the ratcheting strain values over stages I and II increase. This figure may suggest that the mean stress is less influential in controlling the rate of ratcheting strain over these stages and the rate of ratcheting is more controlled by the magnitude of the amplitude stress (see figure 4.8).

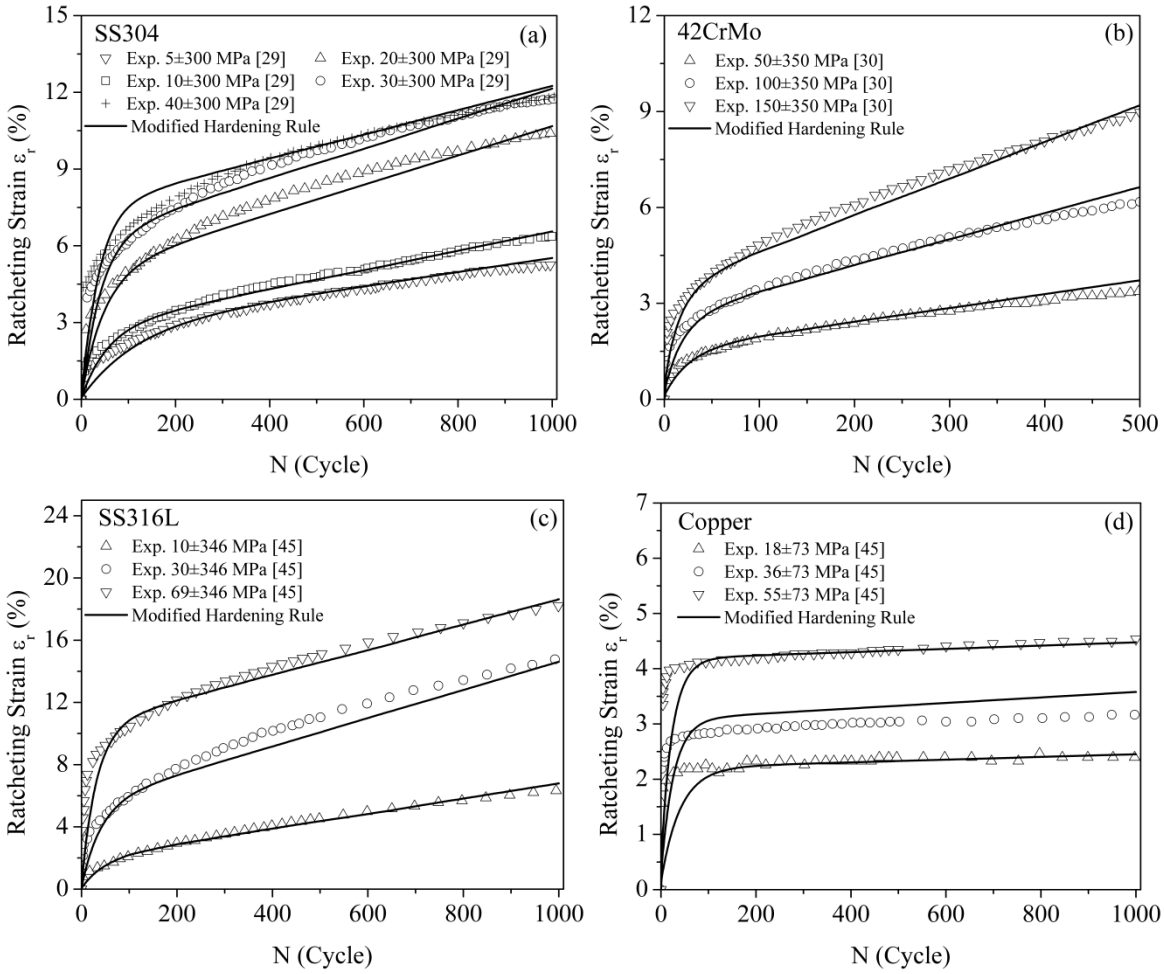

Figure 4.9 The predicted ratcheting strain based on the modified hardening rules versus the experimental ratcheting values over stress cycles at constant stress amplitude and various mean stresses for (a) 304 steel, (b) 42CrMo, (c) 316L, and (d) copper.

Figure 4.10 presents the predicted ratcheting strain values of materials over stress cycles based on the modified hardening rule and compares them with experimental data obtained at various uniaxial stress levels while the maximum cyclic stress stayed constant. The effect of stress ratio is quite vulnerable with the mean stress and amplitude stress magnitudes. In figures 4.8 and 4.9, increases respectively in stress amplitude and mean stress resulted in higher ratcheting strain accumulation over stress cycles. The magnitude of stress amplitude in figure 4.10 dominantly controls the ratcheting strain rate and slopes over stages I and II. Figures 4.10a-4.10d show how the slopes of ratcheting curves vary as stress amplitude level increases. As the magnitude of stress amplitude increased ratcheting strains accumulated in faster rates and sharper slopes.

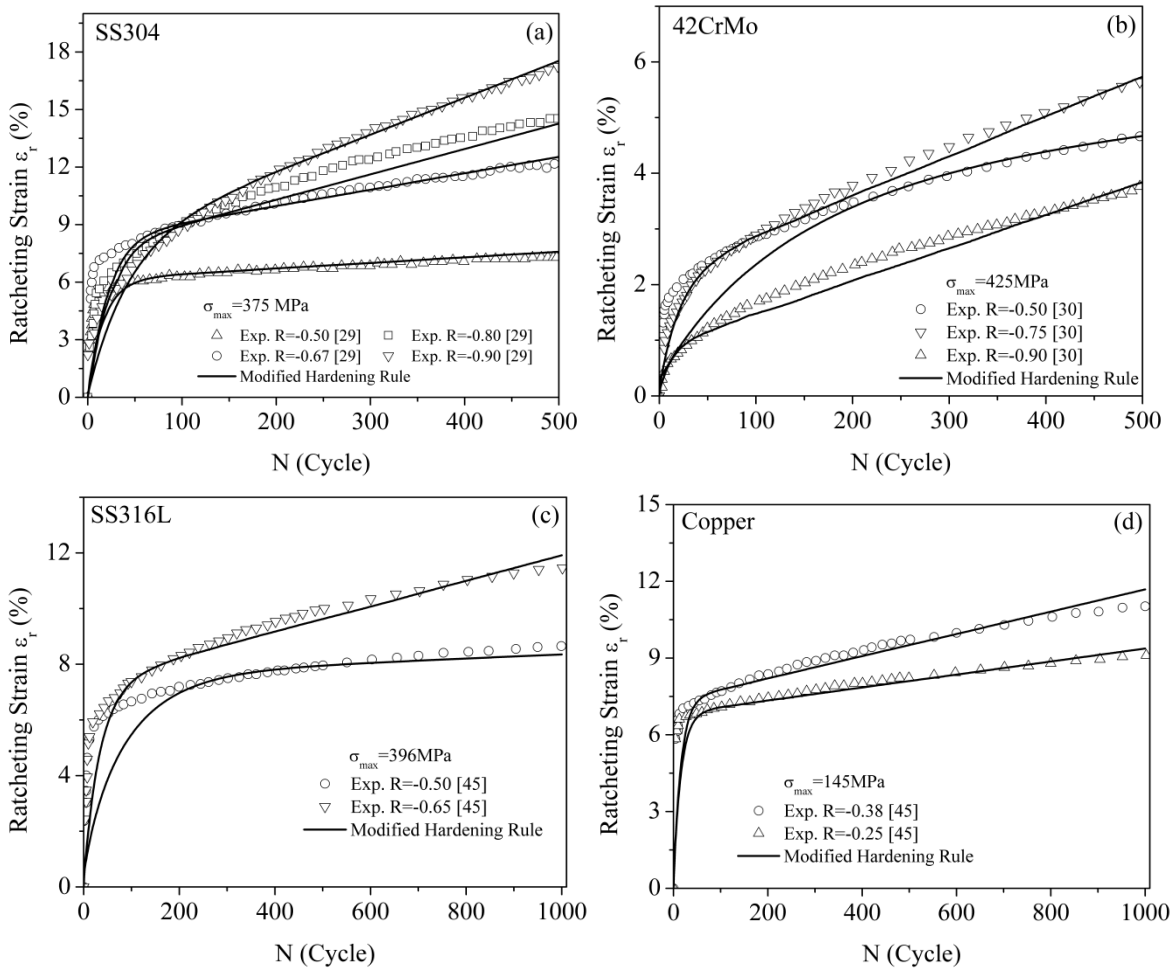

Figure 4.10 The predicted ratcheting strain based on the modified hardening rules versus the experimental ratcheting values over stress cycles at various stress ratios and constant maximum stress for (a) 304 steel, (b) 42CrMo, (c) 316L, and (d) copper.

Figures 4.10a and 4.10d present increases in ratcheting strain curves of 304 steel and copper samples over stress cycles with the magnitude of stress ratios. Increases in ratcheting strains for 42CrMo and 316L steel samples were however overcome by the effect of stress amplitude at various magnitudes of mean stresses (see figures 4.10b and 4.10c). Figure 4.10b presents the ratcheting strain values for annealed 42CrMo steel samples tested by Kang and Liu [29-30] at the constant maximum stress of 425MPa while both stress amplitude and mean stress values varied resulting in different stress ratios of -0.5, -0.75 and -0.9. This figure shows that the highest ratcheting data belonged to the stress ratio of -0.75 rather than -0.9 and further increases in stress ratio shifted the ratcheting data to lower magnitudes. In figure 4.10c similarly the highest magnitude of ratcheting strain data was achieved at stress ratio of -0.65 and stress ratio of

-0.5 corresponded to the lowest magnitudes of ratcheting strains. Such difference in ratcheting response at various stress ratios in 42CrMo (figure 4.10b) and 316L steel (figure 4.10c) samples can be attributed to the type of heat-treatment, cyclic softening/hardening response of materials and the involvement of ratcheting rate coefficients in evaluating the ratcheting response of materials over stress cycles.

4.3. The modified hardening rule and ratcheting assessment under step-loading conditions

The capability of modified hardening rule to characterize ratcheting response of materials subjected to multi-step uniaxial stress cycles is examined. The modified hardening rule was developed based on A-F hardening rule through implementing new ratcheting rate dependent coefficients γ_2 and δ. These coefficients are estimated by means of calibrated curves for any given stress levels defined from the uniaxial single-step ratcheting response at various cyclic stress levels. At a constant mean stress, ratcheting strain progressively increases as stress amplitude over steps of loading history increased. Similar response is also evident for step-loading with constant stress amplitude while the values of mean stress increase. Modified hardening rule is also examined to characterize trend of ratcheting strain for histories with decreasing trend in mean stress values or in stress amplitudes over load steps.

4.3.1. Materials and experimentation

To evaluate the capability of the modified hardening rule in assessing the single/multi-step ratcheting response of materials over stress cycles, four steel alloys of SS316L, SA333, SS316L(N) and 1070 were cyclically loaded under stress-controlled condition at room temperature [11, 38, 74-78]. Uniaxial tests were performed at various stress amplitude, mean stress, and loading histories affecting the ratcheting response of materials. Table 4.5 presents materials properties and ratcheting coefficients C and γ_1 employed in this study.

Table 4.5 Mechanical properties and material dependent ratcheting coefficients

Material	E (GPa)	σ_y (MPa)	C(GPa)	γ_1
SS316L [74-75]	190	175	20	150
SA333 [38, 76]	203	190	60	200
SS316L(N) [77]	210	205	45	650
1070 [11, 78]	210	250	150	420

Tubular test specimens with 7mm gauge diameter and 13mm gauge length of SA333 alloy were tested at stress rate of 50MPa/s. Tests were performed by a 100KN closed loop INSTRON servo-electric testing machine. Cylindrical solid test samples of SS316L(N) steel alloy consisted of gauge length of 23mm and diameter of 8.8mm underwent triangular cyclic loads at the rate of 10MPa/s using 1362 INSTRON servo-mechanic testing machine. Solid test specimens of SS316L steel alloy with gauge length of 30mm and diameter of 10mm were tested under uniaxial cyclic stress rates of 52MPa/s using a MTS809-250KN test machine. The solid test sample bars of 1070 with 12.7mm gauge length and diameter of 10.5mm were subjected to sinusoidal cyclic loading conditions using a 100KN closed loop servo-hydraulic testing system with a frequency of 0.5Hz [11, 38, 74-78]. Stress levels of test samples for single/multi-step loading histories were presented in Table 4.6.

Table 4.6 Uniaxial loading histories of single- and multi-step loading conditions for SS316L, SA333, SS316L(N) and 1070 steel alloys [11, 38, 74-78]

Materials	Test	Step1		Step2		Step3	
		$\sigma_{m1}\pm\sigma_{a1}$	N_1 (Cycle)	$\sigma_{m2}\pm\sigma_{a2}$	N_2 (Cycle)	$\sigma_{m3}\pm\sigma_{a3}$	N_3 (Cycle)
SS316L [74-75]	A1	52±195	20	---	---	---	---
	A2	52±247	100	---	---	---	---
	A3	52±273	100	---	---	---	---
	A4	64±247	200	---	---	---	---
	A5	76±242	200	---	---	---	---
	A6	52±247	100	78±247	100	---	---
SA333 [38, 76]	B1	40±310	500	---	---	---	---
	B2	40±350	1000	---	---	---	---
	B3	80±270	3000	---	---	---	---
	B4	80±310	300	---	---	---	---
	B5	80±350	3000	---	---	---	---
	B6	120±350	2500	---	---	---	---
	B7	40±350	776	80±350	1832	120±350	4584
SS316L(N) [77]	C1	10±210	1000	---	---	---	---
	C2	10±230	1000	---	---	---	---
	C3	10±250	1000	---	---	---	---
	C4	30±230	1000	---	---	---	---
	C5	30±250	1000	---	---	---	---
	C6	10±210	100	10±230	900	---	---
	C7	30±210	100	30±230	900	---	---
	C8	30±210	100	30±250	900	---	---
	C9	30±230	100	30±250	900	---	---
	C10	10±210	100	30±210	900	---	---
	C11	10±210	100	30±230	900	---	---
	C12	10±210	100	30±250	900	---	---
	C13	30±230	100	10±230	900	---	---
	C14	30±230	100	10±210	900	---	---
	C15	30±250	100	10±230	900	---	---
	C16	30±230	100	30±210	900	---	---
1070 [11, 78]	D1	280±375	520	---	---	---	---
	D2	78±403	2050	---	---	---	---
	D3	208±403	4100	---	---	---	---
	D4	208±396	65	---	---	---	---
	D5	204±396	65	78±396	16400	---	---
	D6	208±403	4100	78±403	4100	---	---
	D7	-211±405	4100	-77±437	6200	---	---
	D8	280±375	520	280±425	520	280±375	520
	D9	78±403	2050	202±395	4100	77±391	8200

4.3.2. Verification of the modified hardening rule

4.3.2.1. Low-high step loading condition in SS316L steel alloy

Ratcheting response of SS316L steel alloy undergoing various uniaxial loading histories with different stress levels was characterized by the modified hardening rule. Figure 4.11

presents the predicted and the experimental ratcheting strain values in SS316L steel samples tested at various stress levels for single-step loading histories A1-A5. At constant mean stress of 52MPa, both ratcheting strain data/curves shifted up as the magnitude of stress amplitude increased (figure 4.11a). Figure 4.11b also presents the ratcheting response of 316L steel samples tested at nearly the same stress amplitude and different values of mean stress magnitudes. Since the stress level in both ratcheting tests presented in this figure are close in magnitude, ratcheting diagrams and data overlap each other.

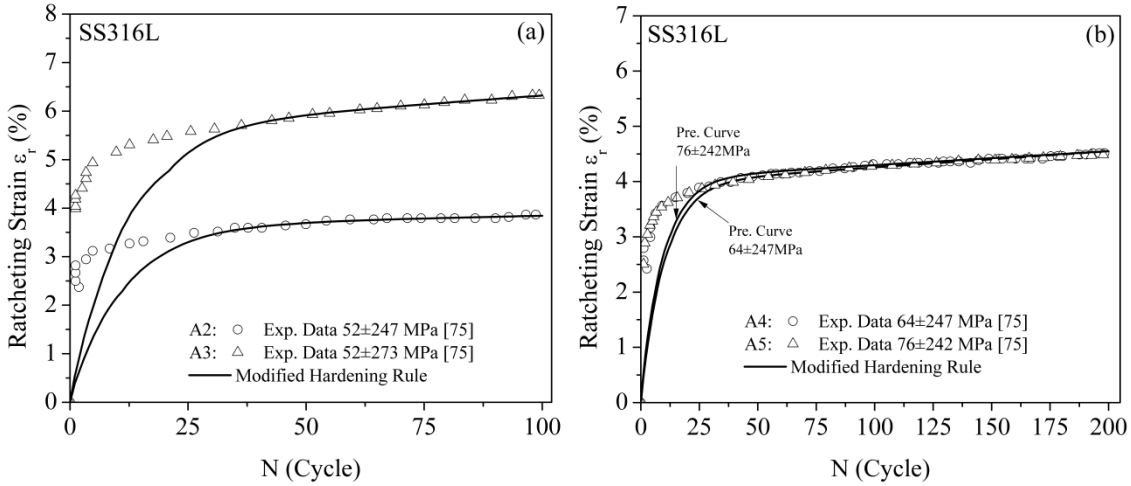

Figure 4.11 Predicted ratcheting strain based on the modified hardening rule versus the experimental data over stress cycles for SS316L steel alloy.

Material and stress dependent coefficients γ_2 and δ in the modified hardening rule play a crucial role to control the ratcheting strain rate in different loading conditions. Figure 4.12 presents variations of these coefficients over stress amplitudes for various constant mean stress curves. A family curve has been constructed from ratcheting strains obtained over uniaxial stress cycles at various stress amplitudes and mean stresses. Curves in figure 4.12 converged and met each other at materials yield stress level and showed decreasing trends as stress amplitude increased. For coefficient γ_2 as the magnitude of mean stress increased the family curves were shifted up while corresponding coefficient δ decreased in magnitude. This readily enabled estimating both γ_2 and δ coefficients for any given stress levels on the curves or by means of interpolation if the curve for the desired stress level is not given among calibration curves. Dashed-curves were interpolated from the continuous master curves which first were plotted to

correlate coefficients γ_2 and δ with tests conducted at various stress amplitudes and constant mean stresses.

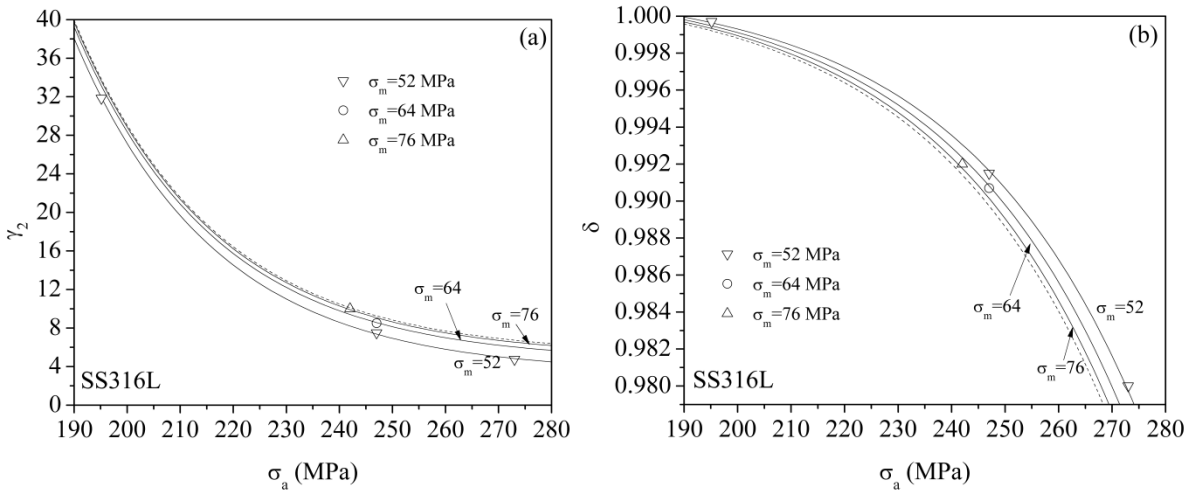

Figure 4.12 Family curves representing the variations of (a) coefficient γ_2 and (b) coefficient δ versus different mean stress and stress amplitude values for SS316L

A set of two-step low-high loading test (A6) with ascending mean stress values as stress amplitude stayed constant is listed in Table 4.6. The low-high loading sequence refers to a testing condition in which a lower mean stress in the first load step is followed by higher value of mean stress applied to the test sample in the second load step as stress amplitude stays unchanged. Over the first 100 cycles, SS316L steel sample is subjected to 52±247MPa followed by the same number of cycles at a higher applied stress level 78±247MPa. Figure 4.13 presents the predicted and experimental ratcheting strain values over two-step low-high loading condition. Both experimental and predicted ratcheting values closely agreed in this figure. A progressive ratcheting strain is evident in this figure as the mean stress value increased from 52MPa to 78MPa. Based on the estimated coefficients γ_2 and δ from calibration curves (see figure 4.12), the modified hardening rule was adapted to predict low-high sequence of step loading for SS316L steel alloy.

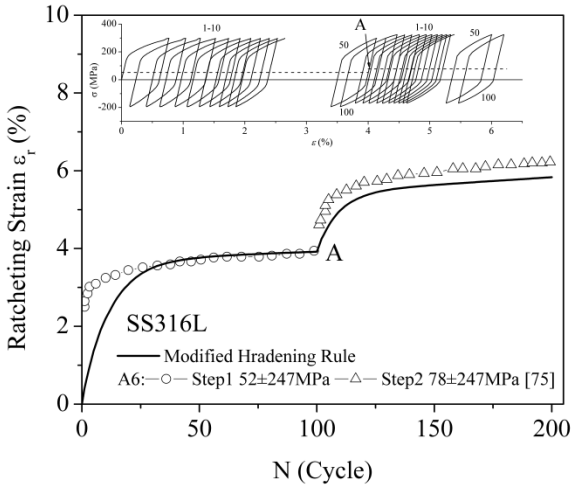

Figure 4.13 Predicted and experimental ratcheting strain values over two-step low-high loading sequence in SS316L steel alloy

4.3.2.2. Low-high step loading condition in SA333 steel alloy

Figure 4.14 presents ratcheting data obtained from single loading tests at various stress levels. As the magnitude of stress amplitude increased (figure 4.14a), ratcheting curves for SA333 steel samples with constant mean stresses shifted up. Such progressive increase in ratcheting response of the material is also evident in figure 4.14b as mean stresses increase in magnitude and the stress amplitude stays unchanged.

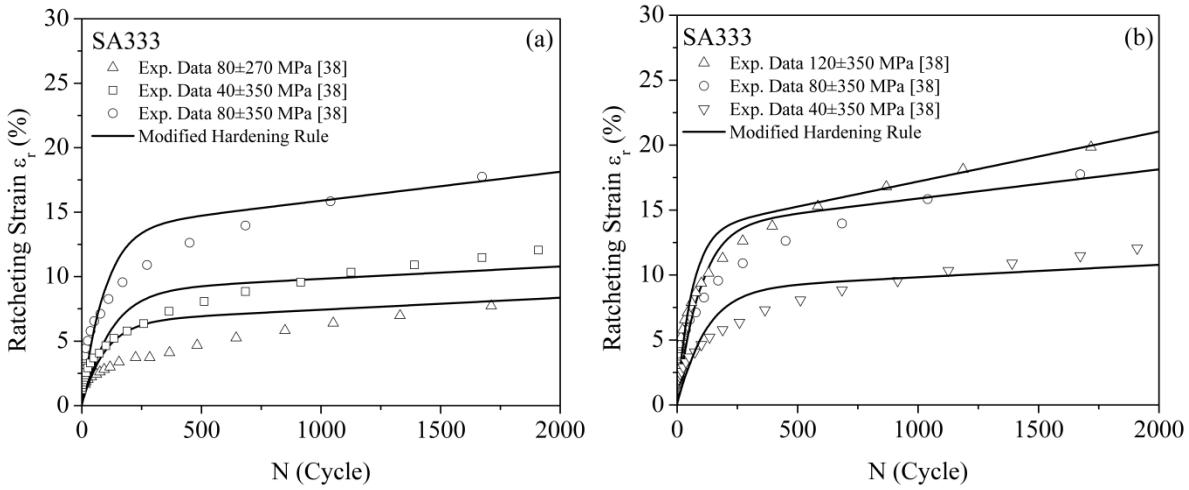

Figure 4.14 Predicted ratcheting strain based on the modified hardening rule versus the experimental data over stress cycles for SA333 steel alloy.

Calibrating family curves were constructed to determine coefficients γ_2 and δ at various mean stress and stress amplitude values in figure 4.15. In this figure at a constant mean stress, as

the magnitude of the stress amplitude increased coefficients γ_2 and δ dropped in magnitudes. The calibration curves were used to predict ratcheting response of SA333 steel alloy tested over a three low-high increasing load steps listed as B7 test in Table 4.6.

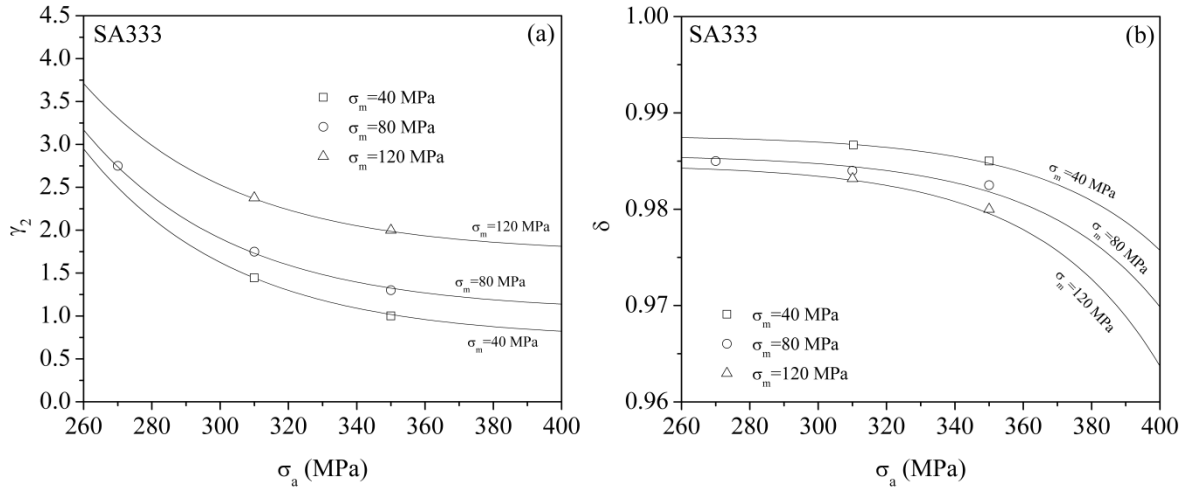

Figure 4.15 Family curves representing the variations of (a) coefficient γ_2 and (b) coefficient δ versus different mean and amplitude stress values for SA333

Figure 4.16 shows how closely the modified hardening rule predicted ratcheting strain over stress cycles in each load step of history B7 when compared with experimental ratcheting strain over three increasing low-high load steps. The load history consisted of constant stress amplitudes of 350MPa with varying mean stress in ascending order of 40, 80 and 120MPa. Ratcheting strain accumulated progressively while the rate of ratcheting decreased as number of cycles advanced. In each step of loading, the modified hardening rule was adjusted to predict ratcheting strain by estimated coefficients γ_2 and δ from the calibration curves constructed based on single load histories (figure 4.15). Change in stress levels (load steps) in figure 4.16 is referenced by A and B.

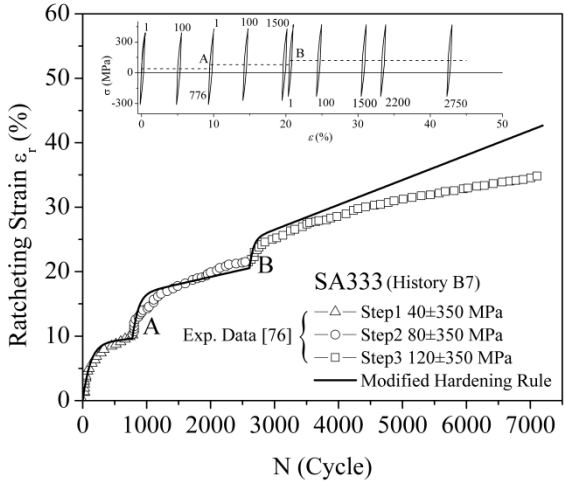

Figure 4.16 Predicted and experimental ratcheting strain values for SA333 Steel alloy under three-step loading condition with increasing (low-high) stress levels

4.3.2.3. Low-high and high-low step loading conditions in SS316L(N) steel alloy

Ratcheting response of 316L(N) steel samples tested under uniaxial single-step loading conditions was evaluated based on the modified hardening rule (Equation (3.13)). Figure 4.17 plots predicted ratcheting curves and those of experimentally obtained for 316L(N) steel samples. At constant mean stress of 10MPa, ratcheting curves shifted up with an increase in stress amplitudes (210, 230 and 250MPa). This shift is also more noticeable at constant stress amplitude of 250MPa as mean stress increases from 10MPa to 30MPa.

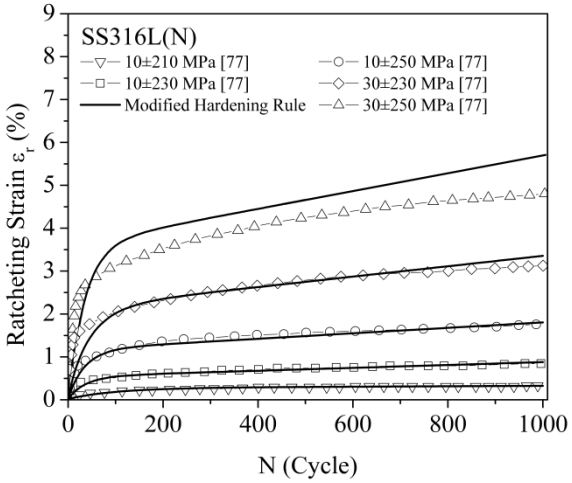

Figure 4.17 Predicted ratcheting strain based on the modified hardening rule versus the experimental data over stress cycles for SS316L(N) steel samples

Corresponding coefficients γ_2 and δ in the predicted ratcheting curves in figure 4.17 were employed to construct calibration curves at various stress levels as shown in figure 4.18. Calibration curves were then employed to predict ratcheting strain values over load steps. These curves in figure 4.18 depict a decreasing trend of coefficients γ_2 and δ as stress amplitude increased at a given mean stress. Constant δ varied in descending pattern as both mean stress and stress amplitude increased.

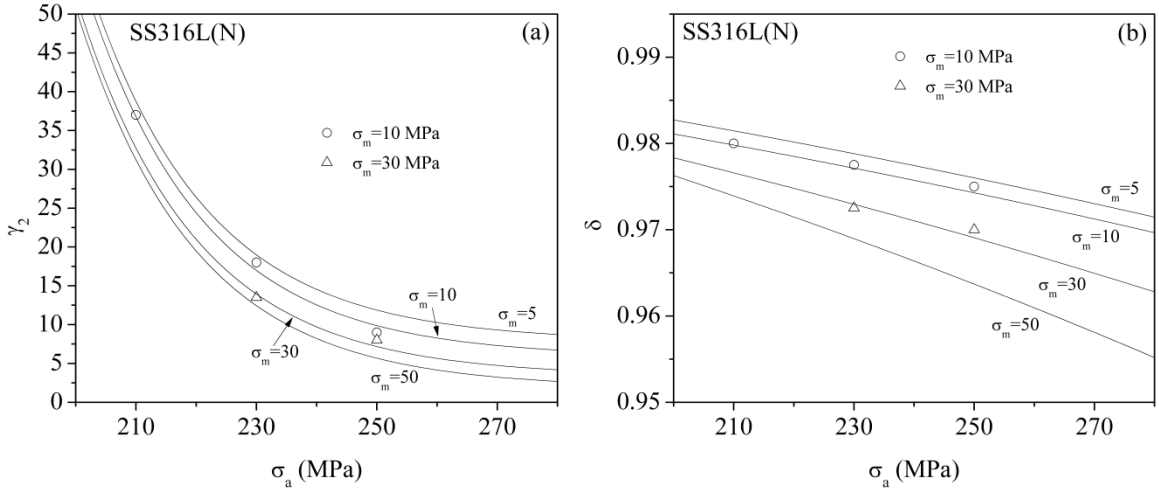

Figure 4.18 Family curves representing the variations of (a) coefficient γ_2 and (b) coefficient δ versus different mean and amplitude stress values for SS316L(N)

Two-step ratcheting tests were performed on SS316L(N) steel samples at different loading sequences of low-high and high-low loading conditions. The modified hardening rule was employed to assess two-step ratcheting response for both dissimilar loading histories. Figure 4.19 presents the predicted ratcheting strain values of SS316L(N) samples based on the modified hardening rule and compares them with experimental data obtained at various stress levels with low-high and high-low loading histories. Figures 4.19a and 4.19b verify that at constant stress amplitude, ratcheting data/curves shift up with an increase in mean stress. The influence of increase in mean stress while stress amplitude stays constant is more prononced in shifting the ratcheting data/curves in figure 4.19a. In this figure, C6 and C7 histories consisted of constant stress amplitudes of 210MPa and 230MPa respectively while magnitude of mean stress over load steps 1 and 2 increased from 10MPa to 30MPa. In figure 4.19c, the ratcheting strain values for all three tests C10, C11 and C12 are identical as the first step in these histories stays the same for its stress levels. Over the second step of loading, an increase in stress amplitude and mean stress

level shifted up the predicted and the experimental ratcheting values for SS316L(N) samples. Ratcheting data predicted in figure 4.19d were obtained through high-low step loading at which both mean stress and stress amplitude drop in magnitude from first step to the second step of loading. Histories C13-C15 consisted of a mean stress level of 30MPa during the first step of loading which reduced to lower magnitude in step 2. The predicted ratcheting response encountered a change in the magnitude of backstress as the stress level droped in the subsequent loading step forming a small peak. The small peaks of experimental data just before the ratcheting progress transits to the second step of loading is evident in figure 4.19d. Figures 4.19e and 4.20f present how influential the sequence of load steps is on the ratcheting response of SS316L(N) steel samples. Histories C7, C9 and C16 in figures 4.19e and 4.19f correspond to low-high and high-low step loads at a constant mean stress of 30MPa and various stress amplitudes. In figure 4.19f the sequence change in the first and second steps of histories C7 and C16 resulted in a noticeable difference in ratcheting strain values.

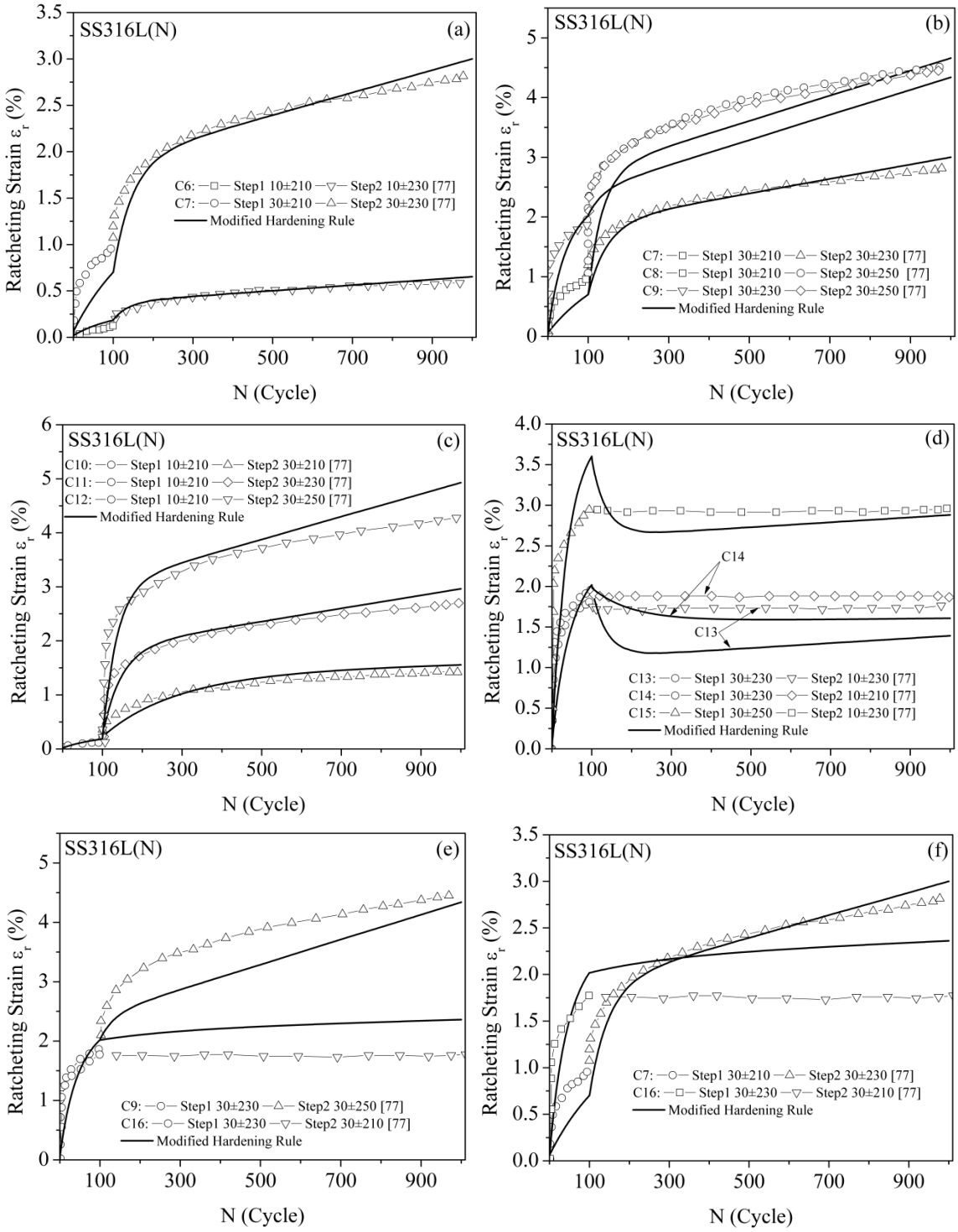

Figure 4.19 Predicted and experimental ratcheting strain values for SS316L(N) Steel alloy under two-step loading with low-high (a-c) and high-low (d-f) sequences

4.3.2.4. Low-high, high-low and low-high-low step loading conditions in 1070 steel alloy

Ratcheting curves of 1070 steel samples predicted by the modified hardening rule were compared with those of experimentally obtained ratcheting data in figure 4.20. These steel samples tested under uniaxial single-step loading histories at different stress levels. Both the predicted and the experimental ratcheting strains in this figure were found in close agreements.

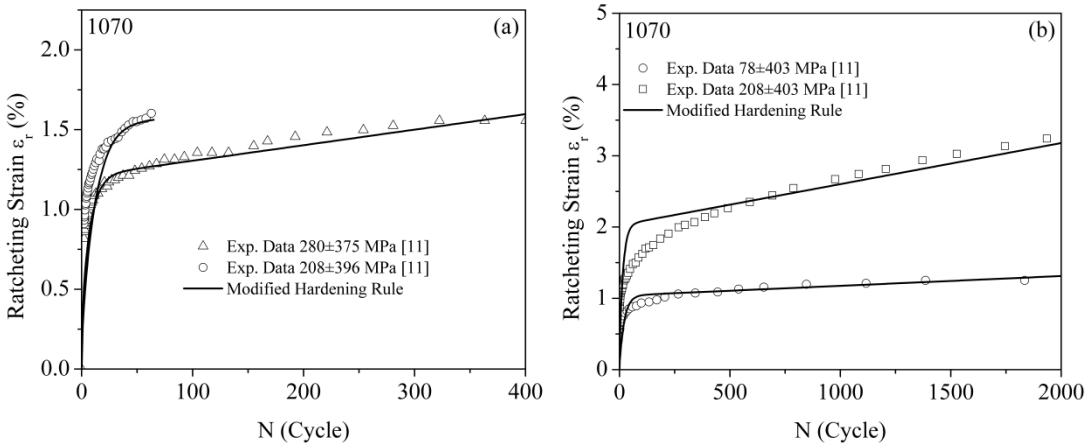

Figure 4.20 Predicted ratcheting strain based on the modified hardening versus the experimental data over stress cycles for 1070 steel alloy

Calibration master curves for 1070 steel alloy were constructed based on single-step uniaxial histories. Coefficients γ_2 and δ were then taken for stress level of interest to predict ratcheting strain values over stress cycles. The family of calibration curves for 1070 steel alloy is presented in figure 4.21.

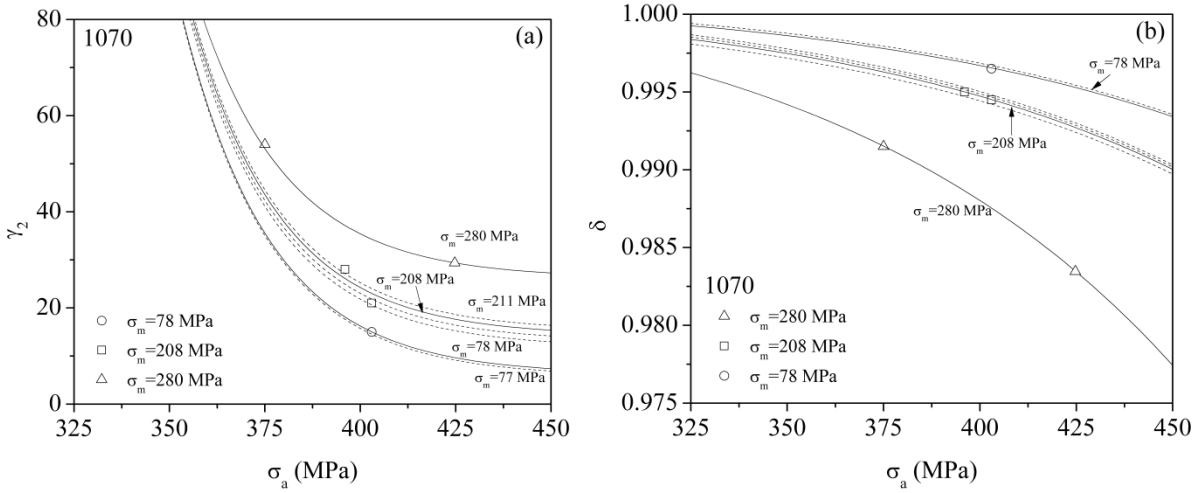

Figure 4.21 Family curves representing the variations of (a) coefficient γ_2 and (b) coefficient δ for different mean stress and stress amplitude values for 1070 steel

Samples made of 1070 steel alloy were tested at high-low load histories of D5 and D6, high-low load history of D7 consists of compressive mean stresses over load steps and load history of D8 with a three-step low-high-low loading sequence at a constant mean stress of 280MPa [78]. A three-step low-high-low load sequence D9 was also performed [78] at a nearly constant stress amplitude while mean stress values changed through steps from 78 to 202 and then 77MPa. Calibrated master curves (figure 4.21) have been employed to estimate coefficients γ_2 and δ required to assess ratcheting response in histories D5-D9. Figure 4.22 presents the capability of the modified hardening rule in ratcheting assessment of 1070 steel samples tested at various low-high (figure 4.22a), high-low (figure 4.22b and 4.22c), compressive high-low (figure 4.22d) and low-high-low (figure 4.22e) sequences. Change in stress levels (load steps) in figure 4.22 is referenced by A and B. Figure 4.22 presents the ratcheting progress over load steps and its increasing or decreasing trends through stress cycles over each load step within histories. In figure 4.22a, the increasing trend of ratcheting response is evident by both the predicted and the experimental ratcheting results verifying the fact that ratcheting strains are accumulated over and within each load step progressively. Ratcheting response within the first load step in figures 4.22b and 4.22c showed a good agreement between the predicted and the experimental results. Over the second step, the modified hardening rule successfully lowered the ratcheting agreeable with the experimental data due to a drop in mean stress magnitude in histories D5 and D6. Predicted ratcheting results over the first load step in figure 4.22d and the first two load steps in figure 4.22e well agreed with the experimental data in histories D7 and D9 respectively. The last load step in histories D5, D6, D7 and D8 presents a change in direction of ratcheting progress over stress cycles. The change in direction of predicted value over the second step of these load histories verifies the capability of the modified hardening rule. The last load step in figures 4.19d-4.19e shows a difference in the predicted ratcheting curves from the experimental data with an order of up to 25%. This discrepancy is observed when mean stress or stress amplitude drops over subsequent loading steps.

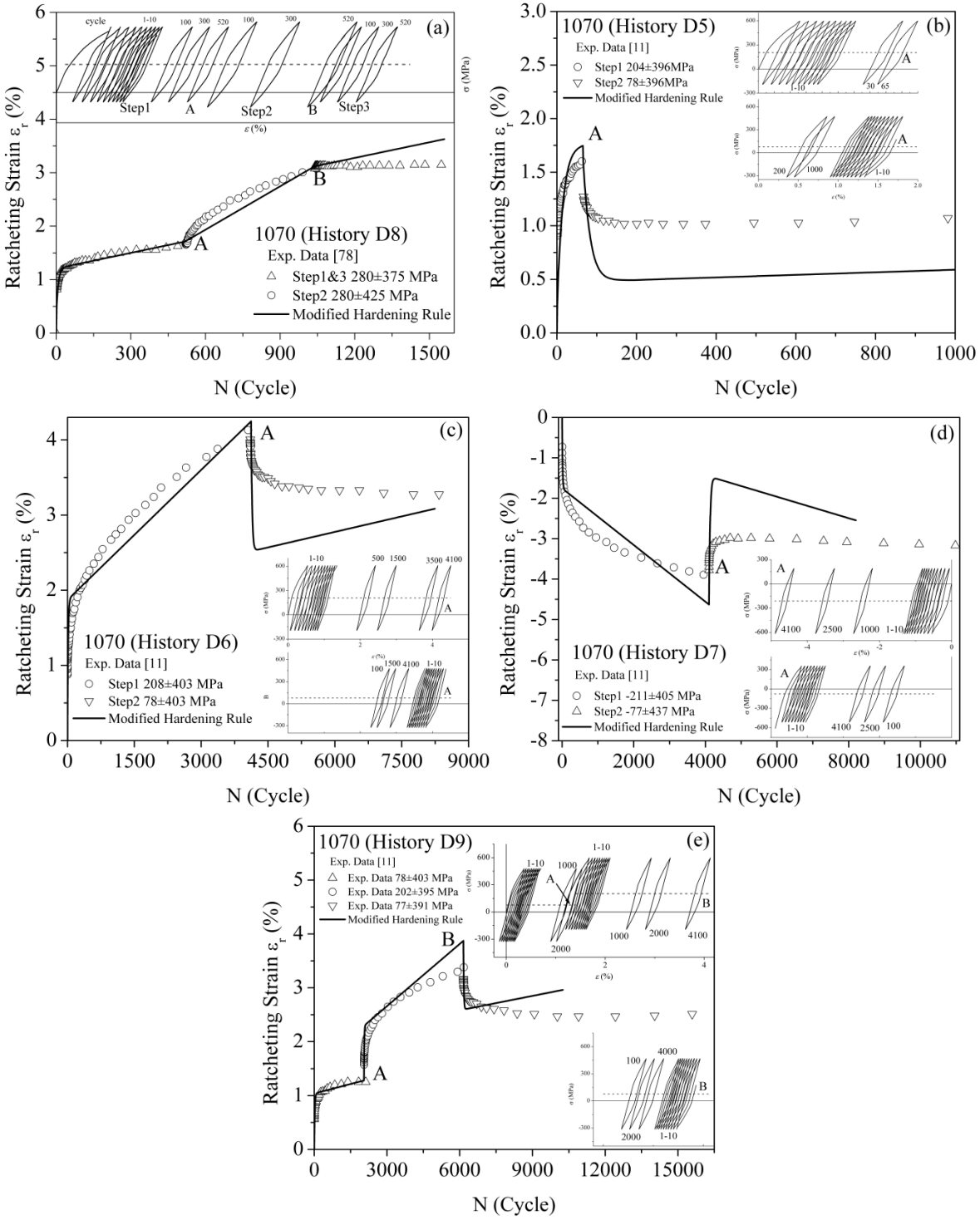

Figure 4.22 Predicted and experimental ratcheting strain values for 1070 Steel alloy under two-step loading with low-high, high-low and three-step loading with low-high-low sequences

4.4. Concurrent ratcheting-fatigue damage analysis

In this section, the concurrent interaction of fatigue damage and ratcheting strain in two steel alloys of 42CrMo and 1020 over uniaxial stress cycles is investigated. The interaction of ratcheting and fatigue damage is defined based on mechanistic parameters involving the effects of mean stress, stress amplitude, and cyclic softening/hardening response of materials. The extent of ratcheting effect is defined by the product of normalized average ratcheting strain rate and maximum cyclic stress, while fatigue damage is analysed based on earlier developed energy-based models of Xia-Kujawski-Ellyin and Smith-Watson-Topper. Overall damage due to ratcheting and fatigue is calibrated through a weighting factor at various mean stress and cyclic stress amplitudes. The estimated lives at different mean stresses and stress amplitudes for 42CrMo and 1020 are compared with those of uniaxially tested.

4.4.1. Materials and testing conditions

In order to evaluate the overall damage of materials under stress cycles, two different materials of 42CrMo and 1020 steel alloys were cyclically loaded under stress-controlled conditions at various mean and amplitude stresses [30,72].Table 4.7 presents fatigue properties of these materials.

Table 4.7 Material and cyclic properties

Material	E (GPa)	σ_y (MPa)	K (MPa)	σ'_f (MPa)	ε'_f	b	c	n
42CrMo [79]	190.5	310	637	894	19.095	-0.094	-0.936	0.097
1020 [79]	203	300	1221	895	0.29	-0.11	-0.47	0.24

Test sample bars of 42CrMo and 1020 steel alloys consisted of 30 mm gauge length and diameter of 10 mm [30,72]. All tests in 42CrMo and 1020 steels were performed under the stress-controlled condition at room temperature. 42CrMo and 1020 steel samples were cyclically tested using a MTS809-250KN test machine with stress rates of 500 MPa/s and 400MPa/s respectively [30,72].

4.4.2. Ratcheting strain data over stress cycles

A typical ratcheting deformation over stress cycles and their corresponding stress-strain hysteresis loops in 42CrMo and 1020 steels are presented in figure 4.23. Over stress cycles ratcheting strain/deformation is accumulated and at longer number of cycles, the subsequent hysteresis loops show slower rate of ratcheting and closeness of loops resulting in a failure at N_f =6130 and N_f =530 cycles for 42CrMo and 1020 steel alloys, respectively.

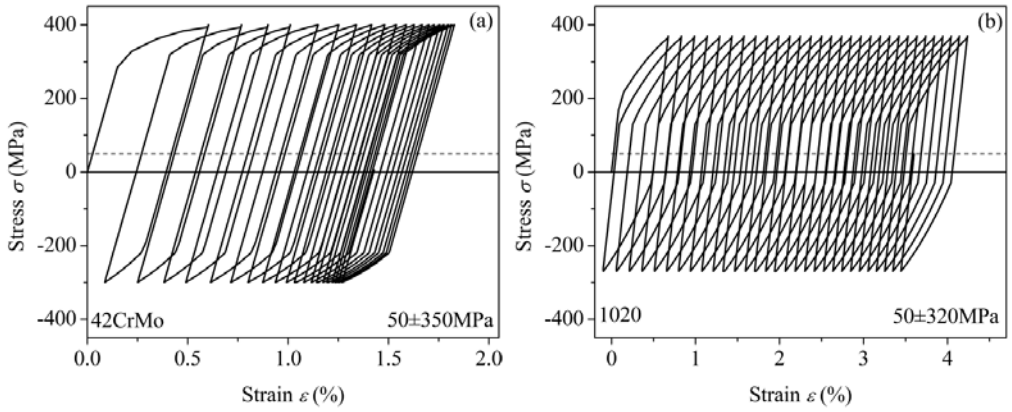

Figure 4.23 Ratcheting response and the corresponding stress-strain hysteresis loops in asymmetrical cyclic stress conditions for (a) 42CrMo and (b) 1020 steel alloys for given stress levels [30,72].

Figure 4.24 represents ratcheting strain values characterized by modified hardening rule and compared with those of obtained experimentally over stress cycles for 42CrMo [30] and 1020 [72] steel alloys at various mean and amplitude stresses.

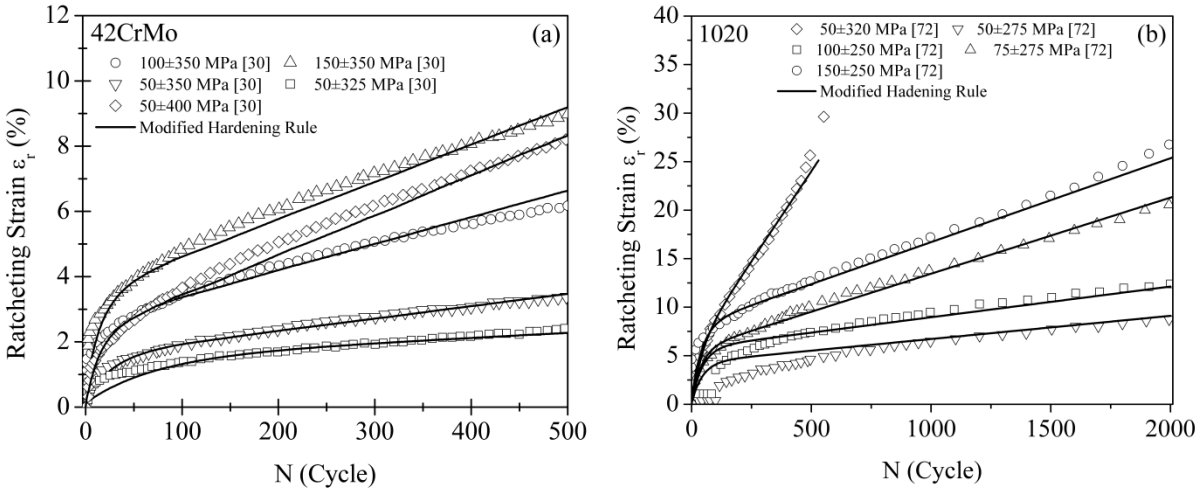

Figure 4.24 Comparison of predicted ratcheting strain with experimental ratcheting data over stress cycles for a) 42CrMo [30] b) 1020 [72] steel alloys

4.4.3. Verification of the overall damage assessment method and results

To evaluate the capability of damage assessment method presented in this research, two different steel alloys of 42CrMo and 1020 were examined. Ratcheting plastic strain and fatigue damage of alloys undergoing stress-controlled cyclic tests were used to assess overall damage of steel alloys when the concurrent ratcheting deformation and fatigue damage were coupled. Two different approaches were examined to assess the overall ratcheting-fatigue damage. In the first approach, ratcheting damage calculated based on the experimental ratcheting strain was integrated with Xia et al. and SWT fatigue damage models to determine the overall damage of 42CrMo and 1020 steel alloys. In the second approach, ratcheting damage was evaluated based on the modified hardening rule. Ratcheting strain of 42CrMo and 1020 steel alloys were predicted based on the modified hardening rule and then Xia et al. and SWT fatigue damage models were coupled to assess overall damage and to estimate life of materials.

To evaluate ratcheting damage component, the average ratcheting strain rate $\dot{\varepsilon}^r_{avg}$ and $\varepsilon^r_{(0-N_f)}$ were calculated over stress cycles and the ratcheting strain damage (D_r) was related to number of cycles through the power-law equation (3.14). Coefficients of this equation were determined from the best fitted curve of the values of $\left(\sigma_{\max}\dfrac{\dot{\varepsilon}^r_{avg}}{\varepsilon^r_{(0-N_f)}}\right)$ versus N_f obtained based on two approaches of the experimental ratcheting strain values and predicted ratcheting strain by means of the modified hardening rule. The modified hardening rule described in chapter 3 was employed to predict ratcheting strain of 42CrMo and 1020 steel alloys. Figure 4.24 represents ratcheting strain values characterized by the modified hardening rule and compared with those of experimentally obtained over stress cycles for 42CrMo [30] and 1020 [72] steel alloys at various mean and amplitude stresses. Terms $\dot{\varepsilon}^r_{avg}$ and $\varepsilon^r_{(0-N_f)}$ were calculated from the predicted ratcheting strain values over stress cycles. The product of the ratio of these terms $\left(\dot{\varepsilon}^r_{avg}\,/\,\varepsilon^r_{(0-N_f)}\right)$ and the maximum stress was related to the life of components through the power-law equation (3.14). The obtained coefficients used for 42CrMo and 1020 steel alloys are listed in Table 4.8. Equation (3.14) corresponds to the normalized average ratcheting strain rate and the applied maximum stress presenting damage and deformation dominantly induced due to ratcheting

phenomenon over stress cycles. The curve of ratcheting damage against number of cycles corresponds to the lower bound curve.

Table 4.8 Ratcheting damage coefficients employed in equation (3.14) for different materials estimated based on the experimental and predicted ratcheting strain values

Material	Based on exp. Ratcheting			Based on pre. ratcheting		
	k_r	χ	C_r	k_r	χ	C_r
42CrMo	4.3×10^5	-1.8	0.04	1.5×10^5	-1.65	0.05
1020	10000	-1.31	0.05	2.7×10^6	-2.1	0.0055

Damage due to fatigue cycles D_m is estimated from energy-based criteria discussed in section 3.4.2.1 and 3.4.2.2. The right-hand side of equations (3.18) and (3.21) relates the damage values calculated using energy-based models to fatigue life N_f through a power-law equation. Coefficients of equations (3.18) and (3.21) are listed in Table 4.9.

Table 4.9 Fatigue damage coefficients employed in equations (3.18) and (3.21) for different materials

Materials	Xia et al. constants			SWT constants			
	k_m	λ	C_m	P	ρ	Q	β
42CrMo	9522000	-1.625	0.6877	4.195	-0.188	17071	-1.03
1020	1.3×10^6	-1.53	1.8	3.946	-0.22	256	-0.58

It should be noted that the coefficient based on the Xia et al. listed in Table 4.9 are determined based on fully reversed uniaxial cyclic data described in reference [57]. Changes in mean and amplitude stresses result in a family of D_m-N_f curves at which their coefficients vary with mean and amplitude stresses. For fully reversed where the mean stress is zero, D_m-N_f curve is considered as the upper bound curve. Various tests with different mean and amplitude stresses along with corresponding ratios of (σ_m/σ_a) have been listed in Table 4.10.

Table 4.10 Fatigue test parameters and results of 42CrMo [30] and 1020 [72] steels

Materials	σ_m (MPa)	σ_a (MPa)	σ_m/σ_a	D_{exp} (MPa) (Xia et al.)	D_{exp} (MPa) (SWT)	N_f (Cycles)
42CrMo	20	380	0.053	6.48	2.74	4000
[30]	21	404	0.053	12.06	4.76	2400
	80	320	0.25	1.18	1.0	11500
	85	340	0.25	2.07	1.42	7500
	150	350	0.43	2.80	1.96	2900
	120	280	0.43	0.45	0.67	11500
	50	350	0.143	2.75	1.57	6130
	100	350	0.285	2.77	1.76	4560
	100	325	0.307	1.36	1.14	7300
	100	300	0.333	0.70	0.80	10600
1020	295	50	0.18	2.17	1.429	5090
[72]	275	50	0.18	1.56	1.093	12065
	250	100	0.4	1.01	0.903	9050
	225	100	0.4	0.64	0.643	23715
	250	150	0.6	1.51	1.032	2100

Sets of experimental results with various (σ_m/σ_a) ratios have been examined. Weighting factors for each ratio have been calculated from experimental data representing the steady value and both upper and lower bound curves. Figure 4.25 plots damage curves of D_r and D_m over life cycles as the lower and the upper bounds representing equations (3.14) and (3.18) or (3.21), respectively. The upper bound curve D_m-N_f was constructed for fully reversed loading condition (σ_m=0) at which fatigue damage was dominant. The lower bound curve D_r-N_f on the other hand corresponded to pure ratcheting damage. The predicted curves placed between these two bounds represent a family of D_m-N_f curves constructed for various non-zero (σ_m/σ_a) ratios in 42CrMo and 1020 steels. Figures 4.25a and 4.25b show that the predicted curves falling between the upper and the lower damage bounds with σ_m/σ_a ratios of 0.053, 0.25, and 0.43 for 42CrMo steel samples. Figures 4.25c and 4.25d plot the lower and the upper curves for 1020 samples for σ_m/σ_a ratios of 0.18, 0.4 and 0.6. The experimental ratcheting-fatigue damage data (listed in Table 4.10) fall on the predicted curves between the upper and lower bounds. In figure 4.25 both the experimental and the predicted ratcheting damage D_r (the lower bound curves) are respectively presented as solid and dashed curves. Ratcheting damage curve predicted based on the modified hardening rule was found in a close agreement with that of obtained experimentally

for both 42CrMo and 1020 steel samples. Family of curves indicating overall damage for various (σ_m/σ_a) ratios based on the experimental and the predicted ratcheting strains was plotted in solid and dashed curves, respectively. These curves were constructed based on the different weighting factors ξ through equation (3.15).

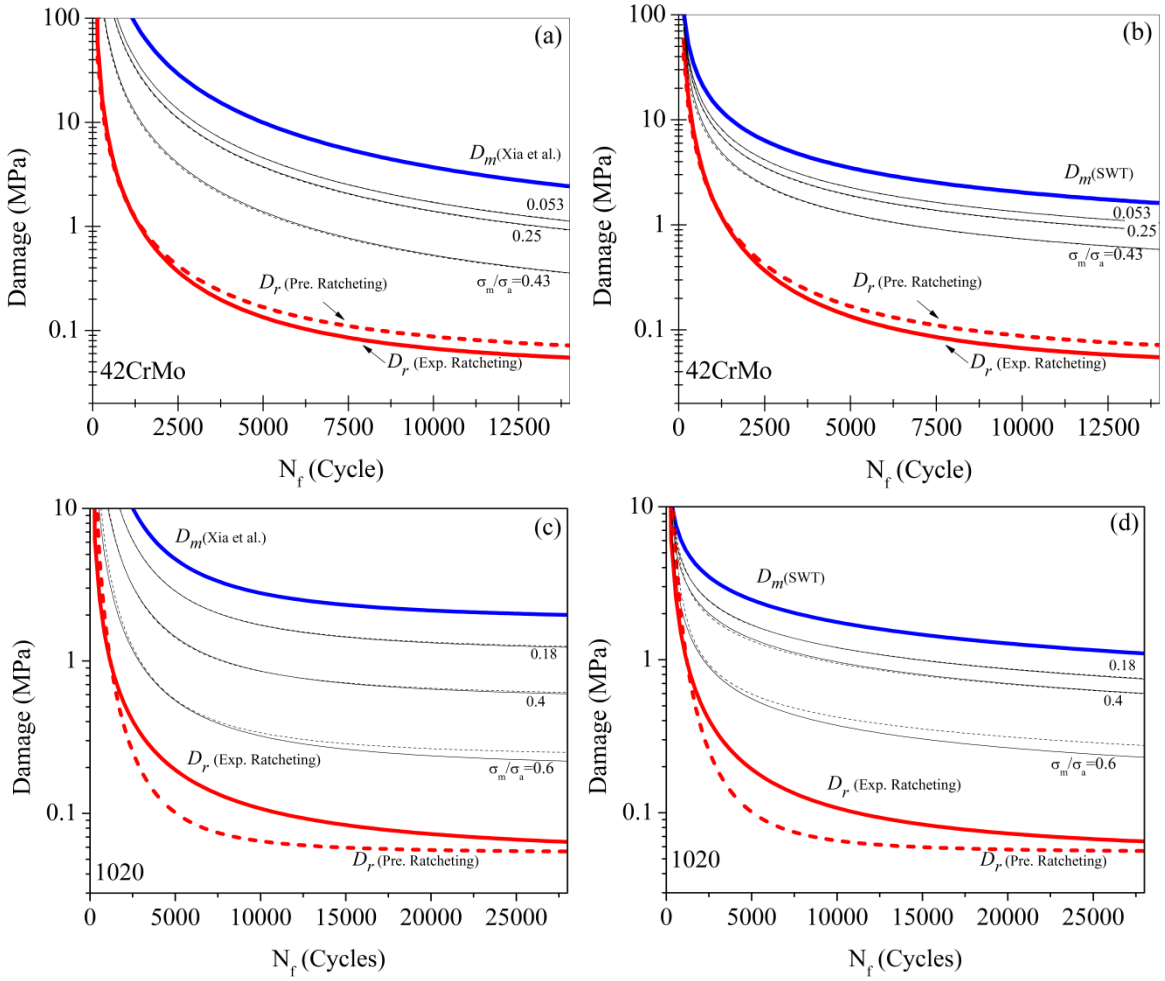

Figure 4.25 Predicted overall damage vs life cycles for 42CrMo and 1020 steels based on Xia et al. (a,c) and SWT (b,d) at different σ_m/σ_a ratios.

4.4.4. Weighting factor ξ versus σ_m/σ_a ratio and overall life estimation

Predicted overall damage curves were found in good agreements with the coupled ratcheting-fatigue damage experimental data tested in 42CrMo and 1020 steel alloys. Figure 4.26 plots values of ξ at various (σ_m/σ_a) ratios employed to construct family curves based on Xia et al. and SWT fatigue damage models (D_m) and the ratcheting damage component (D_r). The lower bound ratcheting damage curves represent both the experimentally obtained ratcheting curve and

the predicted ratcheting curve by means of the modified hardening rule. Values of ξ evaluated by the predicted ratcheting damage were found in good agreement with those obtained from the experimental ratcheting data as shown in figure 4.26.

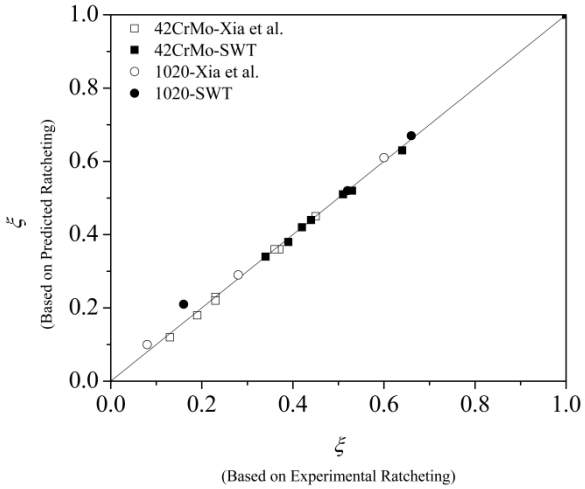

Figure 4.26 Evaluated factor ξ for different (σ_m/σ_a) ratios based on D_m (Xia et al. and SWT) and D_r for 42CrMo and 1020 steel alloys

The typical variations of factor ξ versus (σ_m/σ_a) ratio are plotted in figure 4.27 for 42CrMo and 1020 steel samples tested at various stress ratios.

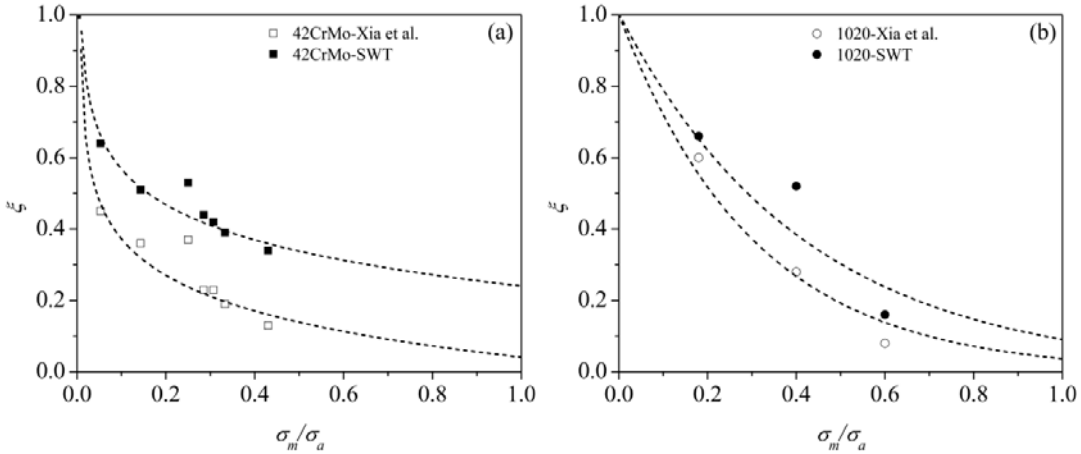

Figure 4.27 Variations of factor ξ versus (σ_m/σ_a) ratio for 42CrMo and 1020 steel alloys based on experimental ratcheting strain and Xia et al. and SWT damage models.

Figure 4.27 presents the trend of factor ξ as stress ratio (σ_m/σ_a) increases for both 42CrMo and 1020 steel alloys. The effect of ratcheting damage on the overall damage for both 42CrMo

and 1020 steel alloys is more pronounced when fatigue damage is assessed through Xia et al. model.

Lives of 42CrMo and 1020 steel samples were predicted based on SWT and Xia et al. fatigue damage models coupled with ratcheting damage evaluated based on the experimental and predicted ratcheting strain and were compared with the experimental life data of these materials tested under uniaxial loading conditions as shown in figure 4.28. To predict life data, ξ values were initially extracted from figure 4.27 for given (σ_m/σ_a) ratios. The curves of overall damage versus life cycles N_f were then constructed using equation (3.15). Life data corresponding to damage values for 42CrMo and 1020 steels listed in Table 4.10 were estimated from the generated curves. Predicted life data were found in good agreements as compared with experimental lives listed in this Table. These agreements fall within a factor of ±2 for predicted life data calculated based on Xia et al. and SWT energy-based damage models and ratcheting damage evaluated by means of the experimental and predicted ratcheting strain values.

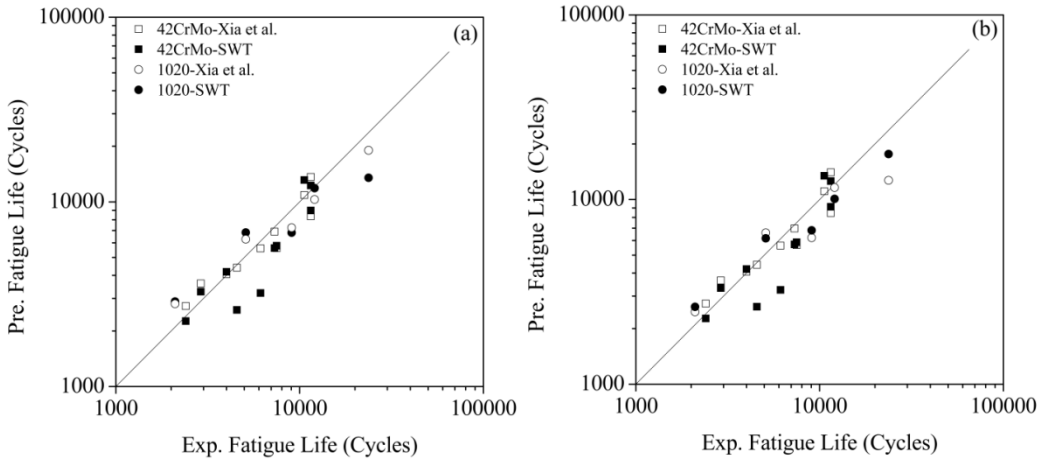

Figure 4.28 The predicted versus experimental lives for 42CrMo and 1020 steels based on Xia et al. and SWT damage models coupled with ratcheting damage evaluated based on a) the experimental and b) the predicted ratcheting strain

4.5. Summary

The formulation of ratcheting strain was defined based on affecting parameters including stress level, material properties and cyclic softening/hardening response of materials. Ratcheting response of steel and copper alloys was evaluated based on the mechanistic equation over uniaxial stress cycles at different mean stresses and stress amplitudes and then were compared with those of experimentally obtained values. The ratcheting strain response of materials was further characterized based on the modified hardening rule developed in this thesis based on the framework of A-F nonlinear hardening rule. Both the mechanistic equation and the modified hardening rule successfully addressed stages I and II of ratcheting strain progress at which ratcheting strain rate decay was followed by constant ratcheting strain rate.

Coefficients γ_2 and δ enabled the modified hardening rule to successfully predict ratcheting strain values between plastic shakedown of Bower's model and overestimated ratcheting response of materials by A-F model. The predicted ratcheting strain values based on the modified hardening rule were found in good agreements with the experimentally obtained ratcheting data over stages I and II for different steel and copper samples. The modified hardening rule was further examined to evaluate ratcheting response of steel alloys under multi-step loading spectra in section 4.3. Over multi-step loading conditions, subsequent load steps were considerably affected by previous load steps. Loading sequence affected ratcheting magnitude and its trend over stress cycles. Low-high loading sequence resulted in a progressive ratcheting process over load steps while high-low loading sequence restrained the ratcheting progress direction or reversed the direction of ratcheting strain. The modified hardening rule was employed to predict multi-step ratcheting strain of steel alloys undergoing load steps with low-high, high-low and low-high-low load histories. The modified hardening rule was employed for each step of load history. Calibration curves were used to estimate coefficients γ_2 and δ. The family of curves was constructed based on single-step ratcheting strain values for various mean stresses and stress amplitudes. Ratcheting strains for low-high stress steps were successfully predicted by the modified hardening rule. High-low loading sequences however resulted in an overestimated-reversed ratcheting strain for 316L(N) and 1070 steel samples respectively with magnitudes of 25% and 50% in the later load step.

The concurrent ratcheting-fatigue interaction in 42CrMo and 1020 steel samples undergoing uniaxial stress cycles was investigated in section 4.4. The interaction of ratcheting and fatigue damage was defined based on mechanistic parameters involving the effects of mean stress, stress amplitude, and cyclic softening/hardening response of materials. The modified kinematic hardening rule was employed to simulate ratcheting strain curve. Damage values generated by the ratcheting phenomenon was defined from the product of the normalized average ratcheting strain rate and the maximum cyclic stress, while fatigue damage was analysed based on energy-based models of Xia-Kujawski-Ellyin and Smith-Watson-Topper. An algorithm was developed to evaluate overall damage due to ratcheting and fatigue phenomena over stress cycles at various mean stresses and stress amplitudes. The estimated lives at different stress levels for 42CrMo and 1020 samples showed good agreements with those of experimentally obtained.

CHAPTER FIVE

DISCUSSION

5.1. Triphasic ratcheting strain prediction

Triphasic ratcheting response for 42CrMo, 20CS, SA333 steels and OFHC copper were evaluated under uniaxial cyclic loading. In figure 4.2 experimental and calculated ratcheting strain values of these materials were plotted over stress cycles. Both mean stress and stress amplitude magnitudes influence the evolution of ratcheting strain and variations of ratcheting strain rate over three stages of life cycles. Figure 4.2 also verifies that an increase in stress level (mean stress and stress amplitude) shifts the ratcheting strain curve to a higher level at shorter lifespan. This further expands the first and the second stages of ratcheting curve while the third stage occurs suddenly resulting in shortening the materials life. The effect of stress amplitude on the entire curve of ratcheting strain versus life cycles in 42CrMo steel was reported to be more influential than the mean stress impact [30]. Figure 4.2a shows a good agreement in predicted ratcheting strain values and experimental data. As shown in this figure, an increase in mean stress while stress amplitude is kept constant and equal to 350MPa leads to over estimation in ratcheting response of 42CrMo steel in the primary stage of ratcheting curve as well as reduction in ratcheting rate. At 50±400MPa loading condition, 42CrMo steel showed a reasonable agreement between the calculated and experimental ratcheting strain values over three stages.

For various amplitude stresses of σ_a= 275, 300, and 320MPa while mean stress is kept unchanged (σ_m= 50MPa), figure 4.2b presents how tightly the calculated ratcheting strain values agree with those of experimentally obtained. Ratcheting strain and ratcheting rate of 20CS increase when stress amplitude and mean stress increase [72]. As shown in this figure, as stress amplitude increases, ratcheting strain at the beginning of the second stage is started in lower

values however rate of ratcheting development in different level of stresses almost follows experimental data.

The accumulation of ratcheting strain with number of cycles for SA333 Gr.6 C-Mn is shown in figure 4.2c. This figure shows the accumulation of ratcheting strain as the number of cycles advances for the stress amplitude of 310MPa with mean stresses of 40MPa, 80MPa and 120MPa respectively. The mean stress influences the ratcheting strain rate and when the mean stress increases the ratcheting strain is accumulated in faster pace and shortens the lifespan. This figure shows good agreements between the predicted and the experimental ratcheting strain values in the very early stage and the last stage of the ratcheting curves.

The ratcheting behaviour of the annealed OFHC copper subjected to various mean stress and stress amplitudes was evaluated as shown in figure 4.2d. This figure depicts the calculated and the experimental ratcheting strain values from uniaxial cyclic tests with the amplitude stress values of 120, 140 and 160MPa and a constant mean stress of 50MPa. Experimentally obtained data of ratcheting strain over life cycles in this material verified that [28] at a constant mean stress as the stress amplitude increases the ratcheting strain rate notably increases at the stages I and III. The higher stress amplitude shortens the intermediate stage of ratcheting life span. Stage I of ratcheting strain curve in the annealed OFHC copper shows a sudden built up. Stage II initially consisted of a small slope and it increased over stress cycles within the intermediate region. Figure 4.2d shows good agreements between predicted ratcheting strain values over three stages.

In figure 4.2c, the calculated values of ratcheting strain in the intermediate stage of SA333 steel underestimate the experimental data. The deviation of the calculated and the experimental values of the ratcheting strain can be attributed to the stress rate at which SA333 steel samples have been tested. These samples were tested at lower stress rate of 50MPa/second which is far less than stress rates for other materials examined (Table 4.2). This evidence was extensively discussed by Kang et al. [60]. They reported that the ratcheting strain produced during the cyclic stressing at lower stress rate is much higher than that at higher stress rates. SA333 steel samples tested at low stress rate of 50MPa/second resulted in ratcheting strain data sitting above the calculated curves.

5.2. Ratcheting assessment based on the modified hardening rule

Ratcheting response of three steel alloys of 304, 42CrMo and 316L and copper under uniaxial loading conditions was evaluated based on A-F, Bower and the modified hardening rule (Equation (3.13)). As shown in figure 3.2, A-F hardening rule overestimated ratcheting response of 42CrMo steel sample at the very early stage of stress cycles. Predicted ratcheting strain values based on Bower's model addressed ratcheting of 42CrMo steel over limited number of stress cycles in stage I. Predicted ratcheting strains in stage I showed the greater capability of Bower's model over this stage where ratcheting strains possessed smaller rates resulting in an increase in the magnitude of ratcheting strain in the first stage. Bower's model however beyond stage I, resulted in an arrest in ratcheting strain progress and a plastic shakedown occurred. The modified hardening rule due to involvement of stress-strain and newly introduced coefficients, addressed the ratcheting response of materials over stages I and II as number of stress cycles increased. Two material stress-strain hysteresis loop constants C and γ_1 employed in Bower's and the modified hardening rule controlled the shape, size and consistency of hysteresis loops over ratcheting process. These constants are independent of applied cyclic stress levels and are solely material dependent. Coefficients γ_2 and δ however in the modified hardening rule governed the rate of strain accumulation in ratcheting stages I and II respectively and were found to be related with stress levels (see Figures 4.4-4.7). Coefficient δ prevented ratcheting to arrest beyond stage I of stress cycles. This coefficient controlled the rate of strain accumulation in stage II of ratcheting process. Jiang and Zhang [73] similarly found that ratcheting rate is sensitive to the applied stresses. Under a load controlled condition, the ratcheting strain is increased with the increase in the applied amplitude stress. The rate of the decay in ratcheting curve over stress cycles was found to be load dependent.

The modified hardening rule was capable to address the stages I and II of uniaxial ratcheting deformation. The hardening rule predicted stage I of ratcheting strain rate decay for limited number of cycles and then predicted ratcheting strain in stage II with constant rate. Figures 4.8-4.10 predicted the ratcheting response of steel and copper samples over uniaxial stress cycles based on the modified hardening rule. The predicted values of ratcheting strain over stages I and II in these figures were compared with experimental ratcheting strains. Figures 4.8-

4.10 presented the dominancy of the stress amplitude on ratcheting strain rate and that of the mean stress influenced greatly on the magnitude of ratcheting over stages I and II.

In 42CrMo steel, the predicted ratcheting strain values in stages I and II stress cycles were found in good agreement with the experimental data. Better correlation is observed by the modified hardening rule in larger cyclic stress levels and ratios. For 316L samples, the modified hardening rule well predicted ratcheting strain rate over stages I/II (see figures 4.8-4.10) at various stress levels.

The interaction of stress amplitude and mean stress on the ratcheting response requires a better understanding of the concurrent influence of both stresses on ratcheting response of materials. Earlier experimental evidences [29-30] have revealed that the ratcheting deformation of steel samples examined over stress cycles were overcome by the influence of applied stress amplitude. These evidences related such interaction to materials heat-treatment, strain hardening/softening and the magnitude of applied stress levels.

Variations of coefficients γ_2 and δ in 304, 42CrMo and 316L steel and copper samples tested under uniaxial stress cycles verified the consistency in the trend of data for materials examined in this research as plotted for various stress levels. Constructed family curves for materials examined in this study enabled estimating both γ_2 and δ coefficients for any given stress levels on the curves or through interpolated dashed-curves for any desired stress level in figures 4.4-4.7. Figures 4.4-4.7 verify the applicability of the generated family curves to readily estimate coefficients γ_2 and δ required to predict ratcheting response of materials over stress cycles as compared with those of experimentally obtained.

Estimated coefficients γ_2 and δ enabled the modified hardening rule to predict ratcheting strain magnitudes and calibrate the ratcheting strain rates over stages I and II over prolonged stress cycles. The modified hardening rule required no further trails to find constants γ_2 and δ to predict ratcheting over stages as these coefficients are calibrated based on stress levels and materials while in earlier modifications such Chen's model developed to predict ratcheting for prolonged stress cycles always trails and arbitrary values were required to estimate the factor χ_i multiplied by the dynamic recovery term.

5.3. The modified hardening rule and ratcheting assessment under step-loading conditions

Ratcheting assessment of SS316L, SA333, SS316L(N) and 1070 steel alloys under uniaxial step-loading conditions was performed. Figures 4.11, 4.14, 4.17 and 4.20 presented good agreements between the predicted ratcheting curves and the experimental data under uniaxial single-step loading conditions. The modified hardening rule due to newly introduced coefficients γ_2 and δ enabled ratcheting assessment of materials over larger number of stress cycles. Coefficients C and γ_1 in the modified hardening rule are two material stress-strain hysteresis loop constants that control the shape and size of hysteresis loops over ratcheting process. Coefficients γ_2 and δ on the other hand are associated with stress levels and govern the rate of strain accumulation in transition and steady stages of ratcheting progress respectively. Calibration curves enabled an accurate estimation of coefficients γ_2 and δ at various mean stress and stress amplitude values under uniaxial stress cycles. Figures 4.12, 4.15, 4.18 and 4.21 presented calibration curves for steel alloys examined in this investigation.

Efficiency of stress level dependent coefficients γ_2 and δ employed in the hardening rule to predict multi-step ratcheting with different loading sequences was evaluated. SS316L stainless steel underwent two-step low-high loading sequence. The first step comprised low mean stress followed by higher mean stress while stress amplitude was kept unchanged over stress steps. The predicted ratcheting strains for the history with two load steps were compared with the experimental data showing close agreement (as shown in figure 4.13). The predicted ratcheting curve at very first cycles of the first step of cyclic stressing fell below the experimental data, but as number of cycles advanced a closer agreement of the predicted and experimental data was achieved. In the second step, the modified hardening rule underestimated slightly the experimentally obtained values. A comparison of ratcheting response of single-step loaded samples in figure 4.11 and multi-step loaded samples in figure 4.13 showed that ratcheting process is influenced by change in mean stress and/or stress amplitude over load steps. Kang et al. also [75] reported that each load step affected the ratcheting strain values over subsequent load steps in a step-load history. The magnitude of this influence very much depends on the sequence of load steps within histories. In SS316L stainless steel with cyclic hardening

characteristics, low-high sequence of loading resulted in a progressive ratcheting process. It is noteworthy that low-high sequence in loading, increases the rate of ratcheting strain accumulation in the material with cyclic softening behaviour and results in drop in component life [75]. Predicted ratcheting response in SS316L alloy under low-high loading sequence in mean stress and at a constant stress amplitude verified the capability of the modified hardening rule to characterize ratcheting strain over load steps. The modified hardening rule was employed to assess ratcheting response in SA333 alloy with loading history B7 consisted of three steps as mean stress values increased and stress amplitude stayed unchanged over load steps. Ratcheting data obtained experimentally showed a build-up in ratcheting response over steps of load histories as mean stress increased [76]. Good agreements between the predicted and the experimental data over prolonged stress cycles in figure 4.16 verified that the modified hardening rule was able to characterize multi-step ratcheting strain of SA333 tested with low-high loading sequences.

The ratcheting response of SS316L(N) samples under low-high and high-low sequences with two-step loading conditions was assessed based on the modified hardening rule and plotted together with experimental data. Figure 4.19a verified that an increase in mean stress at a constant stress amplitude in each step resulted in an overall increase in the magnitudes of ratcheting strain. Ratcheting strain values progressively increased in magnitude over two loading steps in histories C7 and C8 presented in figure 4.19b. Predicted ratcheting values fell below the experimental data beyond the point where step 1-step 2 transitions occurred. In figure 4.19b, histories C8 and C9 with low-high loading sequences, experimental data were expected to address the effect of different stress levels over the first load step on the subsequent ratcheting values emerged from the second load step of these histories with the same applied stress levels. The modified hardening rule however predicted the difference in ratcheting values in step 2.

Figure 4.19c presented histories C10-C12 which increases in both mean stresses and stress amplitudes over the second load steps. The predicted and the experimental ratcheting data plotted in the figure reflected the progressive increase in curves and data over the second step of loading. In figure 4.19d, the modified hardening rule was able to address the sequence of loading. The progressive accumulation of ratcheting strain followed by cessation of ratcheting strain or lowering trend of ratcheting strain was observed as mean stress/stress amplitude

decreased in the subsequent load step of C13-C15 histories. Ratcheting strain values in SS316L(N) samples under high-low loading sequences with decreasing in stress amplitude (history C16 in figure 4.19e) and with decreasing trend in mean stress (history C13 in figure 4.19d) resulted in a small peak in ratcheting strain beyond the first load step. As shown in figure 4.19d, in high-low sequence of step loading cases with decreasing mean stress and maximum stress level, the predicted ratcheting curves corresponded to lower ratcheting values over the second step of load histories. A comparison of low-high and high-low sequence loading histories C7 and C16 in figure 4.19f verified how influential the load sequence is in ratcheting deformation over load steps.

Ratcheting response of 1070 steel samples tested at various step-loading histories was assessed based on the modified hardening rule. Figure 4.22a presenting the low-high ratcheting response of 1070 steel showed that both the predicted and the experimental data progressively increased ratcheting strain over stress cycles within three subsequent load steps. Figure 4.22b and 4.22c however showed both ratcheting curves and data deviated beyond the first load step as the magnitude of mean stress dropped over the second load step. Ratcheting strain of 1070 steel alloy subjected to compressive mean stresses over loading steps was presented in figure 4.22d. For 1070 steel alloy experiencing load history D7 consisted of compressive mean stresses -211MPa and -77MPa respectively over the first and the second load steps, ratcheting strains were progressed in positive directions over the second load steps when mean stress magnitude increased to -77MPa. The modified hardening rule encountered the change in mean stress and resulted in an increase in predicted ratcheting data at this step. The deviation of predicted ratcheting strain curves from experimental data over the second step is attributed to influence of previous load step accumulating ratcheting deformation on the subsequent load steps. The modified hardening rule overestimated ratcheting on the subsequent load steps as evidenced in figures 4.19d and 4.22b-4.22e when stress levels dropped in magnitude over load steps. Figure 4.22e presents ratcheting response of a three-step cyclic loading with low-high-low sequence (history D9). Good agreement was achieved over the first two load steps between the predicted and the experimental ratcheting strain values. Ratcheting curve/data altered its progressive direction. The discrepancy of ratcheting data and predicted curves in the last steps in figures 4.19d and 4.22b-4.22e is associated with yield surface change over stress cycles. The predicted ratcheting values in high-low sequence were deviated from the experimental data respectively

with magnitudes of 25% and 50% for 316L(N) and 1070 steel samples. This may suggest that a combined kinematic-isotropic hardening rule is required to address the yield surface translation and expansion together over deviatoric stress increments.

5.4. Concurrent ratcheting-fatigue damage analysis

The coupled ratcheting-fatigue damage of 42CrMo and 1020 steel alloys were evaluated under uniaxial cyclic loading. Ratcheting damage was evaluated by experimental and predicted ratcheting data and coupled with two energy-based fatigue damage models of Xia et al. (figures 4.25a and 4.25c) and SWT (figure 4.25b and 4.25d). Ratcheting process in materials causes an extra damage and shortens life of components. After a couple of hundred stress cycles the ratcheting strain rate stayed constant and as stress cycles advanced a considerable ratcheting strain was induced in the material resulting in a severe overall damage progress. In annealed 42CrMo and 1020 steel alloys, as mean stress increases while stress amplitude is kept unchanged magnitude of accumulated ratcheting strain over stress cycles sifts up (figure 4.24) and corresponding fatigue life decreases (Table 4.10). Similar trend was evident as stress amplitude increases whereas mean stress was kept constant. The extent of overall damage depends on the magnitude of stress levels. The amount of this damage was related to the effect of magnitude of mean stress and stress amplitude ratio. Mean stress and amplitude stress magnitudes influence the overall damage and result in a family of damage curves. At the small fatigue lives, as the life cycles advance, these curves diverge however in higher cycles they become almost parallel. Weighting factor ξ in equation (3.16) indicated the extent of the influence of ratcheting and fatigue damage at various (σ_m/σ_a) ratios. Factor ξ versus (σ_m/σ_a) ratio for 42CrMo and 1020 steel alloys in figure 4.27 varies between zero and unity. For fully reversed loading condition and in the absence of mean stress (ξ=1), the overall damage in material is associated with only fatigue damage while for cyclic tests conducted in the presence of mean stress factor ξ decreases to values less than unity. As presented in figure 4.27, the factor ξ decreases as (σ_m/σ_a) ratio increases. As the magnitude of (σ_m/σ_a) ratio increased the contribution of ratcheting damage increased. Drop in factor ξ was more pronounced for 42CrMo steel as cyclically tested with non-zero mean stresses. Ratcheting damage in 42CrMo steel was dominant as mean stress magnitude became as large as cyclic amplitude stress corresponding to factor ξ=0.

Energy-based damage models of SWT and Xia et al. were employed to assess fatigue damage in steel alloys. As shown in figure 4.25, the choice of fatigue damage models employed to assess the overall damage calculated from equation (3.15) for 1020 steel was found less crucial as the difference between the predicted overall damage values based on Xia and SWT models for these materials was found insignificant. It is evident from figure 4.27 that for the both steels 42CrMo and 1020, the influence of ratcheting damage is more pronounced by Xia et al. model than SWT.

Ratcheting damage curve was evaluated based on the experimental ratcheting strains and the predicted ratcheting strains by means of the modified hardening rule. Overall damage values obtained based on the modified hardening rule was found in close agreements with those of evaluated experimentally. Factor ξ estimated for different (σ_m/σ_a) ratios by means of the experimental and predicted ratcheting strain values is almost identical (see figure 4.26). Lives of 42CrMo and 1020 test samples were listed in Table 4.10 estimated based on the proposed algorithm (figure 3.3) in figure 4.28. Life data were evaluated based on two energy-based models of Xia et al. and SWT as well as the experimental and predicted ratcheting strain values. Predicted life data were found in good agreements with experimental lives falling within a factor of ±2.

CHAPTER SIX

CONCLUSIONS AND RECOMMENDATIONS

6.1. Conclusions

Several kinematic hardening rules under strain- and stress-controlled conditions were studied. The Prager linear hardening rule underestimated the ratcheting response over stress cycles. Garud multi-surface model estimated the ratcheting strain under stress-controlled conditions during very first few stress cycles. Ratcheting response predicted by A-F hardening rule resulted in a noticeable deviation from the experimental results. Bower's hardening rule was found to better predict ratcheting strain of materials over stress cycles within the early stage of ratcheting. Implementing second kinematic variable in Bower's hardening rule enabled ratcheting prediction for larger number of stress cycles within stages I/II as compared with Prager, Garud, A-F and Chaboche models. Hardening rule of Bower offered a simple hardening rule to assess ratcheting response of materials resulting in an arrest in ratcheting progress beyond stages I/II stress cycles.

Ratcheting assessment of steel and copper alloys was performed based on two approaches of (i) mechanistic and (ii) kinematic hardening rule. Based on the mechanistic approach, ratcheting formulation was developed including affecting parameters such as mean stress, stress amplitude, material properties, and cyclic softening/hardening response. Ratcheting response of steel and copper alloys was evaluated based on the mechanistic equation over uniaxial stress cycles at different mean stresses and stress amplitudes and were found in good agreements when compared with those of experimentally obtained values. The hardening rule approach was also developed to assess ratcheting response of materials based on A-F kinematic hardening rule. The modified kinematic hardening rule approach was characterized by the yield surface translation and the corresponding plastic modulus determined by consistency condition.

Coefficients γ_2 and δ enabled the modified hardening rule to predict ratcheting strain values between plastic shakedown of Bower's model and overestimated ratcheting response of materials by A-F model. These ratcheting strain rate coefficients were related and calibrated for various mean stresses and stress amplitudes. The constructed family curves enabled estimating values of these coefficients from diagrams for any given cyclic stress levels. The predicted ratcheting strain values based on the modified hardening rule were found in good agreement with the experimentally obtained ratcheting data over stages I and II for different steel and copper samples under uniaxial loading conditions.

The modified hardening rule was further examined to evaluate ratcheting response of steel alloys under multi-step loading spectra with low-high, high-low and low-high-low sequences. Over multi-step loading conditions, subsequent load steps were considerably affected by previous load steps. Loading sequence affected ratcheting magnitude and its trend over stress cycles. Calibration curves were used to estimate coefficients γ_2 and δ. The family of curves was constructed based on single-step ratcheting strain values for various mean stresses and stress amplitudes. Ratcheting strains for low-high stress steps were predicted by the modified hardening rule. The deviation of predicted ratcheting strains from experimental values were found up to 25% for 316L(N) steel samples and up to 50% for 1070 steel samples for high-low sequence loading spectra.

Ratcheting-fatigue interaction was formulated to include the influence of both ratcheting and fatigue phenomena over stress cycles. Such interaction was defined based on mechanistic parameters of mean stress, stress amplitude, and cyclic softening/hardening response of steel alloys. The modified kinematic hardening rule was employed to simulate ratcheting strain curve. Induced damage due to ratcheting was defined from the product of the predicted ratcheting strain rate and the maximum applied cyclic stress, while fatigue damage was analysed based on Xia-Kujawski-Ellyin and Smith-Watson-Topper approaches. The predicted overall damage values fell between damage-N curves of fatigue and ratcheting phenomena and closely agreed with the experimental values listed in Table 4.10.

6.2. Recommendations for Future Research

Ratcheting phenomenon is critically important in structural design of load-bearing engineering components subjected to asymmetric cyclic loads of yield stress magnitude particularly when it is coupled with fatigue cycles. To realistically assess ratcheting response of materials a reliable design and damage assessment is necessary. Parameters affecting ratcheting phenomena and its interaction with fatigue phenomenon in one hand and the lack of the volume of ratcheting research results in the literature in other hand prioritize several researchers in the field of cyclic plasticity and stress analysis to pay special attention on mechanistic parameters including stress level, mechanical properties, loading spectra, loading proportionality/non-proportionality, uniaxial, biaxial and multiaxial loading conditions, temperature level, hardening/softening response, microstructural features and materials composition in their research proposals.

The present thesis proposes ratcheting assessment of materials based on parametric equation and the modified kinematic hardening rule and discusses the concurrent interaction of ratcheting-fatigue phenomena over uniaxial stress cycles at room temperature. The modified hardening rule in the present thesis while primarily addresses the effects of stress level and material properties for various single-step and multi-step uniaxial loading conditions, it however requires further modifications to include other affecting parameters. More research work is recommended to include additional parameters for a realistic ratcheting assessment of materials.

- In addition to stress amplitude and mean stress, mechanical properties, such other parameters as stress rate, the softening/hardening responses of materials, loading spectrum (multiaxiality effect), loading frequency, thermal and environmental conditions and materials microstructure are importantly influential in the modelling of ratcheting strain over stress cycles which are recommended as future research outlooks.

- The modified hardening rule was assessed for mainly steel and copper alloys under uniaxial stress-controlled loading conditions. Further research is required to evaluate the capability of the modified hardening rule in assessing ratcheting response of materials

subjected to more complex loading paths such as proportional and non-proportional loading conditions.

- Ratcheting response of materials particularly under thermal cycles and its interaction with corrosive environment requires a detailed future research plan as currently literature lacks enough information and data when both temperature and environment are coupled. Further modifications of ratcheting models to include terms for time-dependency, loading frequency and stress rate are essential.

- Ratcheting strain rate coefficients γ_2 and δ are required to be further calibrated and modeled for various materials. Investigation of other influential terms as cyclic hardening/softening effect, type of heat-treatment, and the influence of microstructural features on such coefficients are required.

- It is further recommended to employ combined kinematic-isotropic hardening rules to assess ratcheting response of materials over stress cycles. It is also required to study the ratcheting response of materials under multi-step loading spectra and to study the effect of hardening rules employed to evaluate ratcheting strain values. The modified hardening rule in this thesis encountered the effect of sequence loading and the trend and magnitude of ratcheting as the loading sequence changed.

- In ratcheting assessment of materials, finite element analysis packages including A-F type hardening rules may face complications such as lack of stability in consistency condition, lack of a robust analysis method, and less accuracy to predict ratchting response of materials. The current modified hardening rule in this thesis because of its promissing predicted ratcheting results is expected to offer more reliable predicted ratcheting values if used in conjunction with FE analysis.

- To address concurrent ratcheting-fatigue damage interaction and assessment of damage contribution due to both ratcheting and fatigue phenomena, more experimentations and ratcheting test data are required. It is also primarily required to develop codes and

standard for ratcheting test conditions and testing specimen as currently no standardized specimen and procedure is available.

APPENDIX A

Appendix A presents experimental data used in chapter two to evaluate stress-strain as well as ratcheting responses of different materials under various loading conditions. Table A.1 presented material properties of 1045, 1070, 42CrMo, SS304, SS316L and rail steel alloys used in section 2.3. The constants of hardening rules employed to predict stress-strain curves in figure 2.5 were listed in Table A.2. Experimental axial and shear stress response of 1045 steel tested subjected to 90° out-of-phase strain-controlled condition presented in figures 2.5 and 2.6 were listed in Table A.3. Experimental ratcheting strain values of 42CrMo, SS304, SS316L and rail steel alloys over uniaxial stress cycles employed in figure 2.7 were presented in Table A.4. Table A.5 presented material constants of Prager, A-F and Bower's hardening rules required to assess ratcheting strain over stages I/II of stress cycles. Corresponding ratcheting hysteresis loops predicted based on Prager, Garud, A-F and Bower models for 42CrMo, SS304, SS316L and rail steel alloys were presented in figure A.1. Experimental ratcheting data for 1070 steel under non-proportional stress-controlled loading condition shown in figure 2.9 were listed in Table A.6. Table A.7 presented material constants of Prager, A-F, Bower and Chaboche hardening rules to assess ratcheting of 1070 steel shown in figure 2.9.

Table A.1 Material properties of steel alloys

Material	E (GPa)	σ_y (MPa)
1045 steel [44]	205	200
1070 steel [44]	210	250
SS304 [29]	190	209
42CrMo [30]	190.5	310
SS316L [45]	210	230
Rail steel [26]	210	400

Table A.2 Hardening rules constants employed to assess stress-strain response in 1045 steel

Model	Material constants
Prager	C=11239 MPa
A-F [11]	C=87674 MPa, γ=412
Bower [11]	C=123690 MPa, γ_1=665, γ_2=40

Table A.3 Experimental data of axial stress versus shear stress for 1045 steel sample tested under 90° out-of-phase cyclic straining condition.

Exp. Data in Fig. 2.5		Exp. Data in Fig. 2.6		Exp. Data in Fig. 2.6	
τ (MPa)	σ (MPa)	ε	σ (MPa)	γ	τ (MPa)
133	0	9.63E-06	80	1.40E-05	34
129	79	1.81E-04	107	2.22E-04	50
116	153	4.00E-04	133	3.88E-04	60
100	195	5.71E-04	157	6.24E-04	72
79	233	7.39E-04	178	7.60E-04	83
63	256	9.34E-04	202	1.00E-03	96
48	274	1.13E-03	226	1.15E-03	107
32	284	1.35E-03	246	1.38E-03	120
16	293	1.52E-03	261	1.55E-03	128
0	293	1.69E-03	273	1.78E-03	131
-16	293	1.81E-03	279	1.76E-03	119
-32	284	1.84E-03	261	1.64E-03	103
-48	274	1.72E-03	231	1.50E-03	88
-63	256	1.59E-03	202	1.29E-03	70
-79	233	1.40E-03	157	1.10E-03	52
-100	200	1.20E-03	118	9.00E-04	35
-116	158	9.85E-04	80	6.80E-04	17
-127	88	7.39E-04	32	5.00E-04	1
-133	0	5.44E-04	-1	2.50E-04	-15
-127	-84	3.50E-04	-33	-9.00E-06	-29
-116	-144	1.81E-04	-60	-2.50E-04	-44
-100	-191	9.63E-06	-87	-5.12E-04	-61
-79	-233	-2.36E-04	-119	-7.48E-04	-77
-63	-256	-4.55E-04	-149	-1.01E-03	-94
-48	-274	-6.74E-04	-173	-1.34E-03	-114
-32	-284	-9.41E-04	-206	-1.56E-03	-128
-16	-288	-1.21E-03	-236	-1.81E-03	-136
0	-293	-1.50E-03	-259	-1.93E-03	-132
16	-293	-1.70E-03	-271	-1.91E-03	-115
32	-288	-1.84E-03	-283	-1.81E-03	-100
48	-270	-1.87E-03	-262	-1.65E-03	-83
63	-260	-1.75E-03	-224	-1.44E-03	-65
79	-237	-1.55E-03	-185	-1.29E-03	-52
100	-195	-1.33E-03	-137	-1.10E-03	-39
116	-149	-1.11E-03	-99	-8.44E-04	-20
129	-88	-9.17E-04	-66	-5.36E-04	0
133	0	-7.22E-04	-33	-2.76E-04	17
---	---	-5.51E-04	-1	---	---
---	---	-3.56E-04	32	---	---
---	---	-1.37E-04	59	---	---

Table A.4 Experimental ratcheting strain for 42CrMo, SS304, SS316L and rail steel alloys at different stress levels used in figure 2.7

42CrMo				SS304				SS316L				Rail Steel	
50±325MPa		50±350MPa		65±260MPa		65±325MPa		56±242MPa		76±242MPa		56±562MPa	
N (Cycle)	ε_r (%)	N (Cycle)	ε_r (%)	N (Cycle)	ε_r (%)	N (Cycle)	ε_r (%)	N (Cycle)	ε_r (%)	N (Cycle)	ε_r (%)	N (Cycle)	ε_r (%)
0	0	0	0	0	0	0	0	0	0	0	0	0	0
2	0.12	2	0.49	11	0.73	6	2.63	1	1.12	1	2.50	15	0.34
4	0.42	4	0.65	25	0.84	12	3.01	4	1.46	2	2.87	48	0.72
7	0.62	6	0.82	39	0.95	20	3.15	6	1.93	3	3.05	100	1.04
9	0.78	8	0.92	65	1.00	27	3.53	9	2.40	4	3.22	199	1.46
12	0.83	10	0.99	81	1.03	40	3.76	11	2.47	6	3.37	398	1.97
15	0.88	16	1.08	95	1.07	62	3.95	17	2.57	8	3.45	---	---
20	0.98	20	1.18	109	1.11	76	4.10	22	2.67	9	3.53	---	---
24	1.01	25	1.28	138	1.16	111	4.30	28	2.71	11	3.62	---	---
27	1.04	31	1.34	152	1.19	132	4.45	33	2.74	15	3.70	---	---
33	1.08	37	1.41	194	1.22	160	4.59	38	2.78	19	3.77	---	---
38	1.11	43	1.47	222	1.25	181	4.70	43	2.81	22	3.82	---	---
45	1.15	49	1.51	264	1.29	209	4.79	50	2.83	26	3.87	---	---
50	1.18	54	1.56	292	1.31	237	4.88	56	2.84	29	3.90	---	---
54	1.21	58	1.61	334	1.33	266	4.96	63	2.86	33	3.94	---	---
60	1.25	64	1.64	391	1.36	293	5.05	69	2.87	38	3.98	---	---
64	1.27	70	1.71	433	1.38	329	5.14	77	2.89	43	4.01	---	---
68	1.28	74	1.73	475	1.41	364	5.22	85	2.91	47	4.05	---	---
72	1.30	78	1.74	503	1.41	400	5.31	93	2.92	55	4.09	---	---
76	1.31	83	1.77	531	1.43	434	5.34	101	2.94	63	4.13	---	---
80	1.33	87	1.80	588	1.45	469	5.42	112	2.98	73	4.18	---	---
84	1.34	93	1.84	644	1.46	519	5.51	122	3.01	81	4.21	---	---
88	1.36	97	1.86	658	1.47	561	5.57	133	3.05	92	4.25	---	---
91	1.38	100	1.87	700	1.48	610	5.65	143	3.08	100	4.28	---	---
95	1.41	---	---	728	1.49	646	5.69	153	3.10	105	4.28	---	---
100	1.44	---	---	784	1.50	687	5.74	162	3.12	115	4.32	---	---
---	---	---	---	813	1.53	730	5.80	171	3.13	125	4.35	---	---
---	---	---	---	883	1.53	765	5.85	180	3.15	134	4.37	---	---
---	---	---	---	910	1.54	800	5.88	188	3.15	143	4.39	---	---
---	---	---	---	939	1.54	835	5.91	195	3.15	152	4.41	---	---
---	---	---	---	981	1.55	870	5.94	200	3.15	162	4.43	---	---
---	---	---	---	1000	1.56	899	5.97	---	---	172	4.45	---	---
---	---	---	---	---	---	933	6.00	---	---	182	4.46	---	---
---	---	---	---	---	---	969	6.03	---	---	191	4.48	---	---
---	---	---	---	---	---	1000	6.07	---	---	200	4.48	---	---

Table A.5 Material constants used in Prager, A-F and Bower models to evaluate the ratcheting strain

Material	Stress level (MPa)	Prager Constant	A-F Constants		Bower constants		
		C(GPa)	C(GPa)	γ	C(GPa)	γ_1	γ_2
42CrMo	50±325	12	42.6	557	25	300	35
	50±350	7.9	42.6	557	25	300	26
SS304	65±260	25.2	44.3	290	55	250	15.5
	65±325	18.6	44.3	290	55	250	3.5
SS316L	76±242	23.7	15	250	3.5	40	19
	56±242	21.6	15	250	3.5	40	21
Rail Steel	56±562	56.5	52.8	286	33.9	8.3	0.41

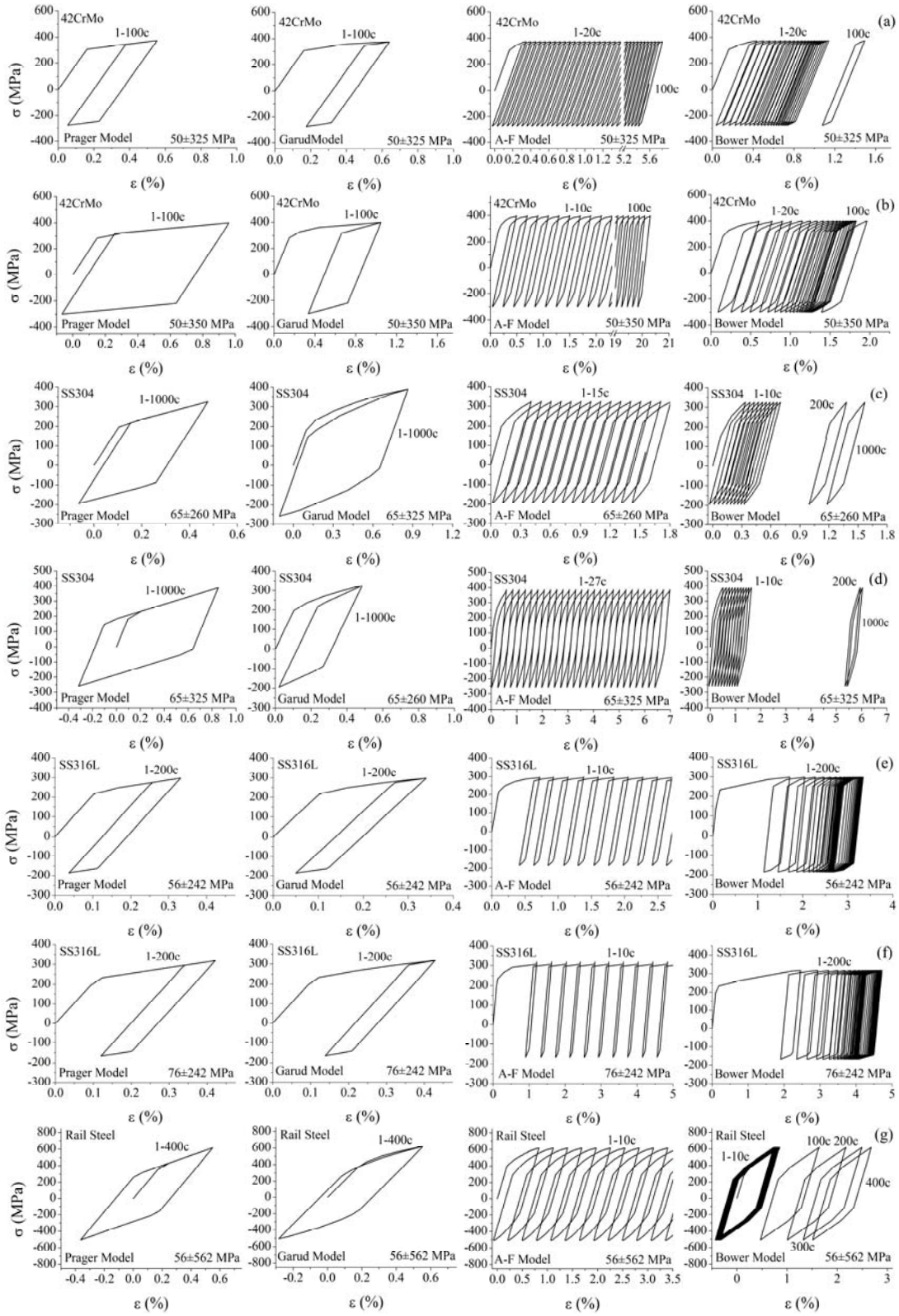

Figure A.1 Ratcheting hysteresis loops predicted based on Prager, Garud, A-F and Bower models for different steels of (a and b) 42CrMo, (c and d) SS304, (e and f) SS316L, and (g) rail steel undergoing various cyclic stressing

Table A.6 Experimental axial ratcheting strains for the first 100 cycles of 1070 steel used in figure 2.9

N (Cycle)	ε_r	N (Cycle)	ε_r	N (Cycle)	ε_r
1	0.00167	30	0.00778	65	0.01
2	0.00278	32	0.00785	68	0.0101
3	0.00389	33	0.00792	70	0.0103
4	0.00444	35	0.00805	72	0.0104
5	0.005	38	0.00819	73	0.0104
7	0.00542	40	0.00833	75	0.0106
8	0.00583	42	0.0084	78	0.0107
9	0.00625	43	0.00847	80	0.0108
10	0.00667	45	0.00861	82	0.0109
12	0.00674	48	0.00875	83	0.011
13	0.00681	50	0.00889	85	0.0111
15	0.00694	52	0.00899	88	0.0113
18	0.00708	53	0.0091	90	0.0114
20	0.00722	55	0.00931	92	0.0114
22	0.00729	58	0.00951	93	0.0115
23	0.00736	60	0.00972	95	0.0115
25	0.0075	62	0.00979	98	0.0116
28	0.00764	63	0.00986	100	0.0117

Table A.7 Material constants used to assess ratcheting response of 1070 steel based on various hardening rules [11]

Model	Material constants
Prager	C=163222 MPa
A-F	C=96188 MPa, γ=285
Bower	C=127680MPa, γ_1=420, γ_2=55
Chaboche	$C^{(1)}$=95885 MPa, $C^{(2)}$=29274 MPa, $C^{(3)}$=11240 MPa, $C^{(4)}$=4890 MPa, $C^{(5)}$=2477 MPa, $C^{(6)}$=1270 MPa, $C^{(7)}$=762 MPa, $C^{(8)}$=425 MPa, $C^{(9)}$=305 MPa, $C^{(10)}$=171 MPa $\gamma^{(1)}$=1510, $\gamma^{(2)}$=461, $\gamma^{(3)}$=177, $\gamma^{(4)}$=77, $\gamma^{(5)}$=39, $\gamma^{(6)}$=20, $\gamma^{(7)}$=12, $\gamma^{(8)}$=6.7, $\gamma^{(9)}$=4.8, $\gamma^{(10)}$=2.7

APPENDIX B

Experimental data employed in ratcheting-fatigue assessment (in chapter four) were presented in Appendix B. Experimental ratcheting strain of 42CrMo, 20CS, SA333 steels and OFHC copper subjected to uniaxial stress cycles used to verify the proposed equation (3.1) in figure 4.2 was presented in Tables B.1-B.4 respectively. Ratcheting response of 304, 42CrMo, 316L and copper alloys at various mean stresses and stress amplitudes was verified based on modified hardening rule in figures 4.8-4.10. Employed experimental ratcheting strain values in figure 4.8 were listed in Tables B.5-B.8. Experimental ratcheting values over stress cycles at constant stress amplitude and various mean stresses employed in figure 4.9 were listed in Tables B.9-B.12. Tables B.13-B.16 presented experimental ratcheting strain over stress cycles at various stress ratios and constant maximum stress employed in figure 4.10. The modified hardening rule was verified to characterize multi-step ratcheting strain at various stress levels for SS316L, SA333, SS316L(N) and 1070 steel alloys. The experimental single-step and multi-step ratcheting strain for SS316L steel alloy employed in figures 4.11 and 4.13 were presented in Tables B.17, B.18 respectively. Tables B.19 and B.20 respectively, presented experimental single-step and multi-step ratcheting strain for SA333 steel alloy employed in figures 4.14 and 4.16. Experimental data for single-step and two-step ratcheting tests performed on SS316L(N) steel samples depicted in figure 4.17 and 4.19 were listed in Tables B.21-B.26. Experimental ratcheting strain of 1070 steel alloy over Single- and multi-steps loading conditions employed in figure 4.20 and 4.22 were presented in Tables B.27-B.32 of Appendix B.

Table B.1 Experimental ratcheting strain of 42CrMo steel alloy used in verification of triphasic equation (3.1) in figure 4.2a

100±350MPa		150±350MPa		50±400MPa	
N(Cycle)	ε_r(%)	N(Cycle)	ε_r(%)	N(Cycle)	ε_r(%)
0	0	0	0	0	0
52	2.2	15	1.2	50	3.4
71	3.2	33	2.0	78	3.8
127	3.9	52	2.9	106	4.3
240	4.4	89	4.4	134	4.9
333	5.1	127	5.0	162	5.3
409	5.5	164	5.5	190	5.8
521	6.0	221	6.2	218	6.0
595	6.5	277	6.5	246	6.3
671	6.8	314	7.0	276	6.5
746	7.0	389	7.5	304	6.7
802	7.4	446	8.1	332	7.0
896	7.7	521	8.6	360	7.4
970	7.9	558	8.9	388	7.6
1027	8.1	615	9.3	416	7.8
1248	8.6	652	9.6	472	8.1
1395	9.9	690	10.0	500	8.5
1615	10.5	764	10.5	556	9.1
1835	11.1	820	10.8	613	9.6
1982	12.3	877	11.2	641	10.0
2202	13.0	915	11.5	697	10.6
2422	13.6	971	11.9	753	11.0
2642	14.8	1008	12.2	809	11.3
2862	15.4	1248	13.6	865	11.6
3009	16.0	1394	15.4	893	12.5
3229	17.3	1615	17.3	978	13.0
3450	18.5	1835	19.1	1175	15.1
3670	19.7	2055	21.0	1372	17.5
3890	21.0	2202	23.4	1597	20.4
4110	22.2	2422	27.1	1793	24.5
4330	23.7	2642	30.8	---	---
4550	25.6	2789	38.2	---	---
4697	27.7	---	---	---	---
4917	31.8	---	---	---	---

Table B.2 Experimental ratcheting strain of 20CS steel alloy used in verification of triphasic equation (3.1) in figure 4.2b

50±275MPa				50±300MPa				50±320MPa	
N(Cycle)	ε_r(%)	N(Cycle)	ε_r(%)	N(Cycle)	ε_r(%)	N(Cycle)	ε_r(%)	N(Cycle)	ε_r(%)
0	0	3270	11.3	0	0	749	14.1	0	0
110	0.7	3390	11.5	4	0.9	796	14.7	8	1.1
130	1.0	3480	11.8	8	1.4	847	15.3	13	2.2
180	1.5	3580	11.9	13	2.2	898	15.8	17	3.5
200	1.8	3670	12.1	17	2.8	945	16.3	22	4.1
230	2.4	3740	12.3	22	3.4	1002	16.8	32	4.9
300	2.8	3810	12.4	27	3.7	1100	18.0	41	5.4
390	3.5	3900	12.7	36	4.1	1200	19.2	55	6.1
440	3.9	4000	12.8	46	4.2	1302	20.3	65	6.6
510	4.2	4070	12.9	50	4.6	1400	21.5	70	7.1
580	4.6	4160	13.0	60	4.9	1500	23.0	78	7.8
650	5.1	4330	13.3	74	5.2	1602	24.7	88	8.1
740	5.4	4490	13.5	83	5.6	1700	26.5	97	8.6
830	5.6	4630	13.9	97	5.9	1800	28.7	120	9.3
950	5.9	4790	14.3	120	6.1	1902	31.7	139	10.3
1020	6.2	4960	14.4	144	6.4	2000	36.1	158	11.1
1090	6.5	5100	14.8	163	7.0	---	---	181	11.9
1170	6.9	5260	15.2	177	7.2	---	---	200	12.5
1260	7.1	5400	15.4	205	7.6	---	---	220	13.3
1380	7.4	5540	15.8	224	7.9	---	---	238	14.0
1470	7.6	5690	16.0	242	8.3	---	---	256	14.8
1540	7.9	5830	16.2	256	8.5	---	---	280	15.5
1640	8.1	5970	16.5	275	8.8	---	---	298	16.0
1700	8.2	6110	16.7	303	9.2	---	---	322	17.0
1870	8.6	6290	17.1	322	9.4	---	---	341	17.8
1960	8.9	6430	17.6	345	9.6	---	---	355	18.6
2050	9.0	6760	18.0	359	9.7	---	---	378	19.5
2120	9.2	6970	18.7	374	10.0	---	---	397	20.3
2220	9.4	7260	19.3	397	10.3	---	---	416	21.1
2330	9.6	7490	19.9	416	10.7	---	---	439	22.2
2450	9.8	7750	20.5	439	10.8	---	---	458	23.0
2540	10.0	8010	21.4	458	11.1	---	---	477	24.4
2640	10.3	8250	22.1	477	11.4	---	---	495	25.6
2760	10.6	8520	23.0	500	11.6	---	---	552	29.6
2850	10.8	8760	23.8	547	12.0	---	---	---	---
2990	11.0	8990	24.8	599	12.7	---	---	---	---
3080	11.1	9250	26.0	645	13.1	---	---	---	---
3180	11.2	9334	26.3	697	13.6	---	---	---	---

Table B.3 Experimental ratcheting strain of SS333 steel alloy used in verification of triphasic equation (3.1) in figure 4.2c

40±310MPa				80±310MPa				120±310MPa	
N(Cycle)	ε_r(%)	N(Cycle)	ε_r(%)	N(Cycle)	ε_r(%)	N(Cycle)	ε_r(%)	N(Cycle)	ε_r(%)
0	0	2258	16.6	0	0	1158	44.8	0	0
1	1.6	2408	17.6	2	1.0	1172	47.5	3	2.8
2	1.8	2558	18.5	5	1.8	1177	49.8	8	4.2
3	2.0	2735	19.6	8	2.4	1180	53.1	13	5.0
4	2.0	2911	20.6	13	2.8	1184	53.2	44	7.2
5	2.2	2988	22.6	33	3.9	---	---	98	10.0
6	2.2	3065	24.6	50	4.5	---	---	126	11.4
7	2.2	3105	26.1	61	5.1	---	---	163	13.0
8	2.3	3145	27.6	75	5.5	---	---	190	14.2
9	2.3	3145	28.8	89	6.0	---	---	217	15.4
10	2.3	3145	29.4	100	6.4	---	---	239	16.4
20	2.5	---	---	117	7.0	---	---	266	17.6
30	2.7	---	---	134	7.4	---	---	295	19.1
40	2.9	---	---	154	8.0	---	---	347	21.7
50	3.1	---	---	177	8.9	---	---	384	23.9
60	3.3	---	---	204	9.5	---	---	413	25.7
70	3.5	---	---	258	11.0	---	---	438	27.5
80	3.7	---	---	303	12.0	---	---	465	29.7
90	3.7	---	---	365	13.4	---	---	493	32.8
100	3.9	---	---	441	15.3	---	---	513	35.2
200	5.0	---	---	511	17.0	---	---	527	37.4
300	5.8	---	---	587	18.9	---	---	544	41.0
400	6.3	---	---	646	20.3	---	---	556	44.8
500	6.9	---	---	705	22.0	---	---	565	48.3
600	7.7	---	---	759	23.2	---	---	570	57.2
700	8.0	---	---	798	24.7	---	---	---	---
800	8.8	---	---	829	25.5	---	---	---	---
900	9.2	---	---	852	26.5	---	---	---	---
1000	9.6	---	---	894	28.0	---	---	---	---
1125	10.5	---	---	919	28.8	---	---	---	---
1385	11.8	---	---	950	30.1	---	---	---	---
1543	12.7	---	---	989	31.9	---	---	---	---
1700	13.6	---	---	1020	33.6	---	---	---	---
1885	14.3	---	---	1045	35.3	---	---	---	---
2037	14.9	---	---	1071	36.9	---	---	---	---
2092	15.3	---	---	1099	38.6	---	---	---	---
2148	15.8	---	---	1121	40.5	---	---	---	---
2203	16.2	---	---	1144	42.3	---	---	---	---

Table B.4 Experimental ratcheting strain of OFHC copper used in verification of triphasic equation (3.1) in figure 4.2d

50±120MPa		30±140MPa		50±140MPa		50±160MPa	
N(Cycle)	ε_r(%)	N(Cycle)	ε_r(%)	N(Cycle)	ε_r(%)	N(Cycle)	ε_r(%)
0	0	0	0	0	0	0	0
1	1.2	1	1.6	1	2.5	1	2.9
2	3.2	2	3.8	2	5.0	2	6.0
3	4.4	4	5.2	3	6.0	3	7.0
4	4.7	5	6.1	5	8.3	5	10.0
5	5.9	6	6.9	6	9.6	6	11.8
6	6.5	8	8.2	8	11.5	8	14.5
7	7.4	9	8.6	9	12.0	10	16.3
10	8.6	11	9.2	11	12.8	11	17.1
13	8.8	14	9.3	14	13.0	15	17.7
16	8.9	22	9.4	17	13.0	17	17.9
20	8.9	28	9.4	33	13.1	20	17.9
23	8.9	40	9.5	64	13.3	22	18.0
26	8.9	60	9.8	80	13.7	24	18.0
29	8.9	78	10.4	100	14.1	29	18.1
34	8.9	99	10.8	123	14.7	34	18.4
40	9.0	117	11.2	143	15.2	38	18.5
48	9.0	139	11.6	160	15.7	44	18.9
80	9.0	176	12.4	183	16.2	51	19.6
106	9.1	251	13.7	196	16.7	60	20.6
128	9.3	322	14.7	260	18.3	69	21.6
160	9.4	418	16.2	325	19.9	80	22.9
200	9.5	544	17.6	400	21.4	90	23.9
237	10.0	708	19.6	517	24.5	105	25.4
280	10.1	908	22.0	613	26.6	121	27.4
319	10.3	1127	24.3	698	28.6	128	28.3
357	10.5	1315	26.4	795	31.3	143	30.2
430	11.0	1535	29.0	873	33.3	158	32.4
548	11.6	1738	31.6	940	35.2	166	33.9
698	12.4	1879	34.0	1015	37.1	176	34.9
905	13.4	2000	35.6	---	---	186	37.2
1177	14.4	2060	37.2	---	---	---	---
1526	15.6	---	---	---	---	---	---
2018	17.0	---	---	---	---	---	---
2618	18.6	---	---	---	---	---	---
3213	20.0	---	---	---	---	---	---
3803	21.4	---	---	---	---	---	---
4578	23.2	---	---	---	---	---	---
5511	25.2	---	---	---	---	---	---
6400	27.2	---	---	---	---	---	---
7573	29.6	---	---	---	---	---	---
8300	31.8	---	---	---	---	---	---
9294	33.8	---	---	---	---	---	---
9824	35.7	---	---	---	---	---	---
10187	37.1	---	---	---	---	---	---

Table B.5 Experimentally obtained ratcheting strain of 304 steel at a constant mean stress and various stress amplitudes used in figure 4.8a

Exp. Data 10±260MPa		Exp. Data 10±280MPa		Exp. 10±300MPa		Exp. Data 10±350MPa	
N(Cycle)	ε_r(%)	N(Cycle)	ε_r(%)	N(Cycle)	ε_r(%)	N(Cycle)	ε_r(%)
0	0	0	0	0	0	0	0
2	0.05	1	0.23	3	0.53	13	3.98
5	0.19	2	0.46	7	1.10	17	3.51
5	0.33	8	0.52	10	1.31	24	4.40
14	0.35	17	0.59	13	1.48	33	4.88
28	0.38	28	0.71	17	1.65	40	5.51
50	0.39	42	0.82	24	1.77	57	5.98
71	0.40	59	0.94	33	1.90	60	6.40
93	0.42	73	1.05	43	2.06	77	6.82
110	0.44	87	1.11	53	2.15	87	7.23
124	0.43	99	1.17	67	2.31	107	7.79
141	0.44	110	1.17	77	2.43	114	8.14
161	0.44	127	1.23	87	2.56	127	8.33
178	0.47	138	1.23	100	2.64	130	8.54
195	0.49	150	1.23	110	2.76	140	8.75
218	0.49	167	1.34	124	2.85	154	9.03
232	0.51	181	1.34	130	2.93	167	9.24
249	0.56	198	1.34	143	3.01	177	9.44
269	0.56	218	1.40	150	3.10	201	9.65
289	0.58	232	1.40	160	3.18	211	10.00
308	0.61	243	1.40	170	3.22	224	10.35
325	0.61	263	1.40	180	3.26	237	10.56
342	0.60	277	1.46	190	3.35	244	10.82
359	0.61	294	1.46	201	3.47	254	11.03
376	0.62	308	1.52	214	3.51	271	11.24
390	0.61	320	1.52	230	3.63	287	11.52
407	0.63	334	1.63	240	3.67	297	11.79
425	0.63	348	1.70	250	3.76	318	12.00
441	0.65	362	1.70	264	3.84	331	12.21
461	0.65	376	1.70	274	3.92	347	12.49
478	0.68	388	1.70	287	3.97	364	12.77
490	0.70	402	1.70	301	4.09	384	12.96
506	0.70	416	1.70	318	4.13	398	13.10
535	0.70	436	1.70	331	4.17	415	13.24
555	0.73	450	1.70	341	4.26	424	13.52
569	0.73	467	1.76	354	4.30	444	13.59
583	0.75	487	1.82	364	4.34	458	13.80
600	0.77	501	1.88	374	4.38	471	14.07
617	0.80	515	1.88	388	4.42	481	14.21
637	0.80	538	1.88	401	4.47	501	14.42
645	0.82	555	1.88	411	4.55	518	14.56
665	0.82	572	1.93	424	4.59	528	14.70
680	0.83	589	1.99	441	4.63	538	14.84
691	0.82	606	1.99	464	4.72	551	14.98
705	0.84	626	2.11	481	4.72	565	15.19
728	0.87	643	2.11	495	4.76	575	15.31
739	0.87	659	2.16	508	4.80	585	15.31
756	0.87	677	2.16	515	4.88	598	15.52
776	0.87	699	2.16	524	4.92	621	15.80

Table B.5 Experimentally obtained ratcheting strain of 304 steel at a constant mean stress and various stress amplitudes used in figure 4.8a (Continued)

Exp. Data 10±260MPa		Exp. Data 10±280MPa		Exp. 10±300MPa		Exp. Data 10±350MPa	
N(Cycle)	εr(%)	N(Cycle)	εr(%)	N(Cycle)	εr(%)	N(Cycle)	εr(%)
793	0.89	717	2.16	545	4.97	638	15.94
807	0.89	736	2.22	571	5.00	658	16.15
824	0.91	759	2.22	588	5.00	678	16.35
832	0.91	776	2.28	602	5.08	692	16.56
849	0.94	796	2.28	608	5.13	702	16.56
869	0.94	812	2.34	621	5.17	705	16.70
889	0.94	830	2.34	635	5.25	728	16.84
909	0.96	849	2.40	652	5.25	748	17.12
926	0.97	869	2.40	665	5.29	775	17.47
946	0.98	889	2.40	675	5.33	799	17.59
965	0.98	911	2.40	689	5.42	818	17.80
980	0.98	932	2.45	699	5.42	835	18.01
991	0.98	946	2.40	709	5.46	855	18.15
997	0.99	957	2.45	718	5.50	882	18.36
---	---	977	2.51	732	5.58	906	18.63
---	---	991	2.51	742	5.58	936	18.91
---	---	---	---	759	5.63	959	19.26
---	---	---	---	775	5.71	976	19.40
---	---	---	---	785	5.75	986	19.47
---	---	---	---	802	5.83	---	---
---	---	---	---	815	5.88	---	---
---	---	---	---	832	5.96	---	---
---	---	---	---	845	5.96	---	---
---	---	---	---	862	6.00	---	---
---	---	---	---	882	6.08	---	---
---	---	---	---	903	6.17	---	---
---	---	---	---	925	6.17	---	---
---	---	---	---	939	6.25	---	---
---	---	---	---	952	6.25	---	---
---	---	---	---	976	6.33	---	---
---	---	---	---	986	6.33	---	---
---	---	---	---	993	6.37	---	---
---	---	---	---	999	6.37	---	---

Table B.6 Experimentally obtained ratcheting strain of 42CrMo steel at a constant mean stress and various stress amplitudes used in figure 4.8b

Exp. Data 50±350MPa				Exp. Data 50±325MPa				Exp. Data 50±400MPa			
N (Cycle)	ε_r (%)	N (Cycle)	ε_r (%)	N (Cycle)	ε_r (%)	N (Cycle)	ε_r (%)	N (Cycle)	ε_r (%)	N (Cycle)	ε_r (%)
0	0	269	2.69	0	0	238	1.81	0	0	169	4.68
3	0.58	280	2.69	3	0.23	250	1.87	3	0.32	179	4.80
6	0.78	290	2.75	4	0.41	259	1.84	3	0.61	188	4.88
10	0.92	301	2.75	5	0.56	269	1.90	4	0.82	200	5.06
15	1.06	310	2.82	6	0.64	278	1.93	5	1.04	210	5.16
18	1.13	320	2.86	9	0.71	289	1.96	5	1.22	218	5.24
24	1.23	331	2.89	11	0.76	300	1.93	7	1.33	229	5.39
29	1.30	341	2.93	15	0.82	309	1.96	10	1.42	239	5.52
35	1.34	349	2.96	20	0.89	320	1.99	14	1.60	250	5.63
39	1.44	361	2.99	25	0.97	329	1.99	16	1.72	259	5.78
43	1.48	369	2.99	32	1.00	338	2.05	17	1.81	270	5.87
50	1.51	380	2.99	38	1.04	349	2.05	22	1.93	280	5.99
54	1.55	391	3.03	42	1.06	359	2.11	25	2.05	289	6.05
60	1.58	400	3.06	46	1.06	370	2.14	29	2.11	298	6.17
65	1.65	411	3.10	52	1.12	380	2.14	32	2.23	310	6.32
74	1.72	423	3.20	58	1.15	388	2.17	34	2.29	318	6.38
77	1.75	429	3.20	64	1.18	399	2.17	36	2.35	329	6.50
82	1.79	440	3.23	69	1.24	408	2.20	40	2.47	339	6.59
88	1.82	450	3.23	75	1.27	419	2.23	45	2.56	349	6.68
96	1.89	460	3.23	82	1.27	428	2.26	51	2.67	362	6.80
110	1.96	469	3.30	88	1.33	437	2.26	57	2.82	369	6.89
120	2.06	479	3.30	97	1.36	450	2.23	63	2.97	379	6.98
130	2.06	490	3.34	102	1.39	461	2.32	68	3.07	390	7.09
141	2.09	499	3.37	110	1.39	468	2.32	73	3.15	399	7.25
149	2.16	---	---	120	1.48	479	2.35	76	3.25	409	7.34
159	2.20	---	---	128	1.51	488	2.38	80	3.30	420	7.40
170	2.27	---	---	139	1.57	497	2.41	85	3.36	428	7.48
180	2.30	---	---	151	1.57	---	---	91	3.45	438	7.58
189	2.34	---	---	159	1.60	---	---	95	3.51	449	7.70
199	2.37	---	---	169	1.63	---	---	100	3.66	458	7.78
210	2.44	---	---	177	1.66	---	---	109	3.81	468	7.91
220	2.51	---	---	188	1.69	---	---	120	3.93	478	7.96
230	2.55	---	---	199	1.69	---	---	129	4.11	487	8.08
241	2.58	---	---	208	1.72	---	---	139	4.26	498	8.20
249	2.62	---	---	220	1.75	---	---	150	4.38	---	---
259	2.65	---	---	228	1.81	---	---	161	4.56	---	---

Table B.7 Experimentally obtained ratcheting strain of SS316L steel at a constant mean stress and various stress amplitudes used in figure 4.8c

Exp. Data 69±300MPa		Exp. Data 69±327MPa		Exp. Data 69±346MPa	
N(Cycle)	ε_r(%)	N(Cycle)	ε_r(%)	N(Cycle)	ε_r(%)
0	0	0	0	0	0
3	1.67	3	2.43	3	4.58
5	1.96	5	3.07	5	5.10
7	2.31	5	3.47	5	5.68
19	2.66	7	3.95	7	6.39
36	2.84	7	4.58	10	6.97
50	2.89	10	5.16	12	7.37
62	2.95	12	5.39	24	8.19
79	3.01	19	5.93	31	8.66
93	3.07	33	6.22	40	8.95
107	3.13	43	6.45	50	9.24
119	3.13	52	6.68	62	9.48
143	3.07	65	6.79	72	9.83
162	3.07	76	6.97	81	10.12
183	3.13	83	7.14	90	10.23
204	3.18	93	7.31	102	10.46
223	3.18	100	7.37	123	10.87
245	3.24	121	7.55	140	11.22
261	3.30	143	7.79	162	11.52
283	3.24	162	7.96	180	11.86
304	3.24	188	8.19	199	12.15
323	3.30	204	8.31	221	12.44
342	3.30	221	8.43	240	12.67
361	3.36	240	8.60	261	12.91
382	3.36	263	8.72	280	13.14
404	3.30	283	8.83	302	13.38
422	3.41	302	8.95	321	13.50
444	3.36	321	9.12	342	13.73
463	3.41	339	9.24	361	13.90
482	3.41	361	9.29	380	14.02
501	3.41	385	9.41	399	14.31
551	3.41	401	9.54	420	14.48
601	3.47	422	9.65	444	14.65
655	3.47	442	9.71	463	14.83
702	3.53	458	9.83	484	14.94
752	3.47	484	9.94	503	15.13
805	3.59	503	10.00	553	15.47
852	3.65	553	10.12	601	15.88
902	3.59	601	10.35	653	16.23
952	3.65	653	10.52	705	16.52
1001	3.65	702	10.64	752	16.81
---	---	752	10.87	800	17.11
---	---	802	11.04	852	17.45
---	---	854	11.16	904	17.69
---	---	900	11.27	952	17.97
---	---	952	11.40	999	18.21
---	---	1001	11.46	---	---

Table B.8 Experimentally obtained ratcheting strain of copper alloy at a constant mean stress and various stress amplitudes used in figure 4.8d

Exp. Data 18±73MPa		Exp. Data 18±91MPa		Exp. Data 18±109MPa	
N(Cycle)	ε_r(%)	N(Cycle)	ε_r(%)	N(Cycle)	ε_r(%)
0	0	0	0	0	0
1	1.56	1	4.33	4	5.86
4	1.84	4	4.54	7	6.89
10	1.98	7	4.81	10	7.09
26	2.12	10	5.02	12	7.44
35	2.12	21	5.30	23	7.30
49	2.19	35	5.51	32	7.23
60	2.19	46	5.72	38	7.03
77	2.19	57	5.79	52	7.65
94	2.26	77	5.86	63	7.93
108	2.19	89	5.93	72	8.28
122	2.12	99	5.98	80	8.47
139	2.19	122	6.05	91	8.68
164	2.19	142	6.19	102	8.89
181	2.33	162	6.19	122	9.31
201	2.33	181	6.33	142	9.38
221	2.26	201	6.33	164	9.51
249	2.33	221	6.47	181	9.79
274	2.33	243	6.47	201	10.14
302	2.26	263	6.54	221	10.42
325	2.33	280	6.61	243	10.68
347	2.33	302	6.68	263	10.89
364	2.33	322	6.68	282	11.10
387	2.33	344	6.82	299	11.31
401	2.33	364	6.82	319	11.52
423	2.33	384	6.89	342	11.72
443	2.33	398	6.96	358	12.00
460	2.40	418	6.96	381	12.21
479	2.40	440	7.03	401	12.42
496	2.40	460	7.09	420	12.56
553	2.40	482	7.16	440	12.77
597	2.40	502	7.23	460	12.91
654	2.40	547	7.30	482	13.17
696	2.33	597	7.44	499	13.24
752	2.33	651	7.51	550	13.73
797	2.47	702	7.58	597	14.21
845	2.40	750	7.72	648	14.56
899	2.40	797	7.72	699	14.98
952	2.40	851	7.86	750	15.31
997	2.40	896	7.93	797	15.80
---	---	943	8.00	845	16.08
---	---	992	8.14	896	16.42
---	---	---	---	946	16.84
---	---	---	---	994	17.12

Table B.9 Experimentally obtained ratcheting strain of 304 steel at constant amplitude stress and various mean stresses used in figure 4.9a

Exp. Data 5±300MPa		Exp. Data 20±300MPa		Exp. Data 30±300MPa		Exp. Data 40±300MPa	
N(Cycle)	ε_r(%)	N(Cycle)	ε_r(%)	N(Cycle)	ε_r(%)	N(Cycle)	ε_r(%)
0	0	0	0	0	0	0	0
3	0.57	10	2.72	12	3.97	4	4.37
10	0.90	20	3.31	18	4.22	10	4.58
10	1.15	30	3.63	21	4.40	16	4.79
17	1.31	40	3.88	30	4.60	21	5.00
24	1.40	50	4.09	32	4.78	27	5.21
33	1.48	67	4.51	38	4.96	32	5.42
46	1.65	77	4.63	44	5.14	41	5.67
57	1.73	87	4.76	52	5.28	52	5.84
67	1.85	94	4.97	55	5.38	61	6.01
73	1.94	110	5.08	61	5.53	72	6.23
83	2.02	117	5.21	67	5.60	83	6.44
90	2.06	124	5.33	72	5.70	95	6.61
100	2.19	137	5.50	78	5.84	103	6.75
110	2.26	147	5.63	86	5.99	111	6.89
117	2.35	154	5.75	95	6.06	120	7.00
127	2.39	167	5.83	101	6.19	128	7.10
137	2.51	184	6.04	106	6.31	139	7.24
147	2.56	194	6.13	120	6.48	148	7.35
157	2.60	204	6.25	129	6.58	160	7.49
164	2.64	224	6.41	138	6.73	171	7.59
174	2.72	240	6.62	149	6.87	188	7.77
190	2.85	254	6.78	157	7.04	207	7.94
204	2.93	267	6.91	169	7.19	219	8.05
217	3.01	284	6.99	180	7.29	233	8.22
227	3.06	301	7.16	192	7.40	247	8.33
244	3.10	324	7.28	206	7.50	261	8.43
257	3.18	337	7.37	220	7.68	278	8.61
271	3.26	351	7.49	232	7.75	290	8.72
294	3.35	374	7.62	238	7.89	312	8.82
318	3.43	391	7.74	257	8.07	326	8.92
331	3.43	411	7.86	275	8.24	337	8.99
337	3.47	427	7.99	291	8.31	351	9.17
351	3.51	451	8.15	303	8.46	369	9.24
364	3.63	475	8.24	314	8.53	385	9.34
374	3.63	498	8.36	331	8.60	402	9.45
388	3.72	521	8.53	346	8.77	422	9.49
401	3.72	545	8.61	362	8.92	439	9.63
418	3.80	561	8.74	380	8.99	450	9.69
427	3.84	588	8.82	405	9.16	467	9.76

Table B.9 Experimentally obtained ratcheting strain of 304 steel at constant amplitude stress and various mean stresses used in figure 4.9a (Continued)

Exp. Data 5±300MPa		Exp. Data 20±300MPa		Exp. Data 30±300MPa		Exp. Data 40±300MPa	
N(Cycle)	ε_r(%)	N(Cycle)	ε_r(%)	N(Cycle)	ε_r(%)	N(Cycle)	ε_r(%)
444	3.88	608	8.94	425	9.24	487	9.87
458	3.92	628	9.03	439	9.34	513	9.97
464	3.92	652	9.11	457	9.48	543	10.11
485	4.01	668	9.23	485	9.62	557	10.15
501	4.09	689	9.31	471	9.62	529	10.01
515	4.09	709	9.40	502	9.73	504	9.94
528	4.17	728	9.48	517	9.76	575	10.22
541	4.22	755	9.56	531	9.83	594	10.33
558	4.22	779	9.65	554	9.97	608	10.40
565	4.26	799	9.69	573	10.01	622	10.47
585	4.30	829	9.85	590	10.15	640	10.50
602	4.34	859	9.94	607	10.26	654	10.57
615	4.34	876	9.98	619	10.29	671	10.64
625	4.38	899	10.10	636	10.43	690	10.71
631	4.42	922	10.19	656	10.51	710	10.78
641	4.51	942	10.27	681	10.61	727	10.88
655	4.51	966	10.31	699	10.68	738	10.88
672	4.55	983	10.35	715	10.75	755	10.95
682	4.55	996	10.40	738	10.82	772	11.02
695	4.59	---	---	764	10.90	792	11.10
712	4.63	---	---	778	10.93	809	11.13
732	4.67	---	---	792	11.03	823	11.20
752	4.76	---	---	810	11.10	840	11.27
765	4.80	---	---	826	11.17	860	11.34
782	4.84	---	---	844	11.24	877	11.38
799	4.88	---	---	855	11.32	888	11.44
809	4.88	---	---	867	11.35	905	11.48
825	4.97	---	---	878	11.42	919	11.55
835	5.00	---	---	889	11.42	931	11.58
855	5.04	---	---	904	11.53	945	11.62
869	5.04	---	---	920	11.56	956	11.69
889	5.08	---	---	934	11.60	967	11.69
903	5.08	---	---	946	11.60	984	11.72
915	5.17	---	---	960	11.63	993	11.79
929	5.17	---	---	972	11.67	1000	11.83
939	5.17	---	---	980	11.70	---	---
956	5.17	---	---	992	11.70	---	---
973	5.25	---	---	1000	11.74	---	---
986	5.25	---	---	---	---	---	---
996	5.25	---	---	---	---	---	---

Table B.10 Experimentally obtained ratcheting strain of 42CrMo steel at constant amplitude stress and various mean stresses used in figure 4.9b

Exp. Data 100±350MPa				Exp. Data 150±350MPa			
N(Cycle)	ε_r(%)	N(Cycle)	ε_r(%)	N(Cycle)	ε_r(%)	N(Cycle)	ε_r(%)
0	0	269	4.86	0	0	260	6.76
1	1.13	280	4.93	1	1.89	270	6.86
2	1.34	290	5.00	3	2.09	283	6.97
5	1.48	299	5.07	4	2.30	288	7.07
6	1.65	310	5.10	7	2.48	299	7.18
8	1.82	320	5.21	10	2.69	309	7.25
12	1.99	330	5.21	15	2.86	320	7.35
17	2.13	340	5.31	19	2.99	331	7.45
21	2.23	349	5.38	22	3.13	340	7.56
24	2.30	361	5.41	25	3.23	352	7.69
29	2.41	369	5.45	29	3.37	363	7.76
35	2.58	381	5.52	33	3.51	370	7.83
39	2.65	393	5.62	38	3.62	380	7.86
47	2.75	402	5.62	42	3.69	390	8.00
53	2.82	411	5.72	47	3.83	400	8.07
58	2.96	420	5.76	54	4.00	408	8.21
64	3.03	430	5.83	60	4.10	422	8.28
70	3.06	440	5.86	65	4.24	429	8.32
75	3.13	450	5.90	70	4.27	441	8.42
79	3.17	462	5.97	74	4.34	448	8.49
86	3.27	471	6.04	79	4.48	461	8.63
91	3.34	479	6.11	86	4.58	472	8.73
96	3.41	492	6.11	92	4.69	479	8.73
110	3.55	500	6.17	99	4.83	490	8.87
118	3.65	---	---	107	4.97	500	8.97
128	3.72	---	---	118	5.10	---	---
139	3.83	---	---	130	5.24	---	---
149	3.93	---	---	141	5.38	---	---
160	4.03	---	---	149	5.52	---	---
171	4.07	---	---	159	5.62	---	---
181	4.24	---	---	169	5.76	---	---
191	4.31	---	---	180	5.90	---	---
201	4.34	---	---	191	6.00	---	---
210	4.41	---	---	201	6.07	---	---
220	4.48	---	---	209	6.17	---	---
230	4.58	---	---	221	6.38	---	---
241	4.65	---	---	231	6.45	---	---
251	4.72	---	---	239	6.59	---	---
262	4.79	---	---	251	6.66	---	---

Table B.11 Experimentally obtained ratcheting strain of SS316L steel at constant amplitude stress and various mean stresses used in figure 4.9c

Exp. Data 10±346MPa		Exp. Data 30±346MPa			
N(Cycle)	ε_r(%)	N(Cycle)	ε_r(%)	N(Cycle)	ε_r(%)
0	0	0	0	645	12.33
3	0.80	1	1.49	695	12.79
17	1.15	3	2.14	748	13.08
33	1.38	4	2.49	800	13.44
48	1.49	5	2.89	850	13.78
67	1.72	12	3.24	900	14.19
81	1.96	17	3.70	944	14.42
98	2.08	31	4.18	992	14.77
119	2.31	38	4.41	---	---
138	2.43	52	4.81	---	---
159	2.60	60	5.05	---	---
180	2.78	69	5.28	---	---
199	2.95	76	5.57	---	---
219	3.07	88	5.68	---	---
238	3.13	98	5.93	---	---
261	3.30	114	6.33	---	---
283	3.41	128	6.50	---	---
302	3.53	136	6.79	---	---
321	3.65	162	7.14	---	---
342	3.76	183	7.43	---	---
361	3.88	197	7.73	---	---
382	3.95	216	8.02	---	---
399	4.06	240	8.31	---	---
420	4.18	261	8.54	---	---
439	4.29	283	8.83	---	---
461	4.35	297	9.06	---	---
479	4.47	318	9.29	---	---
498	4.53	339	9.48	---	---
548	4.76	359	9.77	---	---
598	4.99	378	10.06	---	---
650	5.16	401	10.17	---	---
698	5.34	418	10.35	---	---
748	5.57	442	10.52	---	---
797	5.68	456	10.64	---	---
847	5.87	477	10.93	---	---
897	6.04	501	11.04	---	---
947	6.22	546	11.57	---	---
994	6.33	598	11.92	---	---

Table B.12 Experimentally obtained ratcheting strain of copper at constant amplitude stress and various mean stresses used in figure 4.9d

Exp. Data 36±73MPa		Exp. Data 55±73MPa	
N(Cycle)	ε_r(%)	N(Cycle)	ε_r(%)
0	0	0	0
1	2.19	1	3.35
3	2.32	2	3.48
5	2.40	3	3.58
7	2.46	4	3.64
12	2.56	10	3.75
21	2.69	12	3.85
29	2.73	18	3.97
46	2.77	29	4.01
57	2.79	49	4.03
69	2.81	60	4.08
80	2.81	77	4.12
91	2.83	94	4.12
105	2.83	111	4.12
122	2.85	128	4.16
139	2.90	147	4.16
162	2.90	164	4.16
181	2.90	184	4.18
204	2.92	204	4.20
223	2.94	226	4.20
243	2.92	246	4.22
263	2.96	260	4.24
282	2.96	282	4.26
305	2.98	299	4.26
325	2.98	322	4.26
339	2.98	339	4.28
361	3.00	364	4.28
381	3.00	384	4.28
404	3.02	401	4.28
420	3.02	426	4.31
440	3.02	445	4.33
462	3.02	462	4.33
482	3.04	479	4.35
502	3.04	499	4.35
550	3.06	553	4.37
600	3.04	600	4.41
654	3.04	648	4.43
702	3.08	699	4.45
752	3.10	758	4.45
803	3.10	797	4.47
851	3.13	848	4.49
901	3.13	901	4.49
949	3.17	949	4.49
997	3.17	1000	4.53

Table B.13 Experimentally obtained ratcheting strain of 304 steel at various stress ratios and constant maximum stress used in figure 4.10a

Exp. Data R=-0.50 (95±281MPa)		Exp. Data R=-0.67 (60±313MPa)		Exp. Data R=-0.80 (40±337MPa)		Exp. Data R=-0.90 (20±356MPa)	
N(Cycle)	ε_r(%)	N(Cycle)	ε_r(%)	N(Cycle)	ε_r(%)	N(Cycle)	ε_r(%)
0	0	0	0	0	0	0	0
1	2.47	2	5.14	2	2.62	1	2.82
2	2.98	3	5.57	4	3.20	7	3.34
3	3.41	4	5.99	5	3.85	10	4.12
4	3.78	5	6.42	7	4.34	15	4.72
5	4.56	7	6.79	8	4.85	25	5.32
7	4.85	12	7.15	9	5.43	31	5.67
8	5.21	17	7.29	12	5.64	36	5.93
9	5.35	25	7.49	17	6.06	42	6.19
14	5.43	33	7.78	25	6.50	47	6.63
22	5.71	40	7.93	31	6.79	53	6.97
26	5.71	47	8.00	38	7.00	61	7.48
31	5.84	56	8.29	44	7.22	67	7.65
39	5.92	63	8.43	52	7.49	75	7.91
47	6.06	71	8.58	58	7.64	84	8.17
53	6.06	76	8.58	62	7.86	89	8.43
59	6.06	82	8.80	69	8.07	96	8.70
66	6.13	90	8.87	76	8.36	106	8.96
73	6.13	97	8.94	83	8.58	111	9.22
78	6.21	109	9.09	90	8.80	117	9.30
87	6.35	120	9.16	97	8.94	123	9.65
95	6.28	128	9.36	104	9.16	130	9.91
103	6.28	137	9.51	112	9.36	138	10.17
109	6.28	147	9.58	120	9.58	146	10.26
119	6.42	158	9.72	129	9.65	153	10.42
128	6.50	168	9.72	136	9.79	164	10.76
139	6.50	178	9.94	146	10.01	175	11.20
148	6.50	188	10.01	157	10.16	184	11.37
159	6.64	198	10.08	164	10.45	194	11.55
171	6.64	209	10.23	150	10.30	203	11.89
179	6.57	220	10.37	173	10.52	215	12.07
190	6.64	229	10.37	184	10.73	224	12.33
199	6.64	238	10.52	199	10.94	234	12.41
208	6.71	249	10.59	192	10.88	244	12.76
218	6.71	259	10.66	209	11.01	255	13.02
229	6.79	268	10.73	220	11.30	264	13.19

Table B.13 Experimentally obtained ratcheting strain of 304 steel at various stress ratios and constant maximum stress used in figure 4.10a (Continued)

Exp. Data R=-0.50 (95±281MPa)		Exp. Data R=-0.67 (60±313MPa)		Exp. Data R=-0.80 (40±337MPa)		Exp. Data R=-0.90 (20±356MPa)	
N(Cycle)	ε_r(%)	N(Cycle)	ε_r(%)	N(Cycle)	ε_r(%)	N(Cycle)	ε_r(%)
239	6.79	278	10.81	229	11.44	273	13.35
249	6.71	288	10.94	238	11.52	285	13.53
260	6.71	299	10.94	250	11.81	295	13.79
269	6.86	309	11.01	260	11.95	305	14.05
281	6.86	318	11.01	271	12.09	316	14.13
290	6.86	327	11.15	281	12.31	327	14.31
299	6.86	339	11.23	288	12.38	334	14.48
308	7.00	349	11.37	298	12.38	344	14.74
315	6.93	359	11.37	308	12.53	355	14.92
323	6.93	369	11.44	320	12.67	365	15.00
332	7.07	377	11.44	327	12.80	376	15.18
344	6.93	390	11.52	339	12.95	387	15.44
356	7.00	398	11.52	349	13.02	397	15.61
368	7.07	408	11.59	359	13.09	408	15.70
376	7.07	419	11.66	369	13.24	420	15.87
387	7.15	427	11.81	378	13.38	429	16.13
399	7.07	437	11.95	386	13.45	439	16.13
413	7.22	449	12.02	396	13.53	447	16.46
422	7.22	458	11.95	408	13.60	461	16.55
433	7.22	469	12.09	419	13.89	469	16.64
442	7.22	477	12.09	429	13.89	479	16.81
452	7.22	487	11.95	437	14.03	489	17.07
464	7.22	495	12.17	449	14.11	499	17.25
472	7.29	---	---	458	14.25	504	17.25
481	7.29	---	---	470	14.32	505	17.51
488	7.29	---	---	480	14.32	---	---
494	7.29	---	---	491	14.53	---	---
498	7.29	---	---	499	14.53	---	---

Table B.14 Experimentally obtained ratcheting strain of 42CrMo steel at various stress ratios and constant maximum stress used in figure 4.10b

Exp. Data R=-0.90 (20±400MPa)				Exp. Data R=-0.75 (50±370MPa)				Exp. Data R=-0.50 (106±319MPa)			
N(Cycle)	ε_r(%)	N(Cycle)	ε_r(%)	N(Cycle)	ε_r(%)	N(Cycle)	ε_r(%)	N(Cycle)	ε_r(%)	N(Cycle)	ε_r(%)
0	0	269	2.71	0	0	220	3.93	0	0	279	3.88
1	0.16	280	2.75	5	0.85	240	4.05	3	1.22	298	3.95
3	0.30	289	2.79	6	0.99	259	4.23	4	1.32	319	4.03
5	0.44	299	2.87	9	1.13	279	4.35	5	1.46	339	4.11
9	0.58	309	2.91	11	1.26	300	4.48	6	1.54	360	4.19
12	0.66	319	2.95	12	1.34	320	4.64	7	1.62	380	4.29
16	0.70	329	2.99	16	1.40	341	4.74	9	1.69	400	4.33
19	0.77	340	3.05	18	1.50	359	4.87	10	1.77	419	4.42
23	0.83	349	3.07	20	1.60	380	4.99	14	1.87	439	4.48
28	0.91	360	3.11	24	1.69	398	5.09	18	1.95	458	4.54
33	0.99	368	3.17	26	1.75	419	5.19	25	2.09	479	4.62
39	1.05	380	3.23	28	1.81	439	5.31	32	2.18	497	4.66
45	1.13	388	3.25	30	1.91	458	5.44	35	2.20	---	---
50	1.22	398	3.29	33	1.99	479	5.56	40	2.30	---	---
57	1.30	409	3.34	38	2.07	497	5.64	44	2.34	---	---
64	1.36	419	3.38	40	2.16	---	---	52	2.42	---	---
70	1.42	428	3.42	44	2.22	---	---	58	2.48	---	---
78	1.48	439	3.46	47	2.26	---	---	64	2.54	---	---
84	1.56	449	3.52	53	2.32	---	---	70	2.60	---	---
91	1.62	460	3.56	60	2.42	---	---	76	2.64	---	---
104	1.71	468	3.60	68	2.54	---	---	80	2.69	---	---
111	1.75	479	3.62	74	2.62	---	---	86	2.75	---	---
120	1.83	489	3.68	83	2.69	---	---	95	2.83	---	---
130	1.89	497	3.76	90	2.77	---	---	111	2.91	---	---
141	1.97	---	---	94	2.83	---	---	102	2.87	---	---
151	2.03	---	---	100	2.89	---	---	119	2.97	---	---
160	2.09	---	---	107	2.93	---	---	130	3.03	---	---
169	2.16	---	---	111	3.01	---	---	140	3.11	---	---
178	2.22	---	---	119	3.07	---	---	151	3.17	---	---
190	2.28	---	---	130	3.19	---	---	160	3.25	---	---
202	2.36	---	---	140	3.29	---	---	169	3.32	---	---
209	2.40	---	---	151	3.38	---	---	180	3.38	---	---
220	2.46	---	---	160	3.46	---	---	191	3.42	---	---
231	2.50	---	---	171	3.56	---	---	201	3.48	---	---
241	2.58	---	---	181	3.66	---	---	221	3.58	---	---
248	2.64	---	---	192	3.66	---	---	241	3.68	---	---
261	2.67	---	---	200	3.78	---	---	258	3.76	---	---

Table B.15 Experimentally obtained ratcheting strain of SS316L steel alloy at various stress ratios and constant maximum stress used in figure 4.10c

Exp. Data R=-0.50 (99±297MPa)			
N(Cycle)	ε_r(%)	N(Cycle)	ε_r(%)
0	0	551	8.06
2	2.37	603	8.17
4	3.03	655	8.24
5	3.45	700	8.31
6	4.01	752	8.41
7	4.64	805	8.44
12	5.30	847	8.48
22	5.76	904	8.55
31	6.00	950	8.62
40	6.14	999	8.65
52	6.24	---	---
62	6.38	---	---
74	6.49	---	---
83	6.56	---	---
100	6.66	---	---
121	6.76	---	---
143	6.94	---	---
162	7.01	---	---
180	7.05	---	---
199	7.19	---	---
223	7.26	---	---
245	7.29	---	---
261	7.36	---	---
283	7.43	---	---
302	7.50	---	---
325	7.53	---	---
344	7.64	---	---
361	7.64	---	---
385	7.71	---	---
406	7.78	---	---
420	7.78	---	---
444	7.85	---	---
461	7.88	---	---
484	7.92	---	---
501	7.96	---	---

Table B.16 Experimentally obtained ratcheting strain of copper at various stress ratios and constant maximum stress used in figure 4.10d

Exp. Data R=-0.25 (55±90MPa)				Exp. Data R=-0.38 (45±100MPa)			
N(Cycle)	ε_r(%)	N(Cycle)	ε_r(%)	N(Cycle)	ε_r(%)	N(Cycle)	ε_r(%)
0	0	702	8.64	0	0	600	9.98
4	5.84	752	8.69	4	5.84	648	10.14
7	6.15	800	8.79	9	6.15	702	10.30
10	6.35	853	8.90	10	6.35	752	10.45
12	6.61	904	8.95	11	6.61	803	10.61
26	6.72	952	9.05	12	6.82	853	10.76
35	6.77	1002	9.11	21	7.03	901	10.82
49	6.82	---	---	32	7.14	952	10.97
60	6.88	---	---	43	7.24	1000	11.02
72	6.98	---	---	55	7.34	---	---
86	7.03	---	---	66	7.40	---	---
102	7.08	---	---	80	7.55	---	---
119	7.19	---	---	91	7.66	---	---
142	7.29	---	---	102	7.71	---	---
162	7.29	---	---	122	7.86	---	---
181	7.40	---	---	139	8.01	---	---
201	7.45	---	---	162	8.17	---	---
223	7.50	---	---	181	8.32	---	---
243	7.55	---	---	201	8.38	---	---
263	7.60	---	---	223	8.48	---	---
282	7.71	---	---	240	8.59	---	---
302	7.76	---	---	263	8.74	---	---
322	7.81	---	---	282	8.85	---	---
342	7.92	---	---	302	8.90	---	---
361	7.92	---	---	322	9.00	---	---
384	8.01	---	---	342	9.11	---	---
401	8.01	---	---	361	9.11	---	---
420	8.06	---	---	381	9.21	---	---
443	8.12	---	---	404	9.31	---	---
462	8.17	---	---	420	9.42	---	---
479	8.22	---	---	443	9.52	---	---
499	8.22	---	---	462	9.57	---	---
553	8.32	---	---	482	9.68	---	---
597	8.43	---	---	502	9.72	---	---
651	8.53	---	---	553	9.83	---	---

Table B.17 Experimentally obtained ratcheting strain of SS316L steel alloy at different stress levels used in figure 4.11

Exp. Data 76±242MPa		Exp. Data 52±247MPa		Exp. Data 52±273MPa		Exp. Data 64±247MPa			
N(Cycle)	ε_r(%)	N(Cycle)	ε_r(%)	N(Cycle)	ε_r(%)	N(Cycle)	ε_r(%)	N(Cycle)	ε_r(%)
0	0	0	0	0	0	0	0	144	4.39
1	2.51	1	2.37	1	3.99	1	2.42	149	4.41
2	2.89	2	2.67	3	4.74	3	2.80	153	4.41
3	3.04	3	2.95	5	4.93	4	3.17	155	4.41
4	3.21	5	3.12	10	5.16	6	3.42	160	4.41
5	3.28	8	3.17	13	5.31	9	3.56	165	4.41
6	3.36	13	3.27	18	5.41	15	3.71	167	4.41
7	3.45	16	3.32	21	5.48	20	3.79	172	4.41
9	3.54	21	3.39	26	5.58	25	3.89	175	4.46
12	3.62	26	3.49	31	5.63	29	3.91	178	4.46
16	3.71	31	3.52	36	5.70	34	3.99	180	4.46
21	3.80	35	3.59	43	5.80	38	3.99	188	4.49
26	3.87	38	3.59	46	5.85	43	4.06	190	4.49
32	3.94	41	3.59	51	5.93	48	4.09	193	4.51
39	3.99	46	3.64	55	5.95	52	4.11	196	4.51
46	4.04	50	3.67	61	6.03	56	4.14	198	4.51
55	4.09	54	3.74	65	6.05	58	4.14	---	---
62	4.12	59	3.77	70	6.10	61	4.14	---	---
70	4.16	64	3.77	75	6.13	64	4.16	---	---
79	4.20	67	3.79	79	6.18	68	4.16	---	---
89	4.25	71	3.79	84	6.23	72	4.19	---	---
99	4.28	74	3.79	89	6.23	76	4.19	---	---
107	4.30	79	3.79	94	6.30	82	4.24	---	---
117	4.32	81	3.79	98	6.33	87	4.24	---	---
126	4.34	86	3.79	99	6.33	91	4.26	---	---
136	4.37	90	3.79	---	---	96	4.29	---	---
144	4.39	93	3.82	---	---	99	4.31	---	---
151	4.39	97	3.86	---	---	105	4.31	---	---
159	4.40	99	3.86	---	---	110	4.31	---	---
166	4.42	---	---	---	---	115	4.34	---	---
172	4.43	---	---	---	---	119	4.34	---	---
179	4.45	---	---	---	---	123	4.34	---	---
187	4.47	---	---	---	---	127	4.34	---	---
193	4.47	---	---	---	---	129	4.36	---	---
198	4.48	---	---	---	---	132	4.36	---	---
---	---	---	---	---	---	136	4.36	---	---
---	---	---	---	---	---	141	4.34	---	---

Table B.18 Experimental ratcheting strain values of SS316L steel alloy over two-step (low-high) loading used in figure 4.13

Step1 (52±247MPa)		Step2 (78±247MPa)	
N(Cycle)	ε_r(%)	N(Cycle)	ε_r(%)
0	0	101	4.61
1	2.65	102	4.74
2	2.84	104	4.96
3	3.02	104	5.11
6	3.09	105	5.26
10	3.24	108	5.38
14	3.32	113	5.51
20	3.44	117	5.61
26	3.52	120	5.70
32	3.56	126	5.73
38	3.59	130	5.78
42	3.67	135	5.88
46	3.67	139	5.90
51	3.71	146	5.93
56	3.77	151	5.95
62	3.79	158	6.05
68	3.79	162	6.05
75	3.79	168	6.05
81	3.82	172	6.10
87	3.86	177	6.15
93	3.86	183	6.15
99	3.94	188	6.18
---	---	192	6.20
---	---	196	6.20
---	---	199	6.23

Table B.19 Experimentally obtained ratcheting strain of SA333 steel alloy at different stress levels used in figure 4.14

Exp. Data 40±350MPa		Exp. Data 80±350MPa		Exp. Data 120±350MPa		Exp. Data 80±270MPa	
N(Cycle)	ε_r(%)	N(Cycle)	ε_r(%)	N(Cycle)	ε_r(%)	N(Cycle)	ε_r(%)
0	0	0	0	0	0	0	0
1	1.42	1	1.61	1	3.30	14	1.66
2	1.61	2	2.57	2	3.49	16	1.85
4	1.80	4	3.11	3	3.68	21	2.04
7	1.99	6	3.49	4	3.87	26	2.04
10	2.18	8	3.68	5	3.87	32	2.23
13	2.38	10	3.87	6	4.25	40	2.23
18	2.57	16	4.44	8	4.44	48	2.42
25	2.92	25	5.02	11	4.64	61	2.42
36	3.30	36	5.78	16	5.21	75	2.61
49	3.68	52	6.55	23	5.78	93	2.80
73	4.06	77	7.12	32	6.55	118	2.99
100	4.64	111	8.26	43	7.12	155	3.37
134	5.21	170	9.57	59	7.88	225	3.72
189	5.78	273	10.91	77	8.65	284	3.72
259	6.35	450	12.62	100	9.38	366	4.11
364	7.31	684	13.96	131	10.14	482	4.68
512	8.07	1040	15.84	189	11.29	645	5.25
684	8.84	1673	17.75	273	12.62	849	5.82
915	9.57	---	---	395	13.77	1051	6.40
1125	10.33	---	---	584	15.30	1330	6.97
1390	10.91	---	---	868	16.79	1711	7.73
1673	11.48	---	---	1187	18.13	---	---
1909	12.05	---	---	1718	19.85	---	---

Table B.20 Experimental ratcheting strain values for SA333 Steel alloy under three-step loading condition with increasing (low-high) stress levels used in figure 4.16

Step 1 Exp. Data 40±350MPa		Step 2 Exp. Data 80±350MPa		Step 3 Exp. Data 120±350MPa	
N(Cycle)	ε_r(%)	N(Cycle)	ε_r(%)	N(Cycle)	ε_r(%)
0	0	780	10.31	2637	21.90
26	1.26	826	12.59	2683	22.96
49	3.80	872	12.98	2729	23.37
76	4.58	899	13.39	2755	23.76
99	4.99	922	13.65	2801	24.18
145	5.79	945	14.04	2847	24.57
190	6.32	1014	14.30	2966	24.98
213	6.86	1037	14.58	3035	25.24
286	7.38	1109	15.23	3131	25.63
332	7.92	1109	15.65	3249	26.30
451	8.44	1178	16.17	3318	26.56
520	8.72	1224	16.58	3437	26.97
592	9.11	1320	16.97	3506	27.37
661	9.53	1415	17.38	3552	27.63
734	9.92	1484	17.77	3647	27.76
780	10.18	1603	18.16	3693	27.91
---	---	1718	18.71	3812	28.04
---	---	1791	18.97	3881	28.30
---	---	1860	19.10	3977	28.56
---	---	1932	19.38	4118	28.97
---	---	1955	19.64	4233	29.49
---	---	2001	19.90	4306	29.75
---	---	2097	20.18	4424	30.03
---	---	2143	20.57	4562	30.30
---	---	2239	20.83	4658	30.43
---	---	2285	21.12	4777	30.69
---	---	2399	21.25	4869	30.97
---	---	2495	21.38	5010	31.23
---	---	2541	21.51	5152	31.49
---	---	---	---	5293	31.77
---	---	---	---	5435	31.90
---	---	---	---	5573	32.16
---	---	---	---	5669	32.42
---	---	---	---	5810	32.55
---	---	---	---	5952	32.83
---	---	---	---	6021	32.96
---	---	---	---	6162	33.22
---	---	---	---	6281	33.36
---	---	---	---	6419	33.64
---	---	---	---	6561	33.90
---	---	---	---	6679	34.03
---	---	---	---	6775	34.16
---	---	---	---	6890	34.29
---	---	---	---	7008	34.55
---	---	---	---	7104	34.83

Table B.21 Experimentally obtained ratcheting strain of SS316L(N) steel alloy at different stress levels used in figure 4.17

Exp. Data 10±210MPa		Exp. Data 10±230MPa		Exp. Data 10±250MPa		Exp. Data 30±230MPa		Exp. Data 30±250MPa	
N(Cycle)	ε_r(%)	N(Cycle)	ε_r(%)	N(Cycle)	ε_r(%)	N(Cycle)	ε_r(%)	N(Cycle)	ε_r(%)
0	0	0	0	0	0	0	0	0	0
7	0.05	3	0.17	3	0.27	3	0.70	7	0.82
24	0.12	10	0.32	7	0.46	7	1.05	10	1.64
46	0.15	26	0.41	13	0.62	10	1.28	13	1.96
77	0.17	53	0.46	20	0.79	13	1.45	16	2.18
114	0.20	80	0.49	36	0.91	24	1.60	21	2.39
150	0.22	114	0.53	60	1.01	45	1.76	27	2.54
177	0.22	143	0.56	87	1.10	73	1.93	36	2.68
214	0.24	177	0.60	114	1.19	105	2.06	59	2.87
247	0.24	211	0.62	150	1.27	140	2.17	88	3.06
277	0.25	247	0.63	197	1.36	181	2.27	123	3.23
308	0.25	287	0.65	244	1.41	216	2.35	160	3.37
337	0.25	324	0.69	297	1.45	259	2.44	192	3.50
368	0.27	361	0.69	351	1.48	294	2.51	224	3.60
401	0.29	401	0.70	398	1.51	325	2.55	268	3.74
434	0.29	441	0.74	454	1.53	366	2.62	314	3.86
471	0.29	481	0.74	501	1.57	398	2.66	357	3.95
508	0.29	521	0.74	551	1.58	441	2.72	392	4.04
545	0.29	565	0.76	605	1.60	482	2.77	439	4.14
571	0.29	602	0.76	655	1.62	532	2.82	491	4.23
605	0.31	641	0.77	702	1.63	575	2.87	534	4.31
635	0.31	678	0.79	748	1.65	621	2.90	580	4.37
665	0.31	718	0.79	806	1.67	664	2.93	627	4.44
695	0.31	759	0.79	855	1.69	708	2.96	668	4.50
725	0.31	792	0.79	903	1.70	757	2.97	717	4.55
759	0.31	832	0.79	949	1.74	801	3.00	769	4.62
796	0.31	872	0.81	986	1.76	850	3.05	810	4.65
822	0.31	919	0.82	---	---	899	3.06	853	4.68
859	0.31	962	0.84	---	---	937	3.09	885	4.71
886	0.31	996	0.84	---	---	969	3.11	931	4.74
912	0.31	---	---	---	---	1000	3.13	972	4.77
939	0.31	---	---	---	---	---	---	1000	4.80
966	0.32	---	---	---	---	---	---	---	---
989	0.32	---	---	---	---	---	---	---	---

Table B.22 Experimental ratcheting strain values for SS316L(N) Steel alloy under two-step loading with low-high sequences used in figure 4.19a

Step1 (10±210MPa)		Step2 (10±230MPa)		Step1 (30±210MPa)		Step2 (30±230MPa)	
N(Cycle)	ε_r(%)	N(Cycle)	ε_r(%)	N(Cycle)	ε_r(%)	N(Cycle)	ε_r(%)
0	0	105	0.20	0	0	100	1.07
2	0.003	109	0.26	2	0.18	102	1.20
16	0.03	132	0.29	5	0.36	103	1.31
34	0.06	160	0.32	8	0.49	114	1.46
48	0.08	195	0.36	16	0.58	128	1.58
65	0.08	229	0.39	31	0.67	143	1.70
77	0.09	261	0.41	45	0.78	160	1.79
91	0.11	299	0.43	57	0.82	180	1.86
100	0.12	330	0.45	71	0.85	209	1.97
---	---	368	0.47	85	0.91	235	2.04
---	---	405	0.48	94	0.95	269	2.12
---	---	439	0.49	---	---	296	2.18
---	---	466	0.51	---	---	333	2.23
---	---	506	0.51	---	---	370	2.29
---	---	549	0.51	---	---	405	2.34
---	---	598	0.52	---	---	445	2.38
---	---	644	0.54	---	---	489	2.43
---	---	693	0.56	---	---	540	2.47
---	---	739	0.56	---	---	592	2.53
---	---	776	0.56	---	---	635	2.56
---	---	828	0.57	---	---	687	2.58
---	---	863	0.57	---	---	727	2.61
---	---	906	0.57	---	---	774	2.65
---	---	937	0.58	---	---	811	2.68
---	---	969	0.58	---	---	848	2.70
---	---	---	---	---	---	891	2.74
---	---	---	---	---	---	932	2.77
---	---	---	---	---	---	961	2.78
---	---	---	---	---	---	978	2.82

Table B.23 Experimental ratcheting strain values for SS316L(N) Steel alloy under two-step loading with low-high sequences used in figure 4.19b

Step1 (30±210MPa)		Step2 (30±250MPa)		Step1 (30±230MPa)		Step2 (30±250MPa)	
N(Cycle)	ε_r(%)	N(Cycle)	ε_r(%)	N(Cycle)	ε_r(%)	N(Cycle)	ε_r(%)
0	0	97	1.95	0	0	103	2.10
2	0.02	100	2.14	2	1.02	110	2.34
2	0.18	103	2.35	5	1.22	117	2.59
5	0.36	109	2.52	16	1.39	140	2.86
8	0.49	123	2.68	28	1.52	169	3.04
16	0.58	137	2.86	51	1.70	209	3.23
31	0.67	157	2.98	74	1.79	255	3.39
45	0.78	189	3.14	97	1.86	292	3.48
57	0.82	215	3.25	---	---	333	3.54
71	0.85	249	3.38	---	---	368	3.63
85	0.91	278	3.45	---	---	413	3.74
94	0.95	310	3.56	---	---	471	3.84
---	---	342	3.66	---	---	517	3.91
---	---	373	3.74	---	---	578	3.99
---	---	405	3.80	---	---	638	4.06
---	---	443	3.89	---	---	704	4.14
---	---	480	3.96	---	---	756	4.21
---	---	520	4.02	---	---	805	4.27
---	---	563	4.08	---	---	843	4.30
---	---	595	4.12	---	---	900	4.38
---	---	635	4.17	---	---	941	4.42
---	---	687	4.23	---	---	969	4.45
---	---	736	4.27	---	---	---	---
---	---	785	4.35	---	---	---	---
---	---	831	4.39	---	---	---	---
---	---	871	4.44	---	---	---	---
---	---	914	4.46	---	---	---	---
---	---	946	4.48	---	---	---	---
---	---	972	4.51	---	---	---	---

Table B.24 Experimental ratcheting strain values for SS316L(N) Steel alloy under two-step loading with low-high sequences used in figure 4.19c

Step1 (10±210MPa)		Step2 (30±210MPa)		Step2 (30±230MPa)		Step2 (30±250MPa)	
N(Cycle)	ε_r(%)	N(Cycle)	ε_r(%)	N(Cycle)	ε_r(%)	N(Cycle)	ε_r(%)
0	0	105	0.36	104	0.64	104	1.23
3	0.03	110	0.51	106	0.92	106	1.57
13	0.06	133	0.63	115	1.18	109	1.90
50	0.10	157	0.74	129	1.40	115	2.16
73	0.12	186	0.82	157	1.57	127	2.35
90	0.12	215	0.92	192	1.71	143	2.58
100	0.22	252	0.96	232	1.85	172	2.76
---	---	286	1.04	277	1.96	203	2.91
---	---	328	1.10	328	2.05	240	3.07
---	---	368	1.11	374	2.14	283	3.23
---	---	408	1.14	422	2.21	331	3.39
---	---	445	1.17	468	2.27	377	3.51
---	---	482	1.21	522	2.32	439	3.63
---	---	522	1.26	585	2.39	502	3.72
---	---	565	1.27	650	2.43	562	3.82
---	---	616	1.30	707	2.49	630	3.89
---	---	647	1.30	761	2.52	696	3.96
---	---	684	1.33	832	2.58	750	4.04
---	---	715	1.33	886	2.61	830	4.11
---	---	747	1.35	934	2.64	895	4.17
---	---	784	1.37	963	2.67	943	4.23
---	---	810	1.37	994	2.70	989	4.27
---	---	846	1.39	---	---	---	---
---	---	878	1.39	---	---	---	---
---	---	909	1.40	---	---	---	---
---	---	941	1.44	---	---	---	---
---	---	972	1.42	---	---	---	---
---	---	992	1.42	---	---	---	---

Table B.25 Experimental ratcheting strain values for SS316L(N) Steel alloy under two-step loading with high-low sequences used in figure 4.19d

Step1 (30±230MPa)		Step2 (10±230MPa)		Step1 (30±230MPa)		Step2 (10±210MPa)		Step1 (30±250MPa)		Step2 (10±230MPa)	
N(Cycle)	ε_r(%)	N(Cycle)	ε_r(%)	N(Cycle)	ε_r(%)	N(Cycle)	ε_r(%)	N(Cycle)	ε_r(%)	N(Cycle)	ε_r(%)
0	0	103	1.72	0	0	105	1.88	0	0	114	2.95
1	0.36	111	1.72	1	0.36	120	1.88	2	0.51	140	2.93
1	0.78	140	1.72	1	0.78	143	1.88	3	1.07	189	2.91
4	1.11	189	1.72	4	1.11	169	1.88	4	1.69	253	2.93
7	1.31	227	1.70	7	1.31	210	1.88	4	2.03	323	2.93
13	1.45	276	1.73	13	1.45	265	1.88	7	2.20	398	2.91
21	1.55	334	1.73	21	1.55	334	1.88	16	2.35	476	2.91
33	1.67	407	1.73	33	1.67	401	1.88	30	2.51	563	2.91
53	1.76	473	1.73	53	1.76	471	1.87	48	2.66	653	2.93
71	1.87	537	1.73	71	1.87	546	1.88	68	2.78	720	2.93
85	1.91	607	1.73	85	1.91	610	1.88	80	2.87	780	2.91
97	1.96	679	1.72	97	1.96	659	1.88	94	2.95	836	2.93
---	---	743	1.73	---	---	711	1.88	---	---	888	2.93
---	---	804	1.73	---	---	760	1.88	---	---	934	2.95
---	---	864	1.73	---	---	818	1.88	---	---	969	2.95
---	---	923	1.73	---	---	876	1.88	---	---	992	2.96
---	---	978	1.76	---	---	920	1.88	---	---	---	---
---	---	---	---	---	---	969	1.88	---	---	---	---
---	---	---	---	---	---	998	1.87	---	---	---	---

Table B.26 Experimental ratcheting strain values for SS316L(N) Steel alloy under two-step loading with high-low sequences used in figures 4.19e and 4.19f

Step1(30±230MPa)		Step2 (30±210MPa)	
N(Cycle)	ε_r(%)	N(Cycle)	ε_r(%)
0	0	141	1.76
2	0.02	205	1.76
4	0.55	285	1.74
7	0.88	360	1.77
10	1.06	419	1.77
13	1.26	508	1.74
30	1.41	594	1.74
52	1.53	691	1.73
74	1.66	769	1.76
99	1.77	847	1.76
---	---	919	1.74
---	---	975	1.76
---	---	1000	1.77

Table B.27 Experimental ratcheting strain values for 1070 Steel alloy under single-step loading condition used in figures 4.20

Exp. 280±375MPa		Exp. 204±396MPa		Exp. 78±403MPa		Exp. 208±403MPa	
N(Cycle)	ε_r(%)	N(Cycle)	ε_r(%)	N(Cycle)	ε_r(%)	N(Cycle)	ε_r(%)
0	0	0	0	0	0	0	0
2	0.82	1	0.95	2	0.56	2	0.88
3	0.92	2	1.00	3	0.62	4	0.98
4	0.96	3	1.03	4	0.63	5	1.04
5	0.97	4	1.08	5	0.66	7	1.09
7	1.02	5	1.11	6	0.67	9	1.11
8	1.03	6	1.16	8	0.72	10	1.13
9	1.04	7	1.18	10	0.72	12	1.15
10	1.06	8	1.20	18	0.76	15	1.18
12	1.09	9	1.22	25	0.80	17	1.20
13	1.10	10	1.23	34	0.82	20	1.25
15	1.10	11	1.25	43	0.85	24	1.27
17	1.13	12	1.27	58	0.88	28	1.29
18	1.13	13	1.29	77	0.89	34	1.32
21	1.17	14	1.32	99	0.94	40	1.36
23	1.14	16	1.31	134	0.95	48	1.41
25	1.17	17	1.35	169	0.98	61	1.48
27	1.19	19	1.38	205	1.02	73	1.50
30	1.19	20	1.38	266	1.06	86	1.57
33	1.20	22	1.39	343	1.07	103	1.62
37	1.21	24	1.42	445	1.09	118	1.70
43	1.21	27	1.43	540	1.13	135	1.71
48	1.24	30	1.44	653	1.16	154	1.75
54	1.26	33	1.45	846	1.20	185	1.84
61	1.27	36	1.49	1117	1.21	223	1.91
67	1.29	39	1.51	1386	1.25	268	2.00
75	1.31	42	1.53	1835	1.25	297	2.03
84	1.31	46	1.55	---	---	339	2.07
93	1.33	50	1.55	---	---	387	2.14
104	1.36	54	1.56	---	---	430	2.19
117	1.36	58	1.57	---	---	491	2.26
132	1.36	63	1.60	---	---	591	2.35
155	1.40	---	---	---	---	692	2.44
168	1.43	---	---	---	---	788	2.55
192	1.46	---	---	---	---	977	2.67
221	1.48	---	---	---	---	1083	2.74
254	1.50	---	---	---	---	1206	2.82
281	1.53	---	---	---	---	1372	2.94
322	1.56	---	---	---	---	1527	3.03
363	1.56	---	---	---	---	1745	3.13
400	1.56	---	---	---	---	1935	3.24

Table B.28 Experimental ratcheting strain values for 1070 Steel alloy under multi-step loading condition used in figures 4.22a

Step1(280±375MPa)		Step2 (280±425MPa)		Step3 (280±375MPa)	
N(Cycle)	ε_r(%)	N(Cycle)	ε_r(%)	N(Cycle)	ε_r(%)
0	0	520	1.67	1040	3.08
2	0.82	521	1.66	1041	3.12
3	0.92	522	1.70	1042	3.13
4	0.96	523	1.67	1043	3.12
5	0.97	524	1.68	1044	3.10
7	1.02	525	1.71	1045	3.12
8	1.03	526	1.68	1046	3.12
9	1.04	527	1.68	1047	3.13
10	1.06	528	1.73	1048	3.13
12	1.09	529	1.77	1049	3.12
15	1.10	531	1.77	1050	3.13
18	1.13	534	1.81	1052	3.13
21	1.17	535	1.84	1053	3.12
23	1.14	539	1.85	1055	3.12
25	1.17	541	1.87	1057	3.12
27	1.19	544	1.90	1059	3.13
30	1.19	547	1.91	1063	3.13
33	1.20	552	1.94	1067	3.12
37	1.21	557	1.97	1071	3.13
43	1.21	563	2.01	1076	3.13
48	1.24	568	2.02	1082	3.13
54	1.26	574	2.07	1091	3.12
61	1.27	585	2.10	1098	3.12
67	1.29	595	2.12	1107	3.12
75	1.31	602	2.18	1118	3.13
84	1.31	614	2.19	1131	3.13
93	1.33	631	2.25	1144	3.13
104	1.36	649	2.31	1167	3.13
117	1.36	672	2.37	1183	3.10
132	1.36	698	2.48	1211	3.10
155	1.40	733	2.52	1232	3.13
168	1.43	760	2.58	1261	3.13
192	1.46	779	2.65	1299	3.13
221	1.48	817	2.71	1337	3.13
254	1.50	842	2.76	1382	3.13
281	1.53	883	2.83	1440	3.15
322	1.56	912	2.88	1482	3.15
363	1.56	945	2.93	1548	3.15
400	1.56	990	3.01	---	---
442	1.60	---	---	---	---
489	1.63	---	---	---	---

Table B.29 Experimental ratcheting strain values for 1070 Steel alloy under multi-step loading condition used in figures 4.22b

Step1 (204±396MPa)		Step2 (78±396MPa)	
N(Cycle)	ε_r(%)	N(Cycle)	ε_r(%)
0	0	67	1.27
2	0.95	68	1.23
3	1.03	69	1.22
4	1.04	70	1.20
5	1.11	71	1.19
6	1.16	73	1.18
7	1.18	74	1.16
8	1.20	76	1.17
9	1.22	78	1.13
10	1.23	81	1.13
11	1.25	85	1.11
12	1.27	90	1.09
13	1.29	97	1.08
14	1.32	103	1.07
16	1.31	117	1.05
17	1.35	130	1.05
19	1.38	145	1.03
20	1.38	169	1.02
22	1.39	200	1.02
24	1.42	230	1.03
27	1.43	266	1.02
30	1.44	317	1.02
33	1.45	373	1.02
36	1.49	495	1.03
39	1.51	606	1.03
42	1.53	747	1.04
46	1.55	982	1.07
50	1.55	---	---
54	1.56	---	---
58	1.57	---	---
63	1.60	---	---

Table B.30 Experimental ratcheting strain values for 1070 Steel alloy under multi-step loading condition used in figures 4.22c

Step1 (208±403MPa)				Step2 (78±403MPa)	
N(Cycle)	ε_r(%)	N(Cycle)	ε_r(%)	N(Cycle)	ε_r(%)
0	0	1372	2.94	4101	4.01
2	0.88	1527	3.03	4102	3.93
3	0.97	1745	3.13	4103	3.90
4	0.98	1935	3.24	4104	3.92
5	1.04	2100	3.37	4105	3.88
6	1.07	2451	3.51	4106	3.83
7	1.09	2660	3.63	4108	3.83
9	1.11	3118	3.77	4109	3.81
10	1.13	3369	3.88	4111	3.77
12	1.15	4054	4.13	4113	3.76
15	1.18	---	---	4115	3.76
17	1.20	---	---	4119	3.72
20	1.25	---	---	4124	3.72
24	1.27	---	---	4131	3.70
28	1.29	---	---	4139	3.68
34	1.32	---	---	4149	3.67
40	1.36	---	---	4157	3.65
48	1.41	---	---	4166	3.63
61	1.48	---	---	4178	3.61
73	1.50	---	---	4195	3.60
86	1.57	---	---	4217	3.60
103	1.62	---	---	4247	3.58
118	1.70	---	---	4274	3.54
135	1.71	---	---	4319	3.52
154	1.75	---	---	4368	3.51
185	1.84	---	---	4419	3.51
223	1.91	---	---	4501	3.49
268	2.00	---	---	4563	3.45
297	2.03	---	---	4651	3.42
339	2.07	---	---	4812	3.38
387	2.14	---	---	4971	3.38
430	2.19	---	---	5196	3.37
491	2.26	---	---	5403	3.35
591	2.35	---	---	5693	3.33
692	2.44	---	---	6103	3.33
788	2.55	---	---	6550	3.33
977	2.67	---	---	7095	3.29
1083	2.74	---	---	7763	3.28
1206	2.82	---	---	8335	3.28

Table B.31 Experimental ratcheting strain values for 1070 Steel alloy under multi-step loading conditions used in figures 4.22d

Step1 (-211±405MPa)		Step2 (-77±437MPa)	
N(Cycle)	ε_r(%)	N(Cycle)	ε_r(%)
0	0	4101	-3.78
2	-0.73	4102	-3.60
3	-1.12	4103	-3.53
5	-1.18	4104	-3.48
6	-1.24	4107	-3.43
10	-1.34	4112	-3.37
15	-1.42	4120	-3.31
23	-1.52	4132	-3.28
32	-1.62	4152	-3.24
47	-1.72	4177	-3.18
68	-1.83	4221	-3.13
95	-1.93	4290	-3.08
131	-2.05	4397	-3.06
170	-2.15	4541	-3.03
223	-2.26	4691	-2.98
289	-2.36	4912	-3.00
366	-2.46	5275	-2.98
478	-2.57	5793	-3.00
591	-2.73	6551	-3.01
748	-2.84	7300	-3.06
948	-2.97	7950	-3.08
1237	-3.08	8977	-3.11
1451	-3.23	9967	-3.14
1745	-3.34	10979	-3.17
2211	-3.47	---	---
2660	-3.61	---	---
3118	-3.71	---	---
3548	-3.81	---	---
3950	-3.89	---	---

Table B.32 Experimental ratcheting strain values for 1070 Steel alloy under multi-step loading condition used in figures 4.22e

Step1 (78±403 MPa)		Step2 (202±395 MPa)		Step3 (77±391 MPa)	
N(Cycle)	ε_r(%)	N(Cycle)	ε_r(%)	N(Cycle)	ε_r(%)
0	0	2052	1.57	6152	3.16
2	0.56	2053	1.61	6153	3.15
3	0.62	2054	1.66	6154	3.12
4	0.63	2055	1.68	6155	3.10
5	0.66	2056	1.69	6157	3.08
6	0.67	2058	1.72	6159	3.06
8	0.72	2059	1.74	6162	3.04
10	0.72	2061	1.76	6166	3.00
18	0.76	2065	1.79	6171	2.98
25	0.80	2069	1.81	6178	2.95
34	0.82	2075	1.82	6189	2.94
43	0.85	2080	1.85	6200	2.91
58	0.88	2088	1.89	6216	2.91
77	0.89	2099	1.93	6236	2.86
99	0.94	2115	1.97	6263	2.84
134	0.95	2132	2.01	6289	2.82
169	0.98	2148	2.04	6338	2.79
205	1.02	2174	2.08	6387	2.76
266	1.06	2206	2.11	6463	2.75
343	1.07	2243	2.16	6564	2.73
445	1.09	2300	2.22	6698	2.70
540	1.13	2360	2.26	6892	2.65
653	1.16	2425	2.32	7108	2.62
846	1.20	2505	2.40	7414	2.61
1117	1.21	2626	2.46	7824	2.58
1386	1.25	2793	2.53	8368	2.53
1835	1.25	3033	2.65	9075	2.51
2126	1.25	3269	2.75	10024	2.47
---	---	3555	2.83	10903	2.47
---	---	3916	2.91	12419	2.47
---	---	4266	3.01	14041	2.48
---	---	4788	3.10	15586	2.51
---	---	5302	3.22	---	---
---	---	5912	3.30	---	---
---	---	6169	3.38	---	---

APPENDIX C

Appendix C presents MATLAB Program listing for triphasic ratcheting strain prediction for 42CrMo, 20CS, SA333 and OFHC copper. MATLAB Programs for modification of hardening rule along with related subroutines of calculation, material properties, stress generation, deviatoric stress and Hook's law are also presented. Table C.1 defines symbols and terms used in the Matlab programming.

Table C.1 Symbols and terms used in the MATLAB programming

MATLAB program symbols for mechanistic ratcheting equation	
Symbol	**Description**
Nf	Life Cycles
E	Young's Modulus
Su	Ultimate Stress
Sy	Yield Stress
np	Cyclic strain Hardening exponent
Sa	Stress amplitude
Sm	Mean stress

MATLAB program symbols for the modified hardening rule	
Symbol	**Description**
E	Young's modulus
ni	Poisson's ratio
n	Unit normal tensor
Dsig	Stress tensor increment
Eps	Total strain
DEps	Total strain increment
DEps_e	Elastic strain increment
DEps_p	Plastic strain increment
Ddev_Sig	Deviatoric stress increment
H	Plastic modulus
a	Backstress
Da	Backstress increment
Db	Second internal variable increment
Cb2	Constant γ_2
Cb1	Constant γ_1
Delta	Constant δ
Ab	Constant C
aexx	Axial ratcheting strain
aexy	Shear ratcheting strain

MATLAB Programs for triphasic ratcheting strain prediction of materials

```
clear all
clc
%42CrMo-1-------------------------------------------------
Life=[0 15  33  52  89  127 164 221 277 314 389 446 521 558 615 652 690 764
820 877 915 971 1008    1247.706422 1394.495413 1614.678899 1834.862385
2055.045872 2201.834862 2422.018349 2642.201835 2788.990826];
Ratcheting=[0   1.15    2   2.87    4.43    4.95    5.46    6.16    6.5 7
7.53    8.05    8.57    8.92    9.26    9.6 9.95    10.47   10.82   11.16
11.5    11.85   12.19   13.56164384 15.4109589  17.26027397 19.10958904
20.95890411 23.42465753 27.12328767 30.82191781 38.21917808];
Nf=Life(end);
E=190500;
Su=670;
Sy=310;
np=0.097;
k=637;
Sa=350;
Sm=150;
SR=500;%MPa/s
[x,y]=lorcoef(Nf,E,Su,Sy,np,Sa,Sm,SR,k,Life);
plot(Life,Ratcheting,'^b',x,y,'b-')
axis([min(Life) max(Life)+.1*max(Life) min(Ratcheting)
max(Ratcheting)+.1*max(Ratcheting)])
xlabel('N_f (Cycle)','fontsize',16)
ylabel('Ratcheting Strain \epsilon_r (%)','fontsize',16)
hold on
% 42CrMo-2-----------------------------------------------------
Life=[0 22  50  78  106 134 162 190 218 246 276 304 332 360 388 416 472 500
556 613 641 697 753 809 865 893 978 1175    1372    1597    1793];
Ratcheting=[0 1.04  3.39    3.82    4.25    4.89    5.32    5.75    5.96
6.28    6.5 6.72    7.04    7.35    7.57    7.78    8.11    8.53    9.07
9.6 10.04   10.57   11  11.32   11.64   12.5    13.03   15.07   17.53   20.43
24.5];
Nf=Life(end);
E=190500;
Su=670;
Sy=310;
np=0.097;
k=637;
Sa=400;
Sm=50;
SR=500;%MPa/s
[x,y]=lorcoef(Nf,E,Su,Sy,np,Sa,Sm,SR,k,Life);
plot(Life,Ratcheting,'^g',x,y,'g-')
axis([min(Life) max(Life)+.1*max(Life) min(Ratcheting)
max(Ratcheting)+.1*max(Ratcheting)])
xlabel('N_f (Cycle)','fontsize',16)
ylabel('Ratcheting Strain \epsilon_r (%)','fontsize',16)
hold on
% 42CrMo-3-----------------------------------------------
Life=[0.00  52.00   71.00   127.00  240.00  333.00  409.00  521.00  595.00
671.00  746.00  802.00  896.00  970.00  1027.00 1247.71 1394.50 1614.68
1834.86 1981.65 2201.83 2422.02 2642.20 2862.39 3009.17 3229.36 3449.54
3669.72 3889.91 4110.09 4330.28 4550.46 4697.25 4917.43];
```

```
Ratcheting=[0.00    2.19    3.22    3.91    4.43    5.12    5.46    5.99
6.50    6.75    7.02    7.36    7.71    7.88    8.05    8.63    9.86    10.48
11.10   12.33   12.95   13.56   14.79   15.41   16.03   17.26   18.49   19.73
20.96   22.19   23.73   25.58   27.74   31.75];
Nf=Life(end);
E=190500;
Su=670;
Sy=310;
np=0.097;
k=637;
Sa=350;
Sm=100;
SR=500;%MPa/s
[x,y]=lorcoef(Nf,E,Su,Sy,np,Sa,Sm,SR,k,Life);
plot(Life,Ratcheting,'^r',x,y,'r-')
axis([min(Life) max(Life)+.1*max(Life) min(Ratcheting)
max(Ratcheting)+.1*max(Ratcheting)])
xlabel('N_f (Cycle)','fontsize',16)
ylabel('Ratcheting Strain \epsilon_r (%)','fontsize',16)
title(['\fontsize{14}','42CrMo','  Stress Rate=',int2str(SR),'MPa/s'])
hold on
% 20CS-1-------------------------------------------------------------------
figure
Life=[0 4   8   13  17  22  27  36  46  50  60  74  83  97  120 144 163 177
205 224 242 256 275 303 322 345 359 374 397 416 439 458 477 500 547 599 645
697 749 796 847 898 945 1002    1100    1200    1302    1400    1500    1602
1700    1800    1902    2000];
Ratcheting=[0   0.91    1.44    2.15    2.84    3.39    3.66    4.07    4.21
4.62    4.9 5.17    5.58    5.86    6.13    6.4 6.96    7.23    7.64    7.91
8.32    8.47    8.75    9.16    9.43    9.56    9.7 9.97    10.26   10.67
10.8    11.08   11.35   11.62   12.03   12.72   13.14   13.55   14.1    14.65
15.33   15.75   16.3    16.84   17.95   19.18   20.28   21.52   23.03   24.67
26.46   28.65   31.68   36.08];
Nf=Life(end);
E=203000;
Su=441;
Sy=350;
np=0.24;
k=1221;
Sa=300;
Sm=50;
SR=400;%MPa/s
[x,y]=lorcoef(Nf,E,Su,Sy,np,Sa,Sm,SR,k,Life);
plot(Life,Ratcheting,'^b',x,y,'b-')
axis([min(Life) max(Life)+.1*max(Life) min(Ratcheting)
max(Ratcheting)+.1*max(Ratcheting)])
xlabel('N_f (Cycle)','fontsize',16)
ylabel('Ratcheting Strain \epsilon_r (%)','fontsize',16)
hold on
% 20CS-2-------------------------------------------------------------------
Life=[0 8   13  17  22  32  41  55  65  70  78  88  97  120 139 158 181 200
220 238 256 280 298 322 341 355 378 397 416 439 458 477 495 552];
Ratcheting=[0   1.05    2.15    3.53    4.07    4.9 5.44    6.13    6.55
7.09    7.78    8.06    8.61    9.3 10.26   11.08   11.9    12.45   13.27
13.96   14.79   15.47   16.03   16.98   17.81   18.63   19.46   20.28   21.1
22.2    23.02   24.4    25.64   29.62];
Nf=Life(end);
```

```
E=203000;
Su=441;
Sy=350;
np=0.24;
k=1221;
Sa=320;
Sm=50;
SR=400;%MPa/s
[x,y]=lorcoef(Nf,E,Su,Sy,np,Sa,Sm,SR,k,Life);
plot(Life,Ratcheting,'^g',x,y,'g-')
axis([min(Life) max(Life)+.1*max(Life) min(Ratcheting)
max(Ratcheting)+.1*max(Ratcheting)])
xlabel('N_f (Cycle)','fontsize',16)
ylabel('Ratcheting Strain \epsilon_r (%)','fontsize',16)
hold on
% 20CS-3-----------------------------------------------------
Life=[0 110 130 180 200 230 300 390 440 510 580 650 740 830 950 1020    1090
1170    1260    1380    1470    1540    1640    1700    1870    1960    2050
2120    2220    2330    2450    2540    2640    2760    2850    2990    3080
3180    3270    3390    3480    3580    3670    3740    3810    3900    4000
4070    4160    4330    4490    4630    4790    4960    5100    5260    5400
5540    5690    5830    5970    6110    6290    6430    6760    6970    7260
7490    7750    8010    8250    8520    8760    8990    9250    9334];
Ratcheting=[0   0.7 1.03    1.5 1.8 2.4 2.82    3.46    3.88    4.2 4.6 5.05
5.37    5.58    5.9 6.22    6.54    6.86    7.07    7.38    7.59    7.92
8.13    8.23    8.55    8.86    8.97    9.18    9.4 9.61    9.82    10.03
10.25   10.56   10.77   10.99   11.1    11.2    11.3    11.52   11.83   11.94
12.05   12.26   12.36   12.68   12.79   12.89   13  13.31   13.53   13.85
14.27   14.38   14.8    15.23   15.44   15.75   15.97   16.18   16.5    16.71
17.14   17.56   17.98   18.72   19.25   19.89   20.53   21.37   22.11   22.96
23.82   24.76   26.04   26.25];
Nf=Life(end);
E=203000;
Su=441;
Sy=350;
np=0.24;
k=1221;
Sa=275;
Sm=50;
SR=400;%MPa/s
[x,y]=lorcoef(Nf,E,Su,Sy,np,Sa,Sm,SR,k,Life);
plot(Life,Ratcheting,'^r',x,y,'r-')
axis([min(Life) max(Life)+.1*max(Life) min(Ratcheting)
max(Ratcheting)+.1*max(Ratcheting)])
xlabel('N_f (Cycle)','fontsize',16)
ylabel('Ratcheting Strain \epsilon_r (%)','fontsize',16)
title(['\fontsize{14}','20CS','   Stress Rate=',int2str(SR),'MPa/s'])
hold on
% SA333-1----------------------------------------------------------------
figure
Life=[0 3   8   13  44  98  126 163 190 217 239 266 295 347 384 413 438 465
493 513 527 544 556 565 570];
Ratcheting=[0   2.75    4.16    4.96    7.18    10  11.4    13.02   14.22
15.44   16.44   17.64   19.06   21.68   23.89   25.7    27.5    29.73   32.75
35.17   37.38   41  44.84   48.26   57.2];
Nf=Life(end);
E=203000;
```

```
Su=494;
Sy=304;
np=.14214;%
k=830;
Sa=310;
Sm=120;
SR=50;%MPa/s
[x,y]=lorcoef(Nf,E,Su,Sy,np,Sa,Sm,SR,k,Life);
plot(Life,Ratcheting,'^r',x,y,'r-')
axis([min(Life) max(Life)+.1*max(Life) min(Ratcheting)
max(Ratcheting)+.1*max(Ratcheting)])
xlabel('N_f (Cycle)','fontsize',16)
ylabel('Ratcheting Strain \epsilon_r (%)','fontsize',16)
hold on
% SA333-2-------------------------------------------------------------------
Life=[0 2   5   8   13  33  50  61  75  89  100 117 134 154 177 204 258 303
365 441 511 587 646 705 759 798 829 852 894 919 950 989 1020    1045    1071
1099    1121    1144    1158    1172    1177    1180    1184];
Ratcheting=[0   0.97    1.8 2.43    2.84    3.87    4.51    5.13    5.54
5.96    6.37    6.99    7.42    8.04    8.87    9.49    10.95   11.98   13.44
15.3    16.97   18.85   20.3    21.96   23.2    24.66   25.49   26.53   27.98
28.82   30.07   31.93   33.6    35.27   36.92   38.59   40.45   42.33   44.82
47.52   49.81   53.13   53.2];
Nf=Life(end);
E=203000;
Su=494;
Sy=304;
np=.14214;%
k=830;
Sa=310;
Sm=80;
SR=50;%MPa/s
[x,y]=lorcoef(Nf,E,Su,Sy,np,Sa,Sm,SR,k,Life);
plot(Life,Ratcheting,'^b',x,y,'b-')
axis([min(Life) max(Life)+.1*max(Life) min(Ratcheting)
max(Ratcheting)+.1*max(Ratcheting)])
xlabel('N_f (Cycle)','fontsize',16)
ylabel('Ratcheting Strain \epsilon_r (%)','fontsize',16)
hold on
% SA333-3-------------------------------------------------------------------
Life=[  0   1   2   3   4   5   6   7   8   9   10  20  30  40  50  60  70
80  90  100 200 300 400 500 600 700 800 900 1000    1125    1385    1542.5
1700    1885    2037    2092.25 2147.5  2202.75 2258    2408    2558
2734.5  2911    2988    3065    3105    3145    3145    3145    ];
Ratcheting=[    0   1.58    1.77    1.96    1.96    2.15    2.15    2.15
2.34    2.34    2.34    2.53    2.72    2.92    3.1 3.3 3.5 3.68    3.68
3.87    5   5.75    6.32    6.9 7.7 8.04    8.8 9.2 9.6 10.52   11.83   12.69
13.55   14.31   14.9    15.325  15.75   16.175  16.6    17.55   18.5    19.55
20.6    22.6    24.6    26.105  27.61   28.755  29.4    ];
Nf=Life(end);
E=203000;
Su=494;
Sy=304;
np=.14214;%
k=830;
Sa=310;
Sm=40;
```

```
SR=50;%MPa/s
[x,y]=lorcoef(Nf,E,Su,Sy,np,Sa,Sm,SR,k,Life);
plot(Life,Ratcheting,'^b',x,y,'b-')
axis([min(Life) max(Life)+.1*max(Life) min(Ratcheting)
max(Ratcheting)+.1*max(Ratcheting)])
xlabel('N_f (Cycle)','fontsize',16)
ylabel('Ratcheting Strain \epsilon_r (%)','fontsize',16)
title(['\fontsize{14}','SA333','   Stress Rate=',int2str(SR),'MPa/s'])
hold on
% OFHC Copper-1-----------------------------------------------------------
figure
Life=[1 2   4   5   6   8   9   11  14  22  28  40  60  78  99  117 139 176
251 322 418 544 708 908 1127    1315    1535    1738    1879    2000
2060];
Ratcheting=[1.59    3.75    5.16    6.13    6.88    8.18    8.61    9.16
9.25    9.37    9.37    9.48    9.8 10.4    10.8    11.2    11.6    12.4
13.7    14.7    16.2    17.6    19.6    22  24.3    26.4    29  31.6    34
35.6    37.2];
Nf=Life(end);
E=70800;
Su=234;
Sy=52;
np=0.443;
k=544.59;
Sa=140;
Sm=30;
SR=500;%MPa/s
[x,y]=lorcoef(Nf,E,Su,Sy,np,Sa,Sm,SR,k,Life);
plot(Life,Ratcheting,'^b',x,y,'b-')
axis([min(Life) max(Life)+.1*max(Life) min(Ratcheting)
max(Ratcheting)+.1*max(Ratcheting)])
xlabel('N_f (Cycle)','fontsize',16)
ylabel('Ratcheting Strain \epsilon_r (%)','fontsize',16)
hold on
% OFHC Copper-2-----------------------------------------------------------
Life=[1 2   3   5   6   8   9   11  14  17  33  64  80  100 123 143 160 183
196 260 325 400 517 613 698 795 873 940 1015];
Ratcheting=[2.48    4.99    5.99    8.25    9.63    11.5    12  12.8    13
13  13.1    13.3    13.7    14.1    14.7    15.2    15.7    16.2    16.7
18.3    19.9    21.4    24.5    26.6    28.6    31.3    33.3    35.2
37.1];
Nf=Life(end);
E=70800;
Su=234;
Sy=52;
np=0.443;
k=544.59;
Sa=140;
Sm=50;
SR=500;%MPa/s
[x,y]=lorcoef(Nf,E,Su,Sy,np,Sa,Sm,SR,k,Life);
plot(Life,Ratcheting,'^r',x,y,'r-')
axis([min(Life) max(Life)+.1*max(Life) min(Ratcheting)
max(Ratcheting)+.1*max(Ratcheting)])
xlabel('N_f (Cycle)','fontsize',16)
ylabel('Ratcheting Strain \epsilon_r (%)','fontsize',16)
hold on
```

```
% OFHC Copper-3-----------------------------------------------------------------
Life=[1 2   3   5   6   8   10  11  15  17  20  22  24  29  34  38  44  51
60  69  80  90  105 121 128 143 158 166 176 186];
Ratcheting=[2.85    5.99    6.98    10  11.8    14.5    16.3    17.1    17.7
17.9    17.9    18  18  18.1    18.4    18.5    18.9    19.6    20.6    21.6
22.9    23.9    25.4    27.4    28.3    30.2    32.4    33.9    34.9
37.2];
Nf=Life(end);
E=70800;
Su=234;
Sy=52;
np=0.443;
k=544.59;
Sa=160;
Sm=50;
SR=500;%MPa/s
[x,y]=lorcoef(Nf,E,Su,Sy,np,Sa,Sm,SR,k,Life);
plot(Life,Ratcheting,'^k',x,y,'k-')
axis([min(Life) max(Life)+.1*max(Life) min(Ratcheting)
max(Ratcheting)+.1*max(Ratcheting)])
xlabel('N_f (Cycle)','fontsize',16)
ylabel('Ratcheting Strain \epsilon_r (%)','fontsize',16)
hold on
% % OFHC Copper-4-----------------------------------------------------------------
Life=[1 2   3   4   5   6   7   10  13  16  20  23  26  29  34  40  48  80
106 128 160 200 237 280 319 357 430 548 698 905 1177    1526    2018    2618
3213    3803    4578    5511    6400    7573    8300    9294    9824
10187];
Ratcheting=[1.24    3.23    4.36    4.74    5.87    6.49    7.38    8.62
8.75    8.87    8.87    8.87    8.87    8.87    8.87    8.99    8.99    8.99
9.13    9.26    9.37    9.5 10  10.1    10.3    10.5    11  11.6    12.4
13.4    14.4    15.6    17  18.6    20  21.4    23.2    25.2    27.2    29.6
31.8    33.8    35.7    37.1];
Nf=Life(end);
E=70800;
Su=234;
Sy=52;
np=0.443;
k=544.59;
Sa=120;
Sm=50;
SR=500;%MPa/s
[x,y]=lorcoef(Nf,E,Su,Sy,np,Sa,Sm,SR,k,Life);
plot(Life,Ratcheting,'^r',x,y,'r-')
axis([min(Life) max(Life)+.1*max(Life) min(Ratcheting)
max(Ratcheting)+.1*max(Ratcheting)])
xlabel('N_f (Cycle)','fontsize',16)
ylabel('Ratcheting Strain \epsilon_r (%)','fontsize',16)
title(['\fontsize{14}','OFHC Copper','  Stress Rate=',int2str(SR),'MPa/s'])
hold on
```

MATLAB Programs for the modified hardening rule.

Main program

```
clc
clear all
% ------------------------------------------------------------------------
fh = figure('Name','Stress courses generation',...
    'Position',[0,40,990,650],...
    'Resize', 'off',...
    'Toolbar','none',...
    'Menubar','none','Color',[0.941176 0.941176 0.941176]);
panel3 = uipanel('Parent',fh,'Title','Hystersis loops',...
    'Position',[.62 .52 .37 .48]);
axeshLoop = axes('Parent',panel3,'units','normalized',...
    'Box','on',...
    'Fontsize',8,...
    'Position',[0.15 0.15 0.81 0.82]);
hLoop=plot(0,0,'-k',0,0,'-r',0,0,'ok',0,0,'or');
xlabel('\epsilon(%), -')
ylabel('\sigma(t), \tau(t), MPa')
% ------------------------------------------------------------------------
 [t, Sig, Tau, mate] = test;
% ------------------------------------------------------------------------
panel4 = uipanel('Parent',fh,'Title','Yield surfaces',...
    'Position',[.62 .01 .37 .51]);
axeshSurf = axes('Parent',panel4,'units','normalized',...
    'Box','on',...
    'Fontsize',8,...
    'Position',[0.13 0.14 0.83 0.83],...
    'XLim',[-1000 1000],...
 'YLim',[-1000 1000]);
set(get(axeshSurf,'xlabel'),'string','\surd 3 \tau(t), MPa','fontsize',8)
set(get(axeshSurf,'ylabel'),'string','\sigma(t), MPa','fontsize',8)
grid on
fi=0:pi/80:2*pi;
x=mate.R*cos(fi);
y=mate.R*sin(fi);
hp=patch(x,y,4); hold on,
h=plot(0,0,'ok','markerfacecolor','r','markersize',8);
hz=plot(0,0,'--b');
axis equal
axis manual
% ------------------------------------------------------------------------
i=0;
a=zeros(1,9);
b=a;
DEps_p=zeros(1,9);
aa=zeros(length(t), 9);
am(1:length(mate.R),9)=0;
ar=a;
Eps=zeros(length(t),9);
Eps_p=zeros(length(t),9);
Debuging=zeros(length(t), 29);
DP=0
```

```
for j=1:length(t)-1,
Sig_start=[Sig(j) 0 0 Tau(j) 0 0 Tau(j) 0 0];
Dsig=[Sig(j+1)-Sig(j) 0 0 Tau(j+1)-Tau(j) 0 0 Tau(j+1)-Tau(j) 0 0];
[Debuging,DEps, i, a, ar, DEps_p, b, DP]=calculation(Sig_start, Dsig, i, a,
mate,j,Debuging, ar, DEps_p, b, DP);
Eps(j+1,:)=Eps(j,:)+DEps;
Eps_p(j+1,:)=Eps_p(j,:)+DEps_p;
aa(j+1,:)=a;
% ------------------------------------------------------------------------
set(hLoop(1),'xdata',Eps(1:j+1,1)*100,'ydata',Sig(1:j+1))
set(hLoop(2),'xdata',Eps(1:j+1,4)*100,'ydata',Tau(1:j+1))
set(hLoop(3),'xdata',Eps(j+1,1)*100,'ydata',Sig(j+1))
set(hLoop(4),'xdata',Eps(j+1,4)*100,'ydata',Tau(j+1))
drawnow expose
% ------------------------------------------------------------------------
ay=1.5*aa(j+1,1);
ax=sqrt(3)*aa(j+1,4);
set(hp,'xdata',x+ax,'ydata',y+ay)
set(h,'ydata',Sig(j+1),'xdata',sqrt(3)*Tau(j+1))
j=round(j/50)
end
k=1;
z=1;
% -------------Ratcheting Calculation---------------------------------------
for j=1:length(t)
if rem(t(j),.05)==0
Mexx(z,1)=max(Eps(k:j,1));
Nexx(z,1)=min(Eps(k:j,1));
aexx(z,1)=(Mexx(z,1)+Nexx(z,1))*100/2;
Mexy(z,1)=max(Eps(k:j,4));
Nexy(z,1)=min(Eps(k:j,4));
aexy(z,1)=(Mexy(z,1)+Nexy(z,1))*100/2;
k=j+1;
z=z+1;
end
end
```

Calculation subroutine

```
function [Debuging,DEps, i, a, ar, DEps_p, b,DP]=calculation(Sig_start, Dsig,
i, a, mate,j,Debuging, ar, DEps_p,b, DP )
%-------------------------------------------------------------------%
E=mate.E;
ni=mate.ni;
G=E/(2*(1+ni));
R=mate.R;
%-------------------------------------------------------------------%
Ab=?;
Cb1=?;
Cb2=?;
Delta=?;
%-------------------------------------------------------------------%
    Ddev_Sig=dev(Dsig);
    dev_Sig_start=dev(Sig_start);
%-------------------------------------------------------------------%
    n=nn(dev_Sig_start, a, i);
%-------------------------------------------------------------------%
    [n ,i, ar]=PlasticityCond(i, Ddev_Sig, n, a, ar);
%-------------------------------------------------------------------%
    A_dew=dev_Sig_start;
    C_dew=A_dew+Ddev_Sig;
%-----------------------------------------------------------------------------%
    DEps_p=zeros(1,9);
%-----------------------------------------------------------------------------%
    if F(C_dew, a)>R^2
        if i==0
            A_dew=verify_A(A_dew, a, R);
            [B_dew]=intersection(A_dew, C_dew, a, R);
            A_dew=B_dew;
            AC_dew=C_dew-A_dew;
            i=i+1;
            n=nn(A_dew, a, i);
            D_strain_p=Delta_Strain_p(AC_dew, Delta, i, n, Ab, Cb1, a, b);
            [Da,b,Db]=shiftsurface(Ab,Cb1,Cb2, D_strain_p, a, b, Delta);
            a=a+Da;
            DEps_p=D_strain_p;
        else
            n=nn(dev_Sig_start, a, i);
            D_strain_p=Delta_Strain_p(Ddev_Sig, Delta, i, n, Ab, Cb1, a, b);
            [Da,b,Db]=shiftsurface(Ab,Cb1,Cb2, D_strain_p, a, b, Delta);
            a=a+Da;
            DEps_p=D_strain_p;
        end
    end
    %-------------------------------------------------------------%
    DEps_e=hooklaw(Dsig, 'stress_strain', E, ni);
    DEps=DEps_e+DEps_p;
end
%-------------------------------------------------------------------%
function n=nn(A_dew, a, i)
if i>0
    n=(A_dew-a(1,:))/norm(A_dew-a(1,:));   %eq. (20)
else
```

```
   n=[];
end
end
%-------------------------------------------------------------------%
function [n ,i, ar]=PlasticityCond(i, Delta, n, a, ar)
if i>0
   if n*(Delta)'<0
        i=0;
        n=[];
        ar=a;
   end
else
    n=n;
    i=i;
    ar=ar;
end
end
%-------------- von Mises yield function, Equation (3.7) -------------------%
function y=F(s, aa)
y=(3/2)*(s-aa)*(s-aa)';
end
% Plastic Modulus and plastic strain increment Calculations, Equation (3.10)
(3.5) --------------%
function D_strain_p=Delta_Strain_p(D_dew, Delta, i, n, C, Gama, a, b)
H=C-Gama*(n*(a-Delta*b)'
D_strain_p=(1/H)*(n*D_dew')*n;
end
%--------------- Modified hardening Rule (3.13) ------------------------%
function [Da,b,Db]=shiftsurface(Ab,Cb1,Cb2, D_strain_p, a, b, Delta)

    Db=Cb2*(a-1*b)*sqrt(((2/3)*(D_strain_p*D_strain_p')));
    b=b+Db;
    Da=(1/1)*Ab*D_strain_p-Cb1*(a-
Delta*b)*sqrt(((2/3)*(D_strain_p*D_strain_p')));
end
%-------------------------------------------------------------------%
function [B_dew, k0]=intersection(DewLower, DewHigher, aa, RR)
w(1)=(DewHigher-DewLower)*(DewHigher-DewLower)'; w(2)=2*(DewLower-
aa)*(DewHigher-DewLower)'; w(3)=(DewLower-aa)*(DewLower-aa)'-(2/3)*RR^2;
k0=roots(w); k0=max(k0); k0=k0(1);
B_dew=DewLower+k0*(DewHigher-DewLower);
end
%-------------------------------------------------------------------------%
function A_dew=verify_A(A_dew, aa, RR)
delta=(1e-012)*(A_dew-aa);
if F(A_dew, aa)-RR^2>=0,
[A_dew]=intersection(aa, A_dew, aa, RR);
    A_dew=A_dew-delta;
else
end
end
```

Material properties subroutine

```
function mate = matproperty

fh = figure('Name','Material properties,...
    'Position',[100,150,640,500],...
    'Resize', 'off',...
    'Toolbar','none',...
    'Menubar','none','Color',[0.941176 0.941176 0.941176]);
panel1 = uipanel('Parent',fh,'Title','Coefficients',...
    'Position',[.01 .66 .98 .32]);
Dtextedit=0.18;
y1=0.55; %first row
y2=0.08; %second row
%--Young modulus----------------------------------%
edithE = uicontrol(panel1,'Style','edit',...
    'Units','normalized',...
    'String','210000',...
    'BackgroundColor','white',...
    'Fontsize',9,...
    'Position',[0.02 y1 0.2 Dtextedit]);
texthE = uicontrol(panel1,'Style','text',...
    'Units','normalized',...
    'String','Young modulus, MPa',...
    'Position',[0.02 0.76 0.2 0.14]);
%--Poisson ratio-----------------------------------%
edithni = uicontrol(panel1,'Style','edit',...
    'Units','normalized',...
    'String','0.3',...
    'BackgroundColor','white',...
    'Fontsize',9,...
    'Position',[0.02 y2 0.2 Dtextedit]);
texthni = uicontrol(panel1,'Style','text',...
    'Units','normalized',...
    'String','Poisson ratio, -',...
    'Position',[0.02 0.27 0.2 0.14]);
%--Coefficient of cyclic hardening, K'-----------------%
edithK = uicontrol(panel1,'Style','edit',...
    'Units','normalized',...
    'String','1485',...
    'BackgroundColor','white',...
    'Fontsize',9,...
    'Position',[0.27 y1 0.2 Dtextedit]);
texthK = uicontrol(panel1,'Style','text',...
    'Units','normalized',...
    'String','Coefficient of cyclic hardening, K'', MPa',...
    'Position',[0.27 0.76 0.2 0.23]);
%--Yield stress----------------------------------%
edithSigy = uicontrol(panel1,'Style','edit',...
    'Units','normalized',...
    'String','449',...
    'BackgroundColor','white',...
    'Fontsize',9,...
    'Position',[0.27 y2 0.2 Dtextedit]);
texthSigy = uicontrol(panel1,'Style','text',...
    'Units','normalized',...
```

```
    'String','Yield stress, MPa',...
    'Position',[0.27 0.27 0.2 0.14]);
%--Exponent of cyclic hardening, n'-----------------%
edithn = uicontrol(panel1,'Style','edit',...
    'Units','normalized',...
    'String','0.17',...
    'BackgroundColor','white',...
    'Fontsize',9,...
    'Position',[0.52 y1 0.2 Dtextedit]);
texthn = uicontrol(panel1,'Style','text',...
    'Units','normalized',...
    'String','Exponent of cyclic hardening, n'', -',...
    'Position',[0.52 0.76 0.2 0.23]);
%--Radius increment of yield surfaces---------------------------%
edithDSig = uicontrol(panel1,'Style','edit',...
    'Units','normalized',...
    'String','50',...
    'BackgroundColor','white',...
    'Fontsize',9,...
    'Position',[0.52 y2 0.2 Dtextedit]);
texthDSig = uicontrol(panel1,'Style','text',...
    'Units','normalized',...
    'String','Radius increment of yield surfaces, MPa',...
    'Position',[0.52 0.27 0.2 0.23]);
%--Maximum stress, MPa-----------------%
edithSigmax = uicontrol(panel1,'Style','edit',...
    'Units','normalized',...
    'String','900',...
    'BackgroundColor','white',...
    'TooltipString','Maximum stress must be higher than Yield stress !',...
    'Fontsize',9,...
    'Position',[0.77 y1 0.2 Dtextedit]);
texthSigmax = uicontrol(panel1,'Style','text',...
    'Units','normalized',...
    'String','Maximum stress, MPa',...
    'TooltipString','Maximum stress must be higher than Yield stress !',...
    'Position',[0.77 0.76 0.2 0.23]);
axesh = axes('Parent',fh,'units','normalized',...
    'Box','on',...
    'Fontsize',8,...
    'Position',[0.1 0.11 0.86 0.51]);
set(get(axesh,'xlabel'),'string','\epsilon_a, -','fontsize',8)
set(get(axesh,'ylabel'),'string','\sigma_a, MPa','fontsize',8)
%---buttons---------------------------------------%
bhApply = uicontrol(fh,'Units','normalized',...
    'Position',[0.81 0.23 0.13 0.08],...
    'String','Apply',...
    'Callback',@buttonApply);
bhOk = uicontrol(fh,'Units','normalized',...
    'Position',[0.81 0.13 0.13 0.08],...
    'String','OK',...
    'Callback',@buttonOK);
uiwait(fh);
%-----------------------------------------------%
    function buttonApply(hObject,eventdata)
        mate.E=str2double(get(edithE,'String'));
        mate.K=str2double(get(edithK,'String'));
```

```
        mate.n=str2double(get(edithn,'String'));
        mate.ni=str2double(get(edithni,'String'));
        mate.Sig_y=str2double(get(edithSigy,'String'));
        mate.DSig=str2double(get(edithDSig,'String'));
        mate.Sigmax=str2double(get(edithSigmax,'String'));
        if mate.Sigmax<mate.Sig_y,
            f = warndlg('Maximum stress must be higher than the yield
stress.', 'Warning');
            mate.Sigmax=mate.Sig_y+mate.DSig;
            set(edithSigmax,'string',num2str(mate.Sigmax))
            uiwait(f)
        end
        Sig_ai=[0:5:mate.Sigmax];
        Eps_ai=Sig_ai/mate.E+(Sig_ai/mate.K).^(1/mate.n);
        Sig_a=[0 mate.Sig_y:mate.DSig:mate.Sigmax];
        Eps_a=Sig_a/mate.E+(Sig_a/mate.K).^(1/mate.n);
        %axes(axesh)
        plot(Eps_ai,Sig_ai,'-k',Eps_a,Sig_a,'+-b')
        xlabel('\epsilon_a, -')
        ylabel('\sigma_a, MPa')
        H=zeros(length(Sig_a)-2,1);
        for i=2:length(Sig_a)-1,
        H(i-1,1)=((3/2)*(((Eps_a(i+1)-Eps_a(i))/(Sig_a(i+1)-Sig_a(i)))-
  1/mate.E))^-1;
        end
        R=Sig_a(2:end)';
        mate.R=mate.Sig_y;
        mate.H=H;
    end
%-------------------------------------------------%
    function buttonOK(hObject,eventdata)
        close(fh)
    end
end
```

Stress generation subroutine

```
function [t, Sig, Tau, mate] = test
global smax
fh = figure('Name','Stress courses generation. Copyright:
reza.ahmadzadeh@ryerson.ca',...
    'Position',[300,200,1000,618],...
    'Resize', 'on',...
    'Toolbar','none',...
    'Menubar','none','Color',[.8 .91 1]);
panel1 = uipanel('Parent',fh,'Title','Sinusoidal stress signals',...
    'Position',[.01 .79 .45 .20],'backgroundColor',[.8 .86 1],'FontWeight',
'bold');
panel2 = uipanel('Parent',fh,'Title','Time signal',...
    'Position',[.01 .58 .16 .20],'backgroundColor',[.8 .86 1],'FontWeight',
'bold');
panel3 = uipanel('Parent',fh,'Title','Slow start',...
    'Position',[.19 .58 .14 .20],'backgroundColor',[.8 .86 1],'FontWeight',
'bold');
panel4=uipanel('parent', fh, 'Title', 'Material Properies',...
     'Position',[.01 .05 .45 .35],'backgroundColor',[.8 .86 1],'FontWeight',
'bold');
%--Equations---------------------------------%
axeshSiga = axes('Parent',panel1,'units','pixels',...
    'Position',[7 53 136 26]);
image(imread('stresseq1.jpg','jpg'));
set(gca,'visible','off')
axeshTaua = axes('Parent',panel1,'units','pixels',...
    'Position',[9 12 136 26]);
image(imread('stresseq2.jpg','jpg'));
set(gca,'visible','off')
%--Sig_a and Tau_a-----------------------------------%
texthSiga = uicontrol(panel1,'Style','text',...
    'Units','pixels',...
    'String','Stress levels (MPa)',...
    'Position',[145 85 70 27],...
    'backgroundColor',[.8 .86 1]);
edithSiga = uicontrol(panel1,'Style','edit',...
    'Units','pixels',...
    'String','400',...
    'BackgroundColor','white',...
    'Fontsize',9,...
    'Position',[155 52 52 27]);
edithTaua = uicontrol(panel1,'Style','edit',...
    'Units','pixels',...
    'String','0',...
    'BackgroundColor','white',...
    'Fontsize',9,...
    'Position',[155 11 52 27]);
%--Mean Stresses-----------------------------------%
texthSigm = uicontrol(panel1,'Style','text',...
    'Units','pixels',...
    'String','Mean Stresses (MPa)',...
    'Position',[220 85 90 27],...
    'backgroundColor',[.8 .86 1]);
edithSigm = uicontrol(panel1,'Style','edit',...
```

```
    'Units','pixels',...
    'String','100',...
    'BackgroundColor','white',...
    'Fontsize',9,...
    'Position',[237 52 52 27]);
edithTaum = uicontrol(panel1,'Style','edit',...
    'Units','pixels',...
    'String','0',...
    'BackgroundColor','white',...
    'Fontsize',9,...
    'Position',[237 12 52 27]);
%--Frequencies---------------------------------%
texthfsig = uicontrol(panel1,'Style','text',...
    'Units','pixels',...
    'String','Frequencies (Hz)',...
    'Position',[310 85 66 27],...
    'backgroundColor',[.8 .86 1]);
edithfsig = uicontrol(panel1,'Style','edit',...
    'Units','pixels',...
    'String','20',...
    'BackgroundColor','white',...
    'Fontsize',9,...
    'Position',[315.5 52 52 27]);
edithftau = uicontrol(panel1,'Style','edit',...
    'Units','pixels',...
    'String','20',...
    'BackgroundColor','white',...
    'Fontsize',9,...
    'Position',[315.5 12 52 27]);
%--Phase shift, rad----------------------------------%
texthd = uicontrol(panel1,'Style','text',...
    'Units','pixels',...
    'String','Phase shift (rad)',...
    'Position',[380 42 60 27],...
    'backgroundColor',[.8 .86 1]);
edithd = uicontrol(panel1,'Style','edit',...
    'Units','pixels',...
    'String','0',...
    'BackgroundColor','white',...
    'Fontsize',9,...
    'Position',[383 12 52 27]);
%--Time signal---------------------------------%
edithS = uicontrol(panel2,'Style','edit',...
    'Units','pixels',...
    'String','1000',...
    'BackgroundColor','white',...
    'Fontsize',9,...
    'Position',[50 55 52 27]);
texthS = uicontrol(panel2,'Style','text',...
    'Units','pixels',...
    'String','Frequency sampling (Hz)',...
    'Position',[10 85 140 16],...
    'backgroundColor',[.8 .86 1]);
edithL = uicontrol(panel2,'Style','edit',...
    'Units','pixels',...
    'String','.5',...
    'BackgroundColor','white',...
```

```
    'Fontsize',9,...
    'Position',[50 5 52 27]);
texthL = uicontrol(panel2,'Style','text',...
    'Units','pixels',...
    'String','Length (s)',...
    'Position',[45 35 60 16],...
    'backgroundColor',[.8 .86 1]);
%--Main axes-----------------------------------------%
axesh = axes('Parent',fh,'units','normalized',...
    'Box','on',...
    'Fontsize',8,...
    'Position',[0.525 0.525 0.45 0.45]);
set(get(axesh,'xlabel'),'string','Time, s','fontsize',8)
set(get(axesh,'ylabel'),'string','\sigma(t), \tau(t), MPa','fontsize',8)
%--Young modulus-------------------------------%
texthE = uicontrol(panel4,'Style','text',...
    'Units','pixels',...
    'String','Young modulus (MPa)',...
    'Position',[10 165 80 27],...
    'backgroundColor',[.8 .86 1]);
    % SS304: 190GPa, , 42CrMo:190.5GPa, SS316L:190GPa, Copper:129
edithE = uicontrol(panel4,'Style','edit',...
    'Units','pixels',...
    'String','190000',...
    'BackgroundColor','white',...
    'Fontsize',9,...
    'Position',[20 133 62 27]);
%--Poisson ratio-------------------------------%
texthni = uicontrol(panel4,'Style','text',...
    'Units','pixels',...
    'String','Poisson ratio',...
    'Position',[95 165 80 27],...
    'backgroundColor',[.8 .86 1]);
edithni = uicontrol(panel4,'Style','edit',...
    'Units','pixels',...
    'String','0.3',...
    'BackgroundColor','white',...
    'Fontsize',9,...
    'Position',[105 133 62 27]);
%--Coefficient of cyclic hardening, K'----------------%
texthK = uicontrol(panel4,'Style','text',...
    'Units','pixels',...
    'String','Coefficient of cyclic hardening, K'' (MPa)',...
    'Position',[180 165 100 27],...
    'backgroundColor',[.8 .86 1]);
    % SS304: 1628 MPa, 42CrMo:637, SS316L:2755GPa, Copper:?
edithK = uicontrol(panel4,'Style','edit',...
    'Units','pixels',...
    'String','1628',...
    'BackgroundColor','white',...
    'Fontsize',9,...
    'Position',[198 133 62 27]);
%--Exponent of cyclic hardening, n'----------------%
texthn = uicontrol(panel4,'Style','text',...
    'Units','pixels',...
    'String','Exponent of cyclic hardening, n''',...
    'Position',[280 165 100 27],...
```

```
    'backgroundColor',[.8 .86 1]);
    % SS304: 0.291, 42CrMo:0.097, SS316L:0.388, Copper:?
edithn = uicontrol(panel4,'Style','edit',...
    'Units','pixels',...
    'String','0.291',...
    'BackgroundColor','white',...
    'Fontsize',9,...
    'Position',[298 133 62 27]);
%--Yield stress---------------------------------%
texthSigy = uicontrol(panel4,'Style','text',...
    'Units','pixels',...
    'String','Yield stress (MPa)',...
    'Position',[10 75 80 27],...
    'backgroundColor',[.8 .86 1]);
    % SS304: 209 MPa, 42CrMo:310MPa, SS316L:285MPa, Copper:60
edithSigy = uicontrol(panel4,'Style','edit',...
    'Units','pixels',...
    'String','290',...
    'BackgroundColor','white',...
    'Fontsize',9,...
    'Position',[20 43 62 27]);
%--Maximum stress, MPa----------------%
texthSigmax = uicontrol(panel4,'Style','text',...
    'Units','pixels',...
    'String','Maximum stress (MPa)',...
    'TooltipString','Maximum stress must be higher than Yield stress !',...
    'Position',[95 75 80 27],...
    'backgroundColor',[.8 .86 1]);
edithSigmax = uicontrol(panel4,'Style','edit',...
    'Units','pixels',...
    'String','900',...
    'BackgroundColor','white',...
    'TooltipString','Maximum stress must be higher than Yield stress !',...
    'Fontsize',9,...
    'Position',[104 43 62 27]);
%--Module of Plasticity , MPa----------------%
texthmplastic = uicontrol(panel4,'Style','text',...
    'Units','pixels',...
    'String','Plastic Modulus (MPa)',...
    'TooltipString','Maximum stress must be higher than Yield stress !',...
    'Position',[295 75 100 27],...
    'backgroundColor',[.8 .86 1]);
edithmplastic = uicontrol(panel4,'Style','edit',...
    'Units','pixels',...
    'String','to be calculated',...
    'BackgroundColor','white',...
    'Fontsize',9,...
    'Position',[294 43 100 27]);
%--Main axes-----------------------------------------%
axesh2 = axes('Parent',fh,'units','normalized',...
    'Box','on',...
    'Fontsize',8,...
    'Position',[0.525 0.06 0.45 0.40]);
set(get(axesh2,'xlabel'),'string','\epsilon_a, -','fontsize',8)
set(get(axesh2,'ylabel'),'string','\sigma_a, MPa','fontsize',8)
%---buttons--------------------------------------%
bhSlow = uicontrol(panel3,'Units','normalized',...
```

```
    'Position',[0.22 0.64 0.54 0.32],...
    'String','Slow start',...
    'Enable','off',...
    'Callback',@buttonSlow);
texthSlow = uicontrol(panel3,'Style','text',...
    'Units','normalized',...
    'String','During time (s)',...
    'Position',[0.2 0.4 0.6 0.14],...
    'backgroundColor',[.8 .86 1]);
edithSlow = uicontrol(panel3,'Style','edit',...
    'Units','normalized',...
    'String','0.010',...
    'BackgroundColor','white',...
    'Fontsize',9,...
    'Position',[0.28 0.1 0.4 .24]);
bhApply = uicontrol(fh,'Units','normalized',...
    'Position',[.35 .66 0.05 0.05],...
    'String','Apply',...
    'Callback',@buttonApply);
bhOk = uicontrol(fh,'Units','normalized',...
    'Position',[0.92 0.07 0.05 0.05],...
    'String','OK',...
    'Callback',@buttonOK);
%---buttons-------------------------------------%
hh= uicontrol(panel4,'Units','pixel',...
    'Position',[380 10 55 30],...
    'String','Apply',...
    'Callback',@buttonApply2);
uiwait(fh);
%-----------------------------------------------%
  function buttonApply(hObject,eventdata)

        Sig_a=str2double(get(edithSiga,'String'));
        Tau_a=str2double(get(edithTaua,'String'));
        fsig=str2double(get(edithfsig,'String'));
        ftau=str2double(get(edithftau,'String'));
        delta=eval(get(edithd,'String'));
        fs=str2double(get(edithS,'String'));
        T=str2double(get(edithL,'String'));
        Sig_mean=str2double(get(edithSigm,'String'));
        Tau_mean=str2double(get(edithTaum,'String'));
        t=0:1/fs:T;
        Sig=Sig_a*sin(2*pi*fsig*(t+0))+ Sig_mean;
        Tau=Tau_a*sin(2*pi*ftau*(t+0)-delta)+ Tau_mean;
        axes(axesh)
        plot(t,Sig,'.-k',t,Tau,'.-r')
        xlabel('Time, s')
        ylabel('\sigma(t), \tau(t), MPa')
        legend('\sigma(t)', '\tau(t)')
        axis tight
        set(bhSlow,'Enable','on')
        smax= max(abs(Sig));
  end
%-----------------------------------------------%
    function buttonSlow(hObject,eventdata)
        T=str2double(get(edithL,'String'));
        T0=str2double(get(edithSlow,'String'));
```

```
        fs=str2double(get(edithS,'String'));

        if T0>T,
            f = warndlg('Time of slow start cannot be longer than time of
stress signals.', 'Warning');
            T0 = T;
            set(edithSlow,'string',num2str(T0))
            uiwait(f)
        end
        nr=T0*fs;
        X=[Sig' Tau'];
        w=sin([0:pi/2/nr:pi/2]');
        w=w*ones(1,size(X,2));
        X(1:size(w,1),:)=w.*X(1:size(w,1),:);
        Sig=X(:,1)';
        Tau=X(:,2)';
        plot(t,Sig,'.-k',t,Tau,'.-r')
        xlabel('Time, s')
        ylabel('\sigma(t), \tau(t), MPa')
        legend('\sigma(t)', '\tau(t)')
        axis tight
    end
%-------------------------------------------------%
    function buttonOK(hObject,eventdata)
        close(fh)
    end
%-------------------------------------------------%
    function buttonApply2(hObject2,eventdata2)
        mate.E=str2double(get(edithE,'String'));
        mate.K=str2double(get(edithK,'String'));
        mate.n=str2double(get(edithn,'String'));
        mate.ni=str2double(get(edithni,'String'));
        mate.Sig_y=str2double(get(edithSigy,'String'));
%         mate.DSig=str2double(get(edithDSig,'String'));
        mate.Sigmax=str2double(get(edithSigmax,'String'));
        mate.R=mate.Sig_y;
        if mate.Sigmax<mate.Sig_y,
            f = warndlg('Maximum stress must be higher than the yield
stress.', 'Warning');
            mate.Sigmax=mate.Sig_y+mate.DSig;
            set(edithSigmax,'string',num2str(mate.Sigmax))
            uiwait(f)
        end
        Sig_ai=[0:5:mate.Sigmax];
        Eps_ai=Sig_ai/mate.E+(Sig_ai/mate.K).^(1/mate.n);
        Eps_a=mate.Sig_y/mate.E+(mate.Sig_y/mate.K).^(1/mate.n);
        Eps_b=smax/mate.E+(smax/mate.K).^(1/mate.n);
        mate.C=((3/2)*(((Eps_b-Eps_a)/(smax-mate.Sig_y))-1/mate.E))^-1
        axes(axesh2)
        plot(Eps_ai,Sig_ai,'-k',[Eps_a,Eps_b],[mate.Sig_y,smax],'+-b')
        xlabel('\epsilon_a, -')
        ylabel('\sigma_a, MPa')
        set(edithmplastic,'string',num2str(mate.C))
    end
end
```

Deviatoric stress subroutine

```
%--------------- Deviatoric stress calculation, Equation (3.6) -------------%
function s=dev(t);
error(nargchk(1,1,nargin))
[m n]=size(t);
if n==3
   I=[1 1 1];
elseif n==6
   I=[1 1 1 0 0 0];
elseif n==9
   I=[1 1 1 0 0 0 0 0 0];
else
   error('Improper matrix dimension')
end
s=t-((1/3)*(t*I'))*I;
```

Hook's law subroutine

```
%--------------- Elastic strain calculation, Equation (3.4) -------------%
function Y=hooklaw(X, td, E, ni);
error(nargchk(4,4,nargin))
[m n]=size(X);
if n==3
   I=[1 1 1];
elseif n==6
   I=[1 1 1 0 0 0];
elseif n==9
   I=[1 1 1 0 0 0 0 0 0];
else
   error('Improper matrix dimension')
end
if lower(td)=='stress_strain'
   Y=((1+ni)/E)*(X-(ni/(1+ni))*(X*I')*I);
   elseif lower(td)=='strain_stress'
      Y=(E/(1+ni))*(X+(ni/(1-2*ni))*(X*I')*I);
   else
      error('Improper name of transform direction')
end
```

REFERENCES

[1] Prager W. (1956). A new method of analyzing stresses and strains in work hardening plastic solids. *Journal of Applied Mechanics*, 23, 493-496.

[2] Mroz Z. (1967). On the description of anisotropic work hardening. *Journal of the Mechanics and Physics of Solids*, 15, 163-175.

[3] Dafalias Y., Popov E. (1975). A Model of Nonlinearly Hardening Materials for Complex Loading. *Acta Mechanica*, 21, 173-192.

[4] Krieg R.D. (1975). A practical two surface plasticity theory. *ASME J. Appl. Mech.*, 42, 641-646.

[5] McDowell D.L. (1985). A Two Surface Model for Transient Nonproportional Cyclic Plasticity: Part I -Development of Appropriate Equations. *ASME J. Appl. Mech.*, 52, 298-302.

[6] Chaboche J.L. (1989). New kinematic hardening rule with discrete memory surfaces. *Recherche aérospatiale*, 4, 49-69.

[7] Chaboche J.L. (1986). Time-independent constitutive theories for cyclic plasticity. *International Journal of Plasticity*, 2, 149-188.

[8] Garud Y.S. (1981). A new approach to the evaluation of fatigue under multiaxial loading. *Journal of Engineering Material Technology*, 103, 118-125.

[9] Garud Y.S. (1982). Prediction of stress-strain response under general multiaxial loading. In: *Mechanical Testing for Deformation Model Development, ASTM STP 765*, 223-238, Baltimore,USA.

[10] Garud Y.S. (1991). Notes on cyclic dependent ratchetting under multiaxial loads including Bauschinger effect, In: *SMiRT 11 Transaction*, L, L23/1, 511-518, Tokyo, Japan.

[11] Jiang Y. (1993). Cyclic plasticity with emphasis on ratcheting. PhD thesis, University of Illinois at Urbana-Champaign.

[12] Hassan T., Corona E., Kyriakides S. (1992). Ratchetting in cyclic plasticity part II: multiaxial behavior. *International Journal of Plasticity*, 8, 117-146.

[13] Armstrong P.J., Fredrick C.O. (1966). A mathematical representation of the multiaxial Bauschinger effect. *CEGB Report RD/B/N731 Berkeley Nuclear Laboratories*.

[14] Chaboche, J.L. (1989). Constitutive equations for cyclic plasticity and cyclic viscoplasticity. *International Journal of Plasticity*, 5, 247-302.

[15] Chaboche J.L., Dang-Van K., Cordier G. (1979). Modelization of the strain memory effect on the cyclic hardening of 316 stainless steel. In: *Proceedings of the 5th International Conference on SMiRT, Div. L.*, Berlin, Germany.

[16] Chaboche, J.L. (1991). On some modifications of kinematic hardening to improve the description of ratcheting effects. *International Journal of Plasticity*, 7, 661–678.

[17] Ohno N., Wang J.D. (1993). Kinematic hardening rules with critical state of dynamic recovery, part I: formulations and basic features for ratcheting behavior. *International Journal of Plasticity*, 9, 375-390.

[18] Ohno N., Wang J.D. (1993). Kinematic hardening rules with critical state of dynamic recovery, part II: application to experiments of ratcheting behavior, *International Journal of Plasticity*, 9, 391–403.

[19] Bari S., Hassan T. (2000). Anatomy of coupled constitutive models for ratcheting simulation. *International Journal of Plasticity*, 16, 381-409.

[20] Jiang Y., Sehitoglu, H. (1996). Modeling of cyclic ratchetting plasticity, part I: development of constitutive relations. *ASME J. Appl. Mech.*, 63, 720–725.

[21] Jiang Y., Sehitoglu, H. (1996). Modeling of cyclic ratchetting plasticity, part II: comparison of model simulations with experiments. *ASME J. Appl. Mech.*, 63, 726-733.

[22] McDowell D.L. (1995). Stress state dependence of cyclic ratcheting behavior of two rail steels. *International Journal of Plasticity*, 11, 397-421.

[23] Bari S., Hassan T. (2002). An advancement in cyclic plasticity modeling for multiaxial ratcheting simulation. *International Journal of Plasticity*, 7, 873-894.

[24] Delobelle P., Robinet P., Bocher L. **(**1995). Experimental study and phenomenological modelization of ratcheting under uniaxial and biaxial loading on an austenitic stainless steel. *International Journal of Plasticity*, 11, 295-330.

[25] Burlet H., Cailletaud G. (1986). Numerical techniques for cyclic plasticity at variable temperature, *Eng. Comput.*, 3, 143-153.

[26] Bower A.F. (1989). Cyclic hardening properties of hard-drawn copper and rail steel. *J. Mech. Phys. Solids*, 37, 455-470.

[27] Bower A.F., Johnson K.L. (1989). The influence of strain hardening on cumulative plastic deformation in rolling and sliding line contact. *J. Mech. Phys. Soild*, 37, 471-493.

[28] Das D., Chakraborti P.C. (2011). Effect of stress parameters on ratcheting deformation stages of polycrystalline OFHC copper. *Fatigue & Fracture of Engineering Materials & Structures*, 34, 734-742.

[29] Kang G.Z., Liu Y.J., Li Z. (2006). Experimental study on ratchetting–fatigue interaction of SS304 stainless steel in uniaxial cyclic stressing. *Mater Sci Eng A*, 435-436, 396-404.

[30] Kang G.Z., Liu Y.J. (2007). Uniaxial ratchetting and low-cycle fatigue failure of the steel with cyclic stabilizing or softening feature. *Mater Sci Eng A*, 472, 258–268.

[31] Kang G.Z., Liu Y.J., Ding J. (2008). Multiaxial ratchetting–fatigue interactions of annealed and tempered 42CrMo steels: experimental observations. *International Journal of Fatigue*, 30, 2104–2118.

[32] Kang G.Z., Ding J., Liu Y.J. (2011). Summary on Uniaxial Ratchetting of 6061-T6 Aluminium Alloy. In: *Aluminium Alloys, Theory and Applications*, 199-216.

[33] Kang G.Z., Dong Y., Liu Y.J., Wang H., Cheng X. (2011). Uniaxial ratchetting of 20 carbon steel: Macroscopic and microscopic experimental observations. *Mater Sci Eng A*, 528, 5610-5620.

[34] Kang G.Z., Li Y.G., Zhang J., Sun Y.F., Gao Q. (2005). Uniaxial ratcheting and failure behaviors of two steels. *Theoretical and Applied Fracture Mechanics*, 43, 199-209.

[35] Kang G.Z., Kan Q., Zhang J. (2005). Experimental study on the uniaxial cyclic deformation of 25CDV4.11 steel. *Journal of Materials Science and Technology*, 21, 5-9.

[36] Lim C.-B., Kim K.S., Seong J.B. (2009). Ratcheting and fatigue behavior of a copper alloy under uniaxial cyclic loading with mean stress. *International Journal of Fatigue*, 31, 501-507.

[37] Paul S.K., Sivaprasad S., Dhar S., Tarafder S. (2010). True stress control asymmetric cyclic plastic behavior in SA333 C-Mn steel. *International Journal of Pressure Vessels and Piping*, 87, 440-446.

[38] Paul S.K., Sivaprasad S., Dhar S., Tarafder S. (2010). Ratcheting and low cycle fatigue behavior of SA333 steel and their life prediction. *Journal of Nuclear Materials*, 401, 17-24.

[39] Gaudin C., Feaugas X. (2004) Cyclic creep process in AISI 316L stainless steel in terms of dislocation patterns and internal stresses. *Acta Materialia*, 52, 3097-3110.

[40] Benham P.P., Ford H. (1961). Low Endurance Fatigue of a Mild Steel and an Aluminium Alloy. *J. Mech. Eng. Sci.*, 3, 119-132.

[41] Cai L., Niu Q., Qiu S., Liu Y. (2005). Ratcheting Behaviour of T225NG Titanium Alloy under Uniaxial Cyclic Stressing: Experiments and Modeling. *Chinese Journal of Aeronautics*, 18, 31-39.

[42] Jiang Y., Sehitoglu H., (1996). Comments of the Mroz multiple surface type plasticity models. *Int. J. Solids Structures*, 33, 1053-1068.

[43] Jahed H., Varvani A., Noban M., Khalaji I. (2007). An energy-based fatigue life assessment model for various metallic materials under proportional and non-proportional loading conditions. *International Journal of Fatigue*, 29, 647-655.

[44] Jiang Y., Kurath P. (1996). Characteristics of the Armstrong-Frederick type plasticity models. *International Journal of Plastcity*, 12, 387-415.

[45] Kang G.Z., Liu Y., Dong Y. Gao Q. (2011). Uniaxial Ratcheting Behaviors of Metals with Different Crystal Structures or Values of Fault Energy: Macroscopic Experiments. *J. Mater. Sci. Technol.*, 27, 453-459.

[46] Fatemi A., (1985). Fatigue and deformation under proportional and non proportional biaxial loading. PhD Thesis, The University of Iowa.

[47] Hassan T., Kyriakides S. (1994). Ratcheting of cyclically hardening and softening materials, Part I: uniaxial behavior. *International Journal of Plasticity*, 10, 149–184.

[48] Benham, P.P. (1965). Some observations of cyclic strain-induced creep in mild steel at room temperature. *Int. J. Mech. Sci.*, 7, 81-86.

[49] Coffin L.F.Jr. (1960). The Stability of Metals Under Cyclic Plastic Strain. *J. Basic Engineering, trans. ASME, Series D*, 82, 671-682

[50] Moyar G. J., Sinclair M. (1963). Cyclic strain accumulation under complex multiaxial loading. *Joint international conference on creep, the institution of mechanical engineers,* 2, 47-57

[51] Guionnet C. (1992). Modeling of ratcheting in biaxial experiments. *Journal of Engineering Materials and Technology*, 114, 56-62.

[52] Hassan T, Kyriakides S. (1994). Ratcheting of cyclically hardening and softening materials, Part II: multiaxial behavior. *International Journal of Plasticity*, 10, 185-212.

[53] Hassan T., Kyriakides S. (1992). Ratcheting in cyclic plasticty, Part I: uniaxial behavior. *International Journal of Plasticity*, 8, 91-116.

[64] Bari S., Hassan T. (2001). Kinematic hardening rules in uncoupled modeling for multiaxial ratcheting simulation. *International Journal of Plasticity*, 17, 885-905.

[55] Chen X., Jiao R. (2004). Modified kinematic hardening rule for multiaxial ratcheting prediction. *International Journal of Plasticity*, 20, 871-898.

[56] Chen X., Jiao R, Kim, K.S. (2003). Simulation of ratcheting strain to a high number of cycles under multiaxial loading. *International Journal of Solids and Structures*, 40, 7449-7461.

[57] Xia Z, Kujawski D, Ellyin F. (1996). Effect of mean stress and ratcheting strain on fatigue life of steel. *International Journal of Fatigue*, 18, 335–341.

[58] Rider R.J., Harvey S.J., Chandler H.D. (1995). Fatigue and ratcheting interactions. *International Journal of Fatigue*, 17, 507-511.

[59] Liu Y.J., Kang G.Z., Gao Q. (2008). Stress-based fatigue failure models for uniaxial ratchetting–fatigue interaction. *International Journal of Fatigue*, 30, 1065-1073.

[60] Kang G.Z., Liu Y.J., Ding J. (2007) Uniaxial cyclic deformation behavior of 6061Al alloy and its time-dependence at room and high temperatures, *Key Engineering Materials*, 345-346, 9-12.

[61] Kwofie S., Chandler H.D. (2007). Fatigue life prediction under conditions where cyclic creep-fatigue interaction occurs. *International Journal of Fatigue*, 29, 2117-2124.

[62] Jiang Y., Sehitoglu H. (1999). A model for rolling contact failure. *Wear*, 224, 38-49.

[63] Gao H., Chen X. (2009). Effect of axial ratcheting deformation on torsional low cycle fatigue life of lead-free solder Sn-3.5Ag. *International Journal of Fatigue*, 31, 276-283.

[64] Varvani-Farahani A., Shirazi A. (2007). Prediction of stiffness degradation and damage assessment of unidirectional GRP composites under fatigue cycles. *Sci Eng Compos Mater* 14(3), 197-204.

[65] Ahmadzadeh G.R., Shirazi A., Varvani-Farahani A. (2011). Damage Assessment of CFRP [90/±45/0] Composite Laminates over Fatigue Cycles. *Applied Composite Materials*, 18(6), 559-569.

[66] McDowell D.L. (1994) Description of nonproportional cyclic ratcheting behavior. *Eur. J. Mech. A/Solids*, **13**, 593-604.

[67] Chen X., Jiao R., Kim K.S. (2005). On the Ohno-Wang kinematic hardening rules for multiaxial ratcheting modeling of medium carbon steel. *International Journal of Plasticity*, 6, 161-184

[68] Smith K.N., Watson P., Topper T.H. (1970). A stress strain function for the fatigue of metals. *J Mater JMLSA*, 5, 767-778.

[69] Ellyin F., Xia Z. (1993). General fatigue theory and its application to out-of-phase cyclic loading. *Journal of Engineering Materials and Technology, Transactions of the ASME*, 115, 411-416.

[70] Kujawski D, Ellyin F. (1995). A unified approach to mean stress effect on fatigue threshold conditions. *International Journal of Fatigue*, 17, 101-106.

[71] Liu Y.J., Kang G.Z., Gao Q., Li Z. (2008). Ratcheting-fatigue interaction of annealed 42CrMo steel and its failure model. *Engineering Mechanincs*, 25, 186-191.

[72] Liu Y.J., Kang G.Z., Dong Y. (2008). Experimental study on ratcheting-fatigue interaction of 20 carbon steel in uniaxial cyclic loading. In: *International Conference on Experimental Mechanics*; *Proceedings of SPIE*, 7375, 73751K-1-5, Washington, USA.

[73] Jiang Y., Zhang J. (2008). Benchmark experiments and characteristic cyclic plasticity deformation. *International Journal of Plasticity*, 24, 1481-1515.

[74] Kang G.Z., Gao Q., Cai L., Yang X., Sun Y. (2001). Experimental Study on Uniaxial and Multiaxial Strain Cyclic Characteristics and Ratcheting of 316L Stainless Steel. *Journal of Materials Science and Technology*, 17, 219-223.

[75] Kang G.Z., Li Y., Gao Q., Kan Q.H., Zhang J. (2006) Uniaxial ratchetting in steels with different cyclic softening/hardening behaviours, *Fatigue & Fracture of Engineering Materials & Structures*, 29, 93-103.

[76] Paul S.K., Sivaprasad S., Dhar S., Tarafder S. (2011). Cyclic plastic deformation behavior in SA333 Gr. 6 C–Mn steel. *Materials Science and Engineering A*, 528, 7341-7349.

[77] Haupt A., Schinke B. (1996). Experiments of the ratchetting behavior of AISI 316L(N) austenitic steel at room temperature. *Journal of Engineering Materials and Technology*, 118, 281-284.

[78] Jiang Y., Sehitoglu H. (1994) Multiaxial cyclic ratchetting under multiple step loading. *international journal of plasticity*, 10, 849-870.

[79] ASM Handbook, Volume 19- Fatigue and Fracture, ASM International, Cleveland, (1996), 968-979